



HAL
open science

Preparation of highly thermostable materials by modification and functionalization of bisphthalonitrile resin

Ya-Jie Lei

► **To cite this version:**

Ya-Jie Lei. Preparation of highly thermostable materials by modification and functionalization of bisphthalonitrile resin. Food and Nutrition. Université de Lorraine, 2013. English. NNT : 2013LORR0265 . tel-01750720

HAL Id: tel-01750720

<https://hal.univ-lorraine.fr/tel-01750720>

Submitted on 18 Sep 2023

HAL is a multi-disciplinary open access archive for the deposit and dissemination of scientific research documents, whether they are published or not. The documents may come from teaching and research institutions in France or abroad, or from public or private research centers.

L'archive ouverte pluridisciplinaire **HAL**, est destinée au dépôt et à la diffusion de documents scientifiques de niveau recherche, publiés ou non, émanant des établissements d'enseignement et de recherche français ou étrangers, des laboratoires publics ou privés.



AVERTISSEMENT

Ce document est le fruit d'un long travail approuvé par le jury de soutenance et mis à disposition de l'ensemble de la communauté universitaire élargie.

Il est soumis à la propriété intellectuelle de l'auteur. Ceci implique une obligation de citation et de référencement lors de l'utilisation de ce document.

D'autre part, toute contrefaçon, plagiat, reproduction illicite encourt une poursuite pénale.

Contact : ddoc-theses-contact@univ-lorraine.fr

LIENS

Code de la Propriété Intellectuelle. articles L 122. 4

Code de la Propriété Intellectuelle. articles L 335.2- L 335.10

http://www.cfcopies.com/V2/leg/leg_droi.php

<http://www.culture.gouv.fr/culture/infos-pratiques/droits/protection.htm>



UNIVERSITÉ
DE LORRAINE

Ecole Nationale Supérieure des
Industries Chimiques
(ENSIC)

en co-tutelle avec l'Université des Sciences et
Technologies de Chine

Ecole Doctorale : Ressources Procédés
Produits Environnement (RP2E)

Laboratoire Réactions et Génie des Procédés
(LRGP-CNRS UMR 7274)

**Elaboration de matériaux hautement stable thermiquement par modification et
fonctionnalisation de la résine bisphthalonitrile**

**Preparation of highly thermostable materials by modification and
functionalization of bisphthalonitrile resin**

THESE

présentée en vue de l'obtention du

DOCTORAT DE L'UNIVERSITE DE LORRAINE

Spécialité : Génie des Procédés et des Produits

par

Ya-Jie LEI

Soutenue le 24 juillet 2013

Composition du jury:

Rapporteurs :	Jinbo BAI Jie Yang	Directeur de recherche au CNRS, Ecole Centrale de Paris, France Professeur à l'Université de Sichuan, Chine
Examinateurs :	Guo-Hua HU Xiao-Bo LIU	Professeur à l'Université de Lorraine, France Professeur à l'Université des Sciences et Technologies Electroniques, Chine

Table of contents

Table of contents	I
Chapter 1 Introduction	1
1.1 Motivation and objectives	1
1.2 Overview of thesis.....	6
1.3 References	10
Chapter 2 Experimental.....	13
2.1 Materials.....	13
2.1.1 Materials for chapter 3	13
2.1.2 Materials for chapter 4	13
2.1.3 Materials for chapter 5	13
2.1.4 Materials for chapter 6	13
2.2 Sample preparation.....	14
2.2.1 Preparations of samples for chapter 3	14
2.2.2 Preparations of samples for chapter 4	16
2.2.3 Preparations of samples for chapter 5	18
2.2.4 Preparations of samples for chapter 6	19
2.3 characterization	21
2.3.1 Differential Scanning Calorimetry (DSC) analysis	21
2.3.2 Thermogravimetry analysis (TGA).....	21
2.3.3 Rheological measurements.....	21
2.3.4 X-ray diffraction (XRD) analysis.....	22
2.3.5 Mechanical Properties analysis	22
2.3.6 Resistance measurements	22
2.3.7 Intrinsic viscosity measurements.....	23
2.3.8 Dielectric properties analysis	23
2.3.9 Magnetic properties analysis	23
2.3.10 Fourier-transform infrared spectroscopy analysis (FTIR).....	24
2.3.11 Scanning electron microscopy analysis (SEM).....	24
2.3.12 Transmission electron microscopy analysis (TEM)	24
2.4 References	24
Chapter 3 Preparation Process and Properties of Exfoliated Graphite Nanoplatelets filled Bisphthalonitrile Nanocomposites	25
3.1 Introduction	25
3.2 Results and discussion.....	27
3.2.1 Structure of xGnP.....	27
3.2.2 Rheological behavior of the xGnP/BPh pre-polymer system.....	29
3.2.3 Thermal properties of the xGnP/BPh nanocomposites.....	30
3.2.4 Mechanical properties of the xGnP/BPh nanocomposites	31
3.2.5 Resistivity of the xGnP/BPh nanocomposites	34
3.3 Conclusions	35
3.4 References.....	36
Chapter 4 Mechanical and thermal properties of graphite nanoplatelets reinforced polyarylene ether nitriles / bisphthalonitrile IPN system	39

4.1. Introduction	39
4.2. Results and discussion.....	40
4.2.1 FTIR spectra of the PEN-BPh IPN system	40
4.2.2 Thermal properties of the PEN-BPh IPN system	41
4.2.3 Mechanical property of the PEN-BPh IPN system	42
4.2.4 Thermal properties of xGnP/PEN-BPh composite.....	45
4.2.5 Mechanical property of xGnP/PEN-BPh composites.....	46
4.3 Conclusions	47
4.4 References.....	47
Chapter 5 Production of empty and iron-filled multiwalled carbon nanotubes from iron-phthalocyanine polymer and their electromagnetic properties	49
5.1. Introduction	49
5.2. Results and discussion.....	51
5.2.1 DSC analysis of the iron phthalocyanine (FePc) oligomer	51
5.2.2 Microstructure of the CNTs.....	51
5.2.3 XRD analysis of the CNTs	56
5.2.4 Dielectric properties of the CNTs.....	58
5.2.5 Magnetic properties of the CNTs	64
5.3. Conclusions	65
5.4 References	66
Chapter 6 Electromagnetic, Microwave-Absorbing Properties of Iron- phthalocyanine and its composites based on phthalocyanine polymer.....	68
6.1. Introduction	68
6.2. Results and Discussion.....	70
6.2.1 Conductivity of the FePc after a series of high temperature sintering	70
6.2.2 Microwave absorption properties of the iron- phthalocyanine (S700).....	74
6.2.3 The effect of catalysis amount on the microwave absorption properties of FePc after 700 °C sintering.....	80
6.2.4 Dielectric and microwave absorption properties of the FePc/BPh composites.....	85
6.2.5 Mechanical properties of FePc/BPh composites	90
6.3. Conclusions	93
6.4 References	94
Chapter 7 Conclusion.....	96
Acknowledgements.....	99
ABSTRACT.....	100

Chapter 1 Introduction

1.1 Motivation and objectives

Nowadays, the application of polymer composites as engineering materials has become the state of the art. In order to meet a special target of engineering application, polymer composites can be designed by selecting the correct composition and choosing the appropriate manufacturing process, as schematically illustrated in Fig. 1.1. There are many possibilities to create polymer composites containing different fillers and/or reinforcements (Fig. 1.2)[1]. In addition, not only different kinds but also various properties of matrix materials and fillers/reinforcements, as well as the fiber orientations and, in case of continuous fiber composites, the laminate parameters can be considered.

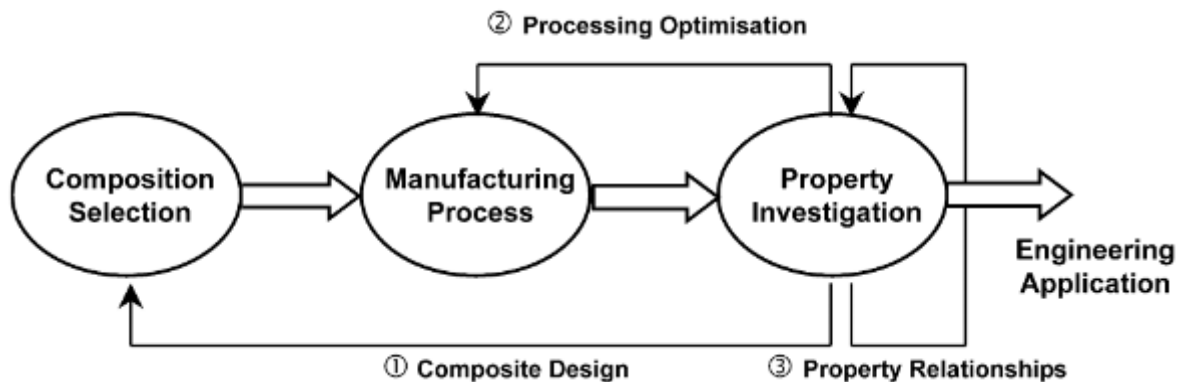


Fig. 1.1 Schematic presentation of composition selection, manufacturing process, and property investigation for the development of composite materials

In the manufacturing process, some key parameters, e.g. curing temperatures and manufacturing speed, which govern the final quality of the composites, should also be analyzed. Property investigation plays a key role in materials science to evaluate composites designed for special engineering applications. All three stages shown in Fig. 1.1 are not separated, but interconnected, and the integration can be summarized as composite design, process optimization and structure-property relationship (as indicated additionally in Fig. 1.1). The first two fields correspond to the interaction between the selected compositions or the manufacturing process and the properties investigated, whereas the last relates to

possible correlations between some simple measured parameters (e.g. modulus, strength and failure strain) and more complex properties (e.g. fatigue, thermostability, combined loading and creep). The understanding of all these relationships is important in composite materials science, in order to meet the requirements for particular engineering applications.

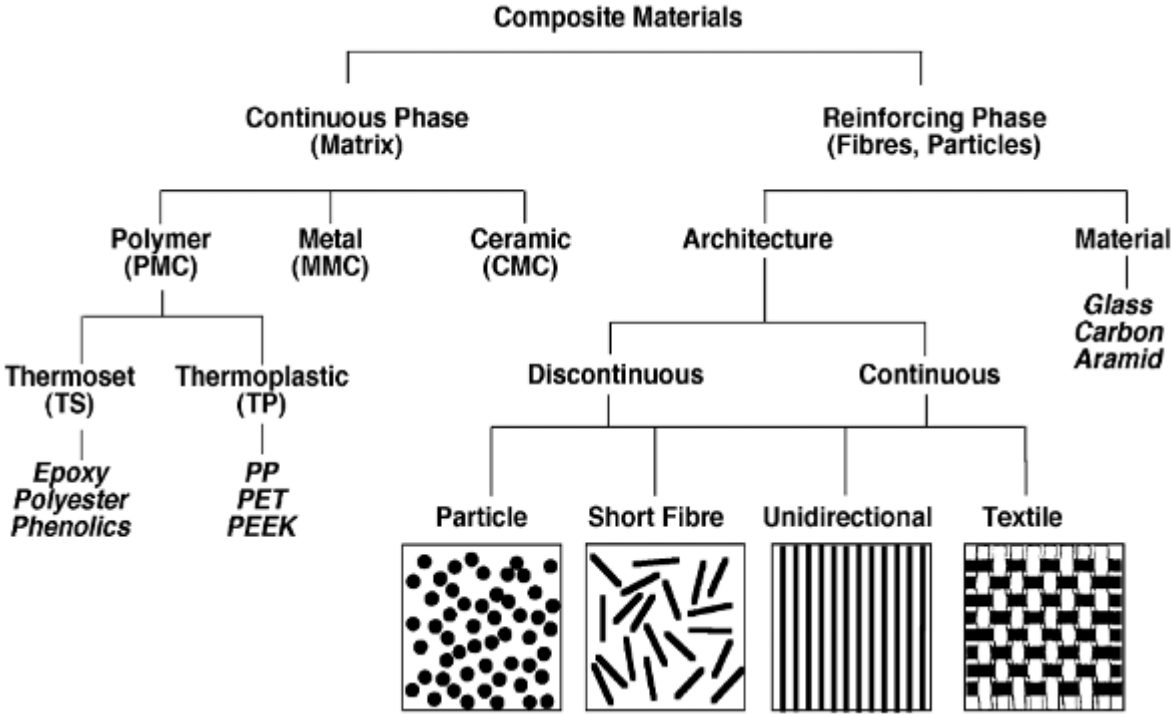


Fig. 1.2 Systematic illustration of the structural components of composite materials [1]

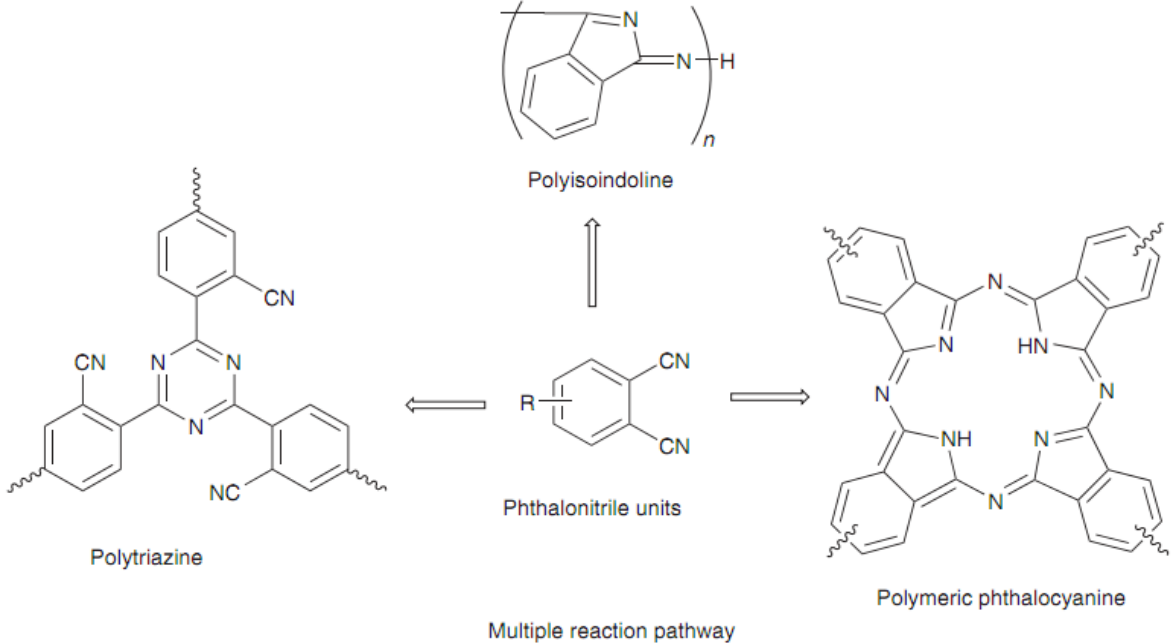


Fig. 1.3. Multiple cure pathways for phthalonitrile resins

High-temperature/performance polymers are an important class of materials for aerospace, marine, and microelectronic applications. The interest in polymeric composites versus metallic materials arises from the need for a reduction in weight and an enhancement in performance. For composite applications, it is essential to have polymeric materials that have fairly low melting points, a large processing window defined as the difference between the melting point and the polymerization temperature, and a low viscosity for the fabrication of composite components by cost-effective methods such as resin transfer molding, resin infusion molding, and filament winding. Bisphthalonitrile polymers are an important class of high-performance polymers. They are derived by heating phthalonitrile derivatives for an extended period of time at elevated temperatures by addition curing reaction of cyano groups from phthalonitrile derivatives. Multiple cure pathways for phthalonitrile resins shown in Fig. 1.3 probably depend on the type of the curing agent used and proceed through a multiple mechanism. For example, polymeric phthalocyanine is the major product when metallic salts are used [2-7]. A low concentration of cure agents such as aromatic amine, strong organic acid/amine salts and strong organic acid probably promote the polymerization reaction of phthalonitrile resin with the polytriazine as the major product and polymeric phthalocyanine as the minor product. Therefore, the properties and processing of the phthalonitrile resins can be controlled by the curing agent used.

Because of their outstanding thermal and thermal-oxidative stability, good mechanical properties, low flammability, good water and chemical resistance, and easy processing, bisphthalonitrile polymers are recognized as a better class of excellent candidate matrices for advanced composites than other traditional high temperature/performance resin-based advanced composites, such as epoxy, cyanate resin, polyimide and bismaleimide (BMI).

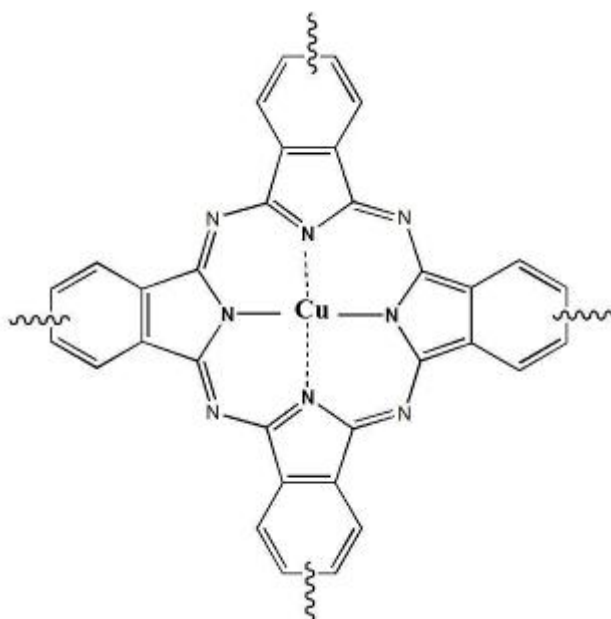
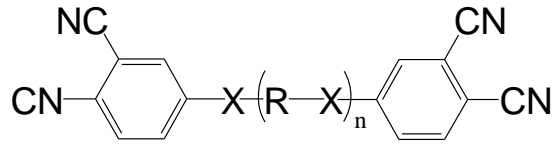


Fig. 1.4. Structure of copper phthalocyanine

In fact, phthalonitrile monomers have been used to synthesize phthalocyanine dyes for several decades. In 1934, Dent and Linstead found that copper phthalocyanine (Fig. 1.4) could be sublimed under nitrogen at 560 °C without decomposition [8]. That phenomenon induced researchers to synthesize heat resistant polymeric phthalocyanines. In 1958, Marvel and Martin attempted to see whether or not the phthalocyanine unit might be incorporated into a polymeric structure to produce an equally thermostable polymer [9, 10]. Unfortunately, only low molecular weight polymers were produced. After that, other researchers synthesized various phthalonitrile monomers and the corresponding polymeric phthalocyanines [11–19]. The polymerization was catalyzed by metals or their salts and the resultant polymers were mainly composed of phthalocyanine units as the linkages. As a result, the polymers were found to have poor oxidative thermostability due to metal-catalyzed oxidation. Therefore, these polymers were not suitable for using as resin matrices for advanced composites. In 1980, Keller and Price found that the polymerization of phthalonitrile monomers could be promoted by small amounts of primary amines and much more stable polymers were obtained [5]. Since then, a way to advanced composites was open for phthalonitrile resins.

To date, several phthalonitrile monomers having structural variations at molecular level have been synthesized and polymerized into thermosets [20, 21]. Typical structures of phthalonitrile monomers are shown in Fig. 5.



$n=1\sim 8,$ $\text{X}=\text{O}, \text{S}, \text{N}, \text{etc.}$

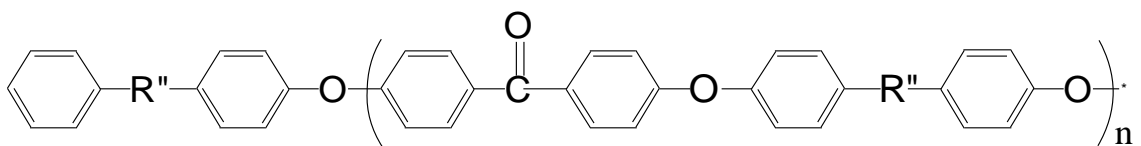
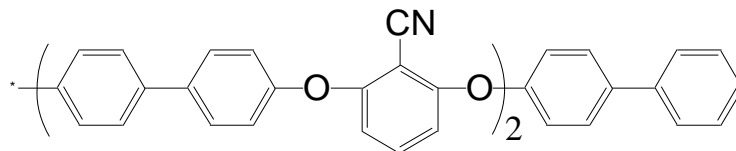
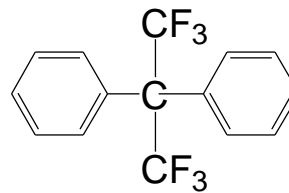
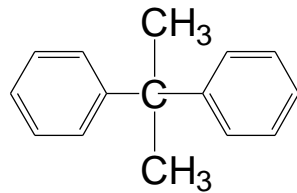
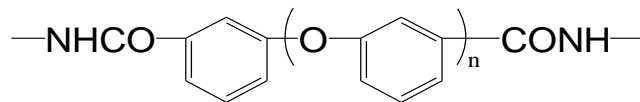
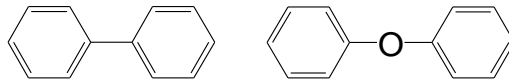
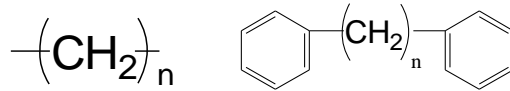
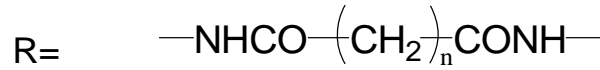


Fig. 1.5 Typical structures of phthalonitrile monomers.

Among them, 4, 4' bis-(3, 4-dicyanophenoxy)biphenyl (BPh) is one of the typical phthalonitrile monomers which has been effectively used as a matrix resin for composite formulations. Its structure is shown in Fig. 1.6. Composite panels have been processed by conventional prepreg consolidation, resin infusion and filament winding methods with different reinforcements such as carbon tape [22], carbon fabric, and glass fabric [23, 24]. Due to its relatively low initial melt viscosity (0.1–0.2 Pa.s), BPh-based phthalonitrile

composites are amenable to processing by a resin transfer molding process which is more cost-effective. Moreover, mechanical properties and thermal and oxidative stabilities of BPh-based composites are superior to those of many state-of-the-art high-temperature composites. Phthalonitrile polymers show potential as high-temperature polymers for use in a wide variety of applications such as composite matrices [25], adhesives [26], and electrical conductors [27-30]. However, their performances are limited by the following disadvantages:

(1) Mechanical properties of bisphthalonitrile polymers are adversely affected by their intrinsic brittleness of the network structure.

(2) High melting temperature, narrow processing window, high curing temperature, low curing rate and long curing time.

(3) According to the existing report, the processing temperature of bisphthalonitrile resin-based composites is controlled at 500 °C or less, while there are few studies on its materials formed above 500 °C.

(4) Works on the functionalization of bisphthalonitrile resin have not been abundant enough and its application range needs to be expanded.

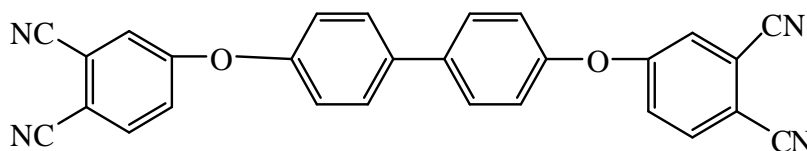


Fig. 1.6. Typical structures of 4, 4' bis-(3,4-dicyanophenoxy) biphenyl monomers

Based on the above statement, this thesis is focused on the modification and functionalization of bisphthalonitrile resins. Bisphthalonitrile resins were modified by a variety of methods, resulting in improvement of their mechanical properties. Moreover carbon nanotubes with different morphologies and microwave absorbing materials were obtained by pyrolysing bisphthalonitrile resins with different metal iron catalysts in the range of 600 ~ 900 °C. An approach for functionalization of bisphthalonitrile resins was developed and its application field expanded.

1.2 overview of thesis

A brief overview of this thesis is as follows.

Chapter 2 describes the main experiments in this study.

Polymer nanocomposites have been an area of major scientific and technological interest since they have potential to exhibit multifunctional and high-performance characteristics owing to the presence of small amounts of nanofillers in polymer matrices [31-38]. Under such circumstances, the intrinsic properties of the nanofillers as well as the strong polymer-nanofiller interfacial interactions alter the properties of the polymer matrix [31, 32, 39], which may have the potential of significantly improving its mechanical, thermal and electrical properties. All these properties depend on the type of nanofiller. Many nanofillers could be considered for nanocomposite fabrication and property enhancements. Among the most studied nanofillers are layered silicates such as montmorillonite and bentonite [40-42], graphite, and carbon nanotubes [43, 44]. Exfoliated graphite nanoplatelets (xGnP) are a potential alternative to other nano-reinforcements such as nano-clays and carbon nanotubes since they combine the low cost and layered structure of nano-clays and the superior thermal and electrical properties of carbon nanotubes [45, 46].

In Chapter 3, xGnP filled 4,4'-bis (3,4-dicyanophenoxy) biphenyl (BPh) nanocomposites were prepared by a resin transfer molding process. The rheological behavior of the BPh pre-polymer, and the morphology, electrical, mechanical and thermal properties of the xGnP/BPh nanocomposites were systematically investigated. The results showed that the xGnP/BPh pre-polymer possessed a higher complex viscosity and storage modulus than the pure BPh and that the xGnP could significantly enhance the mechanical and electrical properties of the resulted nanocomposites. The electrical percolation threshold of the xGnP/BPh nanocomposites was between 5 and 10 wt % xGnP. The flexural strength and modulus of the xGnP/BPh nanocomposites with 10 wt% xGnP exhibited maximum values and their thermal stability was greatly improved. Those novel xGnP/BPh nanocomposites could have advanced applications in areas like aerospace and military industry.

The mechanical properties, thermal and oxidative stability of BPh-based composites are superior to those of many state-of-the-art high-temperature composites. A previous

work showed that xGnP/BPh composites with 10 wt% xGnP content exhibited maximum values and the thermal stability were greatly improved. However, the performances of this BPh-based system are still limited by the intrinsic brittleness of the network structure that adversely affects its mechanical properties.

To overcome this limitation, in Chapter 4 the thermoset-thermoplastic interpenetrating polymer networks (IPN) tend to be effective. The IPN, with an intimate combination of two kinds of polymers in network formation [47-49], can exhibit synergistic properties of both the component polymers, which is often more excellent than single component. As a kind of engineering thermoplastic, polyarylene ether nitrile (PEN) has attracted much interest from both industry and academia due to its excellent property similar to polyether ether ketone (PEEK). Owing to its rigid molecular structure, PEN exhibits high mechanical strength, high toughness, good radiation resistance, and high thermo-oxidative stability [50-52], which make it very attractive for the composites used at toughening mechanism, aggressive chemical environments and so on. Herein, we chose PEN as the guest polymer in BPh system. However, the introduction of thermoplastic resin always increases the tenacity but decreases the modulus and thermal stability of the thermoset resin. Therefore, it is necessary to introduce a third component to offset losses of the flexural modulus and thermal stability lowered by PEN. Then the xGnP reinforced PEN-BPh IPN system was prepared and the results demonstrated that xGnP could improve the flexural strength of BPh and also offset losses of the flexural modulus and thermal stability lowered by PEN. The high performance xGnP reinforced PEN-BPh IPN composite is believed to have potential applications in military industry, aerospace, and other fields where solvent resistance and/or exposure to high temperature is necessary.

Carbon nanotubes (CNTs), first reported by Sumio Iijima in 1991[53], have attracted tremendous attention due to their unique structural, electronic, magnetic and mechanical properties [54]. To date, CNTs can be obtained by many methods such as arc-discharge [55, 56], laser ablation [57] and chemical vapor deposition (CVD) [58]. Among them, CVD method is highly preferred for the preparation of aligned CNTs in the presence of carbon sources (e.g. graphite, metal carbonyls, metallophthalocyanines and metallocenes [59, 60])

and catalysts (e.g. pure metals, metal salts and organic metals [61]). Further industrial preparation of CNTs by CVD method, however, is hindered due to cumbersome separation and purification process of catalysts from the CNTs. And the CVD method needs a supply of hydrogen to maintain catalysts activity during the high-temperature process, and the control of tube morphology is also limited. To solve the problem, solid-state pyrolysis of organometallic precursors for CNT preparation could be effective, simple and controllable [62~64], for that the organometallic materials serve as both the carbon source and the catalyst, and the pyrolysis process could be carried out in a controllable manner at “low” temperature in the solid states rather than in the gas phases. Moreover, compared with organometallic precursors such as cobalt–oligoalkyne complexes, iron, cobalt and nickel phthalocyanines molecular [65], the use of metal phthalocyanine molecular as carbon sources exhibited excellent performances during the synthesis of CNTs. Synthesis of CNTs using small molecule phthalocyanine as carbon sources has been studied a lot, but preparing CNTs from its polymer has not been reported yet.

In Chapter 5, a simple and efficient method for in situ synthesis of multiwalled carbon nanotubes (CNTs) from the pyrolysis of a mixture formulated from $\text{Fe}(\text{CO})_5$ powder and nano-iron powder respectively various high temperature bisphthalocyanine polymer under nitro atmosphere was described. SEM, TEM, XRD were employed to figure out the detailed structure information on the CNTs, meanwhile the conductive, dielectric and magnetic properties were studied. This research opened up a new application area of bisphthalocyanine resin which is different with other traditional thermosetting ones.

Phthalocyanine (Pc) is a class of thermoset resins obtained by the addition polymerization of phthalonitrile cyano groups at high temperature. It is a planar heterocyclic molecule of about 1.3 nm diameter with four fused phenyl and pyrrole subunits through aza bridges. The Pc macromolecule is also able to coordinate various metal cations (Fe, Ni, Co, etc.) in its center with the four central nitrogens belonging to the pyrrolic subunits. With iron, it is called iron-phthalocyanine (FePc) [66]. FePc, known for its high symmetry, planarity, and electron delocalization, is a porphyrin derivative consisting of a central Fe atom bound to a π -conjugated ligand. It has attracted a great deal of attention due to a wide variety of potential applications.

In Chapter 6, BPh monomer and ferrocenecarboxaldehyde were employed to synthesize FePc via a series of high temperature sintering: 500, 700 and 900 °C. The products with best electromagnetic properties were obtained after 700 °C sintering process while 4 wt% ferrocenecarboxaldehyde loading catalyst has been used. So, we mainly focus on the microwave absorption properties of the FePc after 700°C sintering process. Theoretical simulation for the microwave absorption using Cole-Cole semicircle theory agrees well with the experimental results: the microwave absorption of these composites can be mainly attributed to the dielectric loss rather than magnetic loss. Then we choose BPh resin as the vector of FePc (after 700 °C sintering process) absorbent to prepare FePc/BPh composites. After curing reaction, the FePc particles provided the composite with novel dielectric and microwave-absorbing properties and the mechanical properties of the resin were greatly improved. The high value of microwave reflection and mechanical property suggests that the composite can be a promising microwave absorbing material.

1.3 References

- [1] Verpoest I. Personal communication, 1998.
- [2] Walton TR., Griffith R., O'Rear JG. Phthalonitrile Resins. *Polym Sci Technol*, 1975, 9B:665
- [3] Snow AW, Griffith JR.. Syntheses and characterization of heteroatom-bridged metal-free phthalocyanine network polymers and model compounds. *Macromolecules*, 1984, 17: 1614-1624
- [4] Marullo NP, Snow AW. Polymerization of Bisphthalonitriles: Metal Free Phthalocyanine Formation. *ACS Symposium Series*, 1982, 195: 325-335
- [5] Keller TM, Price TK. Amino-cured bisphenol-linked phthalonitrile resins. *J Macromol Sci Chem*, 1982, 18: 931-937
- [6] Keller TM, Griffith JR. Polymerization studies on aromatic bis(phthalonitrile)monomers. *ACS Org Coat Plast Chem Prepr*, 1980, 43: 804-807
- [7] Keller TM, Dominguez DD. High temperature resorcinol-based phthalonitrile polymer. *Polymer*, 2005, 46: 4614-4618
- [8] Dent CE, Linstead RP. *J Chem Soc*, 1934, 1027–1031.
- [9] Marvel CS, Martin MM. *J AmChemSoc*, 1958, 80:1197–1199.
- [10] Marvel CS, Martin MM. *J AmChemSoc*, 1958, 80:6600–6604.
- [11] Griffith JR, Walton TR. *Am Chem Soc Polym Prepr*, 1974, 15:787.
- [12] Walton TR, Griffith JR, O'Rear JG. *Am Chem Soc Div Org Coat Plast Chem Prepr* 1974, 34:446–453.

- [13] Griffith JR, O'Rear JG, Walton TR. *Adv Chem Ser*, 1975, 142:458–464.
- [14] Keller TM, Griffith JR. *Am Chem Soc Div Org Coat Plast Chem Prepr*, 1978, 39:546–548.
- [15] Keller TM, Griffith JR. *Am Chem Soc Symp Ser*, 1980, 132:25–34.
- [16] Keller TM, Price TR, Griffith JR. *Synthesis* 1980, 8:613.
- [17] Walton TR, Griffith JR, Reardon JP. *J Appl Polym Sci* 1985, 30:2921–2939.
- [18] Achar BN, Fohlen GM, Parker JA. *J Appl Polym Sci* 1984, 29:353–359.
- [19] Woehrl D, Schulte B. *Makromol Chem* 1988, 189:1229–1238.
- [20] J. A. Hinkley. *J Appl Polym Sci*, 1984, 29: 3339–3347
- [21] M. L. Warzel, T. M. Keller. *Polymer*, 1993, 34: 663–666
- [22] Sastri SB, Armistead JP, Keller TM. *Polym Compos*, 1996, 17: 816-822.
- [23] Sastri SB, Armistead JP, Keller TM, Sorathia U. *Polym Compos* 1997, 18: 48-54.
- [24] Sastri SB, Armistead JP, Keller TM, Sorathia U. *SAMPE Symp Ser*, 1996, 42: 1032-1038.
- [25] Keller T. M., *Chem. Mater.* 1994, 6: 302-305.
- [26] Keller T. M.. C. M. Roland, US Patent. 1993, 5242755.
- [27] Keller T. M.. *Chemtech.* 1988, 18: 635-640.
- [28] Keller T. M.. *J Polym Sci: Part A: Polym. Chem.* 1988, 26: 3182-3199.
- [29] Keller T. M.. *SAMPE Symp.* 1986, 31: 528-529.
- [30] Guilani J. F., Keller T. M.. *Sens. Mater.* 1989, 1: 2244-2247.
- [31] Dang, ZM., Yuan, JK., Zha, JW., Zhou, T., Li, ST., Hu, GH. *Prog. Mater Sci.* 2012, 57: 660-723.
- [32] Yu ZZ, Hu GH, Varlet J, Dasari A, Mai YW. *J. Polym.Sci., Part B: Polym. Phys.* 2005, 43: 1100-1112.
- [33] Gunes IS, Cao F, Jana SC. *Polymer.* 2008,49: 2223-2234.
- [34] Chinellato AC., Vidotti SE., Hu GH., Pessan LA. *Compos. Sci. Technol.* 2010, 70: 458-465.
- [35] Mohammed H, Al-Saleh, Sundararaj U. *Polymer*, 2010, 51: 2740-2747.
- [36] Vidotti SE., Chinellato AC., Hu GH., Pessan LA. *J. Polym. Sci., Part B: Polym.Phys.* 2007, 45: 3084-3091.
- [37] Chinellato AC., Vidotti SE., Hu GH., Pessan LA. *J. Polym.Sci., Part B: Polym. Phys.* 2008, 46: 1811-1819
- [38] Pavlidou S, Papaspyrides CD. *Prog. Polym. Sci.* 2008, 33: 1119-1198.
- [39] Penu C., Hu GH., Fernandez A., Marchal P., Choplin L. *Polym. Eng. Sci.* 2012, in press. DOI 10.1002/pen.23162
- [40] Vaia RA, Giannelis EP. *Polymer. MRS Bulltin.* 2011, 26: 394-401.
- [41] Manias E, Touny A, Wu L, Strawhecker K, Lu B, Chung TC. *Chem. Mater.* 2001, 13: 3516-3523.
- [42] Hu GH., Hoppe S., Feng LF., Fonteix C. *Chem. Eng. Sci.* 2007, 62: 3528-3537
- [43] Sheng N, Boyce MC, Parks DM, Rutledge GC, Abes JI, Cohen RE. *Polymer.* 2004, 45: 487-506.
- [44] Chen LM., Ozisik R, Schadler LS. *Polymer.* 2010, 51: 2368-2375.
- [45] Kalaitzidou K, Fukushima H, Drzal LT. *Carbon.* 2007, 45: 1446-1452.
- [46] Kalaitzidou K, Fukushima H, Drzal LT. *Compos. A.* 2007, 38: 1675-1682.

- [47] Sperling LH. New York: Plenum Press, 1981.
- [48] Huelck V, Thomas DA, Sperling LH. *Macromolecules*. 1972, 5: 340-348.
- [49] Curtius AJ, Covitch MJ, Thomas DA, Sperling LH. *Polym. Eng. Sci.* 1972, 12: 101-107.
- [50] Saxena A, Sadhana R, Rao VL, KanakavelM, Ninan KN. *Polym. Bull.* 2003, 50: 219-226.
- [51] Saxena A, Rao VL, Ninan KN. *Eur. Polym.* 2003, 39: 57-66.
- [52] Li C, Gu Y, Liu XB. *Mater Lett.* 2006, 60: 137-140.
- [53] Iijima S. *Nature*. 1991, 354: 56-59.
- [54] Baughman RH, Zakhidov AA, Heer WA. *Science*, 2002, 297: 787-792.
- [55] Bethune DS, Kiang CH, Vries MS, Gorman G, Savoy R, Vazquez J, Beyers R. *Nature*. 1993, 363: 605-607.
- [56] Journet C, Maser WK, Bernier P, Loiseau A, Chapelle ML, Lefrant S, Denaiard P, Lee R, Fischer JE. *Nature*, 1997, 388: 756-758.
- [57] Thess A, Lee R, Nikolaev P, et al. *Science*. 1996, 273: 483-487.
- [58] Jose-Yacamán M, Miki-Yoshida M, Rendon L, Santieste-ban TG. *Appl. Phys. Lett.* 1993, 62: 202-204.
- [59] Qin LC. *J. Mater. Sci. Lett.* 1997, 16: 457-464.
- [60] Hou H, Zeng J, Weller F, Greiner A. *Chem. Mater*, 2003, 16: 3170-3175.
- [61] Lyu SC, Liu BC, Lee SH, Park CY, et al. *J. Phys. Chem. B*, 2004, 108: 1613-1616.
- [62] Iyer VS, Vollhardt KPC, Wilhelm R. *Angew. Chem*, 2003, 115: 4515-4519.
- [63] Dosa PI, Erben C, Iyer VS, et al. *J. Am. Chem. Soc.* 1999, 121: 10430-10431.
- [64] Laskoski M, Steffen W, Morton JGM, Smith MD, Bunz UHF. *J. Am. Chem. Soc.* 2002, 124: 13814-13818.
- [65] Tong WY, Djuricic AB, Xie H, et al. *J. Phys. Chem. B*, 2006, 35:17406-17413.
- [66] Milev AS, Tran N, Kannangara GSK, Wilson MA, Avramov I. *J. Phys. Chem. C*. 2008, 112: 5339-5347.

Chapter 2 Experimental

2.1 Materials

2.1.1 Materials for chapter 3

N, N-dimethylformamide (DMF) and K_2CO_3 were purchased from Tianjin BODI chemicals. 4, 4'-biphenol and 4-nitrophthalonitrile were purchased from Beijing Yangcun Co. Ltd., China. Natural graphite was purchased from Qingdao Yanxin Graphite Co. Ltd., China. Diphenyl diamine sulfoxide (DDS) was purchased from Yangzhou Tianchen Meticulous Chemical Co. Ltd., China. All the chemicals and reagents were used without further purification.

2.1.2 Materials for chapter 4

N-methyl-2-pyrrolidone (NMP), 2, 6-dichlorobenzonitrile, hydroquinone, Anhydrous K_2CO_3 and phenolphthalein were purchased from Tianjin BODI chemicals. Anhydrous K_2CO_3 was dried under vacuum at 100 °C before use. DDS was purchased from Yangzhou Tianchen Meticulous Chemical Co. Ltd., China. 4, 4'-bis (3, 4-dicyanophenoxy) biphenyl (BPH) monomer was synthesized in our laboratory,

2.1.3 Materials for chapter 5

$Fe(CO)_5$ powder (micron level) and nano-iron (size: ~40 nm) was supplied by China New Materials Company. N-methyl-2-pyrrolidone (NMP) was obtained from Tianjin BODI Chemicals. 4, 4'-bis (3, 4-dicyanophenoxy) biphenyl (BPh) monomer was synthesized in our laboratory. All materials were used without any further purification.

2.1.4 Materials for chapter 6

4, 4'-bis (3, 4-dicyanophenoxy) biphenyl (BPh) monomer was prepared in our

laboratory. Ferrocenecarboxaldehyde were supplied by China New Materials Company. N-methyl-2-pyrrolidone (> 99%) is obtained from TianJin BODI Chemicals. All the materials are used without any further purification.

2.2 Sample preparation

2.2.1 Preparations of samples for chapter 3

(1) Preparation of BPh monomer

BPh monomer was synthesized via the reaction of 4-nitrothalonitrile and 4,4'-biphenol. The typical procedure of the synthesis of BPh was as follows: In a 100 mL three neck round bottle flask equipped with a mechanical stirrer and refluxing condenser, 4-nitrothalonitrile (17.3 g, 0.1 mol), 4,4'-biphenol (9.3 g, 0.05mol) and DMF (50 mL) were taken. Then, the powdered anhydrous K_2CO_3 (15 g, 0.108 mol) were added into the solution. After refluxing at 80 °C for 6 hours, the reaction mixture was poured into a cold 10% aqueous HCl solution to precipitate the monomer. The synthetic scheme is illustrated in Fig. 2.1. Then the monomer was filtered and washed several times with distilled water until pH value reached 7. Then the light orange monomer was dried at 80 °C over night.

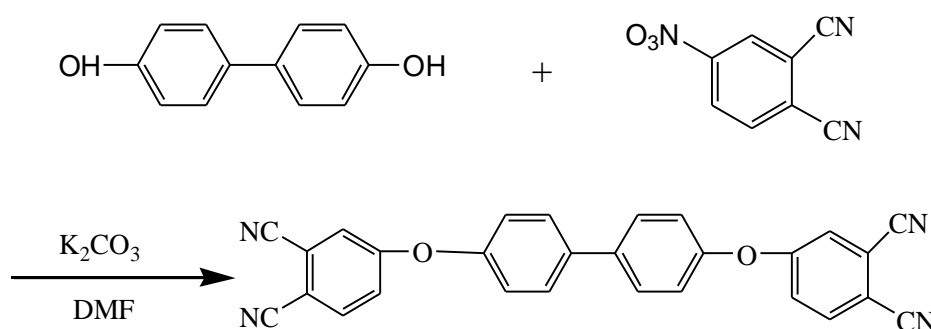


Fig. 2.1 Synthesis of BPh monomer

(2) Preparation of exfoliated graphite nanoplatelets (xGnP)

xGnP was prepared following a method reported in the literature [1-3]. A 4:1 mixture of concentrated sulfuric acid and nitric acid was added slowly, under appropriate cooling and stirring, to graphite flakes. After 24 h of reaction, the mixture was filtered, washed with distilled water, and then dried in an oven at 90 °C. The treated graphite flakes were then put

in an oven at 900 °C for rapid expansion and exfoliation. The expansion ratio was as high as 300.

(3) Preparation of xGnP/BPh nanocomposites

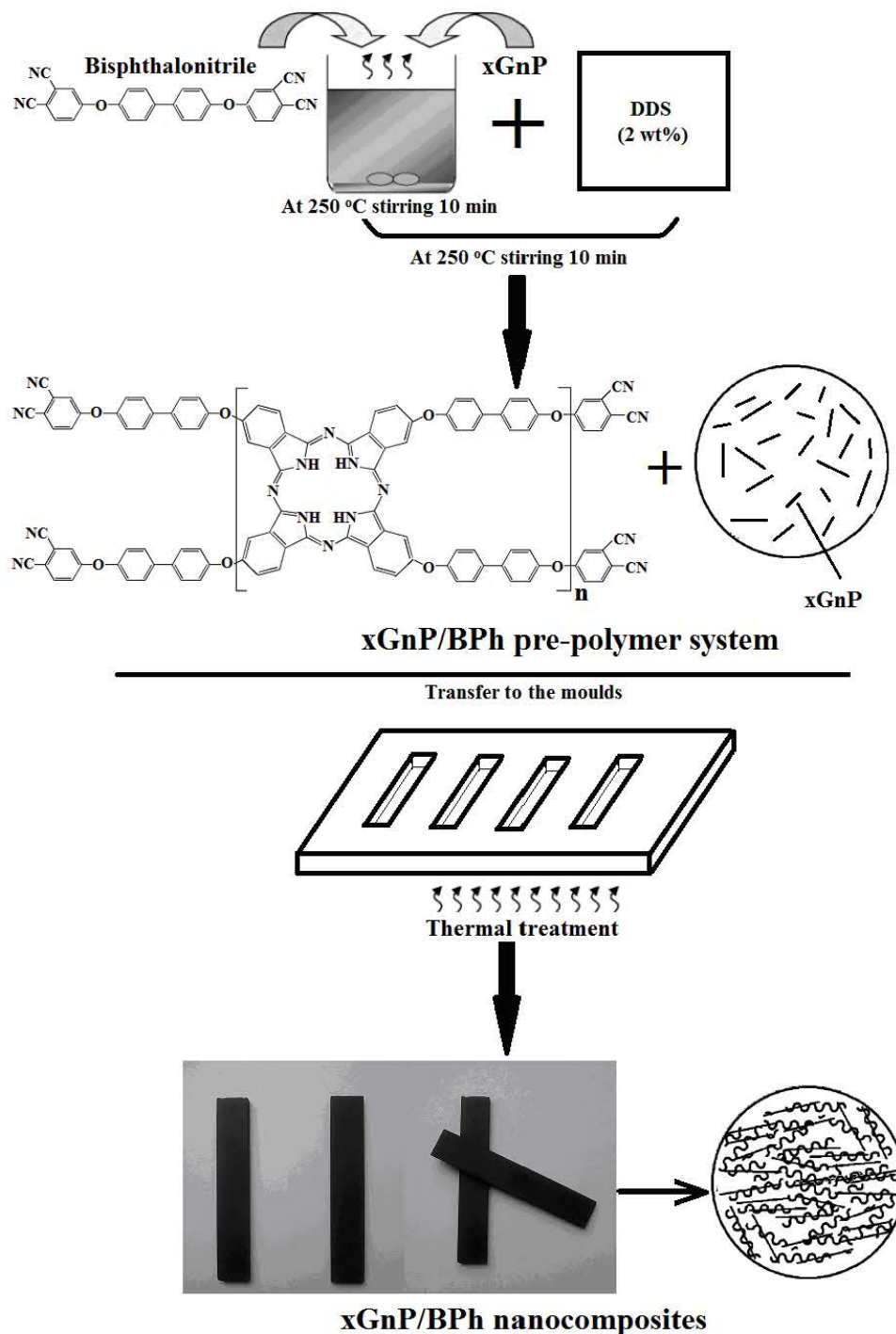


Fig. 2.2 Preparation process of xGnP/BPh nanocomposites.

xGnP/BPh nanocomposites were prepared by a resin transfer process, as shown in Fig. 2.2. 50 g BPh monomer was melted in a beaker of 200 ml at 250 °C (its melting point is 235 °C).

xGnP were then added. After 10 min of stirring at 25 rpm, 2 wt% of DDS (curing agent) was added. The whole mixture was stirring at 25 rpm for another 10 min, yielding a green pre-polymer mixture containing xGnP. Then the xGnP/BPh pre-polymer system was transferred in moulds and cured in the oven following a temperature profile: 250 °C for 4 h; 280 °C for 4 h; 320 °C for 4 h; 350 °C for 4 h; and 375 °C for 6 h. Finally, xGnP/BPh nanocomposites with different weight ratios (xGnP wt%=0, 2, 5, 10, and 15%) were obtained.

2.2.2 Preparations of samples for chapter 4

(1) Preparation of phenolphthalein-based PEN copolymers

Phenolphthalein-based PEN copolymers were prepared following a method reported in the literature [6], and the structure of the synthesized polymer is shown in Fig. 2.3.

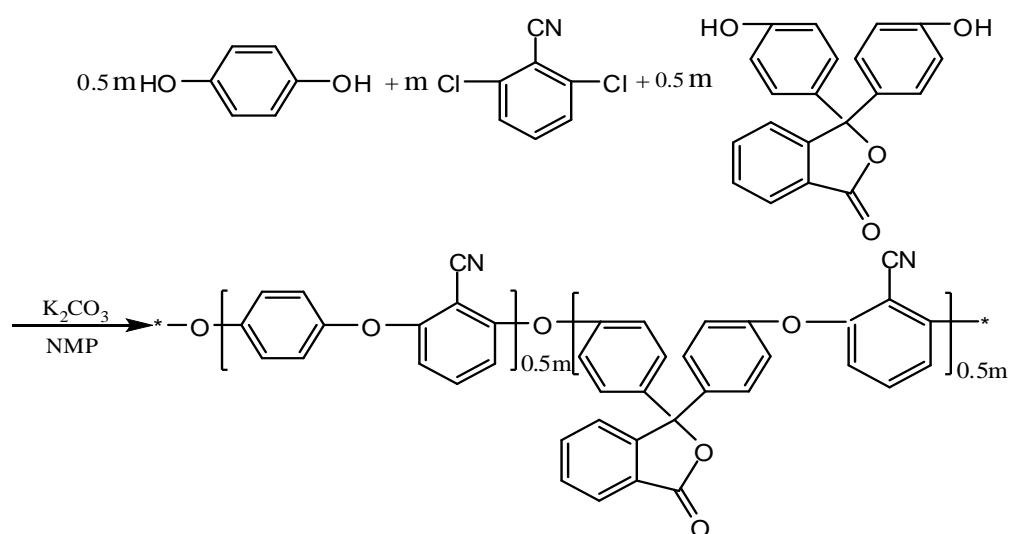


Fig. 2.3 Synthesis of phenolphthalein-based PEN copolymers

The intrinsic viscosity of the synthesized phenolphthalein-based PEN copolymers under room temperature in NMP was 1.14 dL/g.

(2) Preparation of PEN-BPh IPN system

BPh monomer was first melted in a beaker with a volume of 200 mL at 250 °C (the melting point of BPh was 235 °C), and PEN powder was added to the BPh melt. After 10

min of stirring 2 wt% of DDS (curing agent) was added. The resulting melting liquid was transferred into the moulds and cured in the oven by the sequential mode of temperature program as follows: 250 °C, 4 h; 280 °C, 4 h; 300 °C, 4 h; 350 °C, 6h; 375 °C, 2h. Finally, PEN-BPh IPN system with different weight ratios (PEN wt%=0%, 5%, 10%, 15%,) were obtained.

(3) Preparation of xGnP reinforced PEN-BPh IPN system

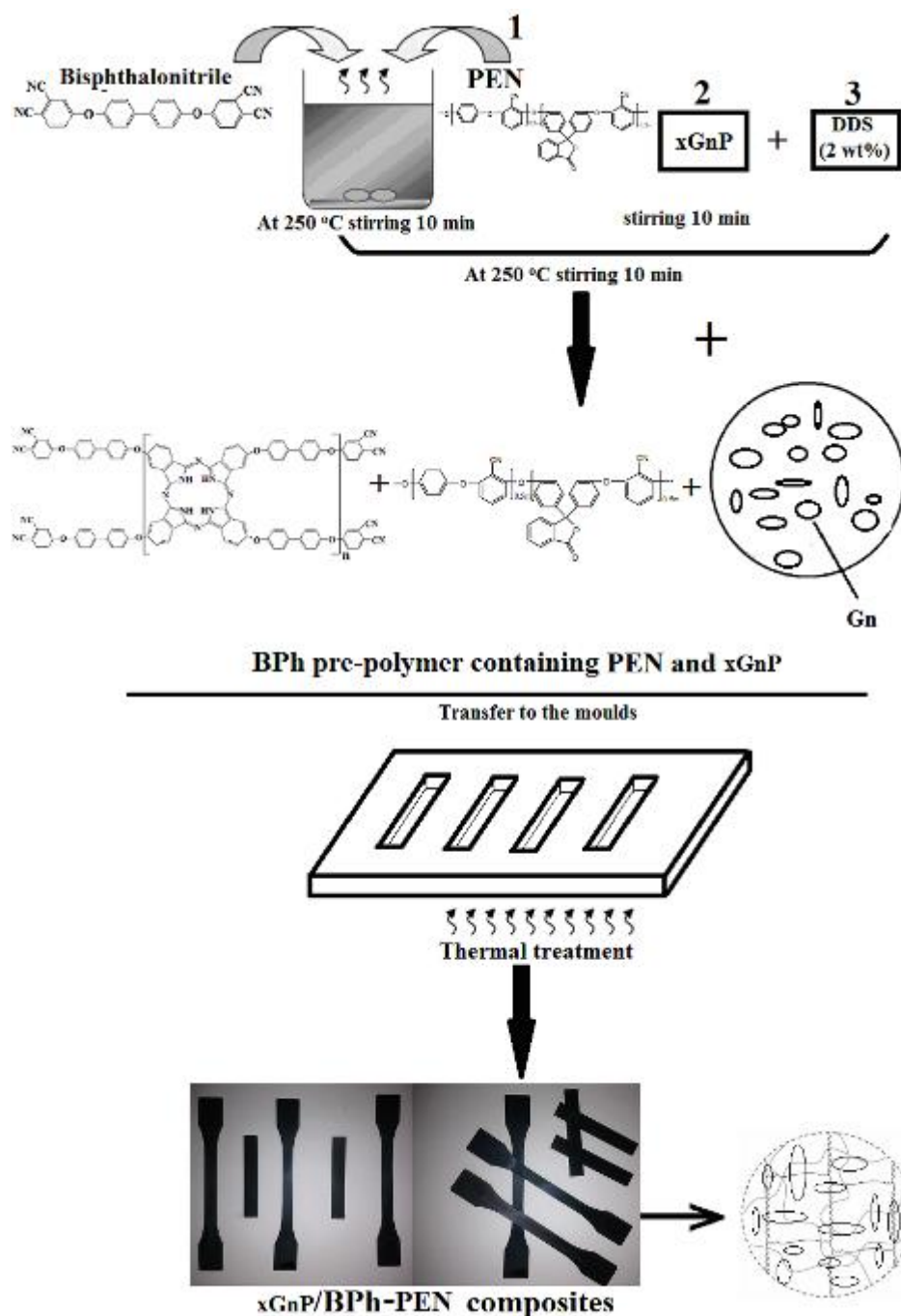


Fig. 2.5 Preparation process of xGnP/BPh nanocomposites

The preparation method of xGnP/PEN-BPh composites was shown in Fig. 2.5. It was

similar to the “Preparation of xGnP/BPh nanocomposites”. The BPh monomer was first melted at 250 °C. PEN (10 wt%) was then added to the BPh monomer melt. After 10 min of stirring 10 wt% of xGnP was added. At last 2 wt% of DDS was added. The resulting melting liquid was transferred into the moulds and cured in the oven by the sequential mode of temperature program as follows: 250 °C, 4 h; 280 °C, 4 h; 300 °C, 4 h; 350 °C, 6h; 375 °C, 2h. Finally, xGnP /PEN-BPh nanocomposites with weight ratios of BPh/PEN/GN=100/10/10 were obtained.

2.2.3 Preparations of samples for chapter 5

Typically, 10 g BPh monomer and 12 ml NMP were stirred and refluxed together at 180 °C for 10 min. The mixture was then cooled to room temperature and 0.4 g (4 wt% of BPh monomer) metallic catalysts ($\text{Fe}(\text{CO})_5$ powder or nano-iron powder) was added to the mixture with vigorous stirring. After being refluxed at 200 °C for 4 h, a dark green oligomer solution was obtained. Finally, it was poured into water to precipitate the oligomer and the excess iron was removed by Millipore filter. The preparation process is shown in Fig. 2.6. The oligomers obtained with two different catalysts, $\text{Fe}(\text{CO})_5$ and nano-iron powder, were labeled as samples (a) and (b), respectively. They were cured in the oven by the following procedure: 250 °C, 4 h; 280 °C, 4 h; 300 °C, 50 h. As a result, two types of cured Pc polymers were obtained. Solid-state pyrolysis of the two Pc polymers for CNT preparation was carried out by heating under N_2 atmosphere at 5 °C min^{-1} to 300 °C (isotherm for 1 h); 5 °C min^{-1} to 350 °C (isotherm for 1 h); 5 °C min^{-1} to 400 °C (isotherm for 1 h); 3 °C min^{-1} to 500 °C (isotherm for 4 h); 2 °C min^{-1} to 800 °C (isotherm for 8 h).

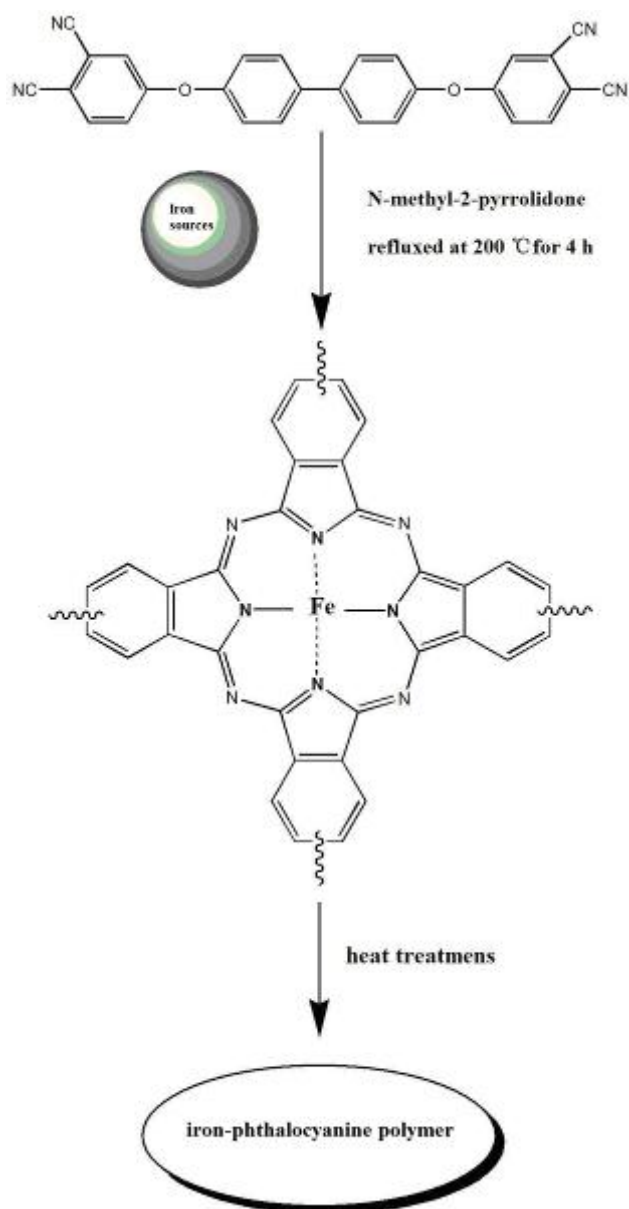


Fig. 2.6 Preparation of iron phthalocyanine polymer.

2.2.4 Preparations of samples for chapter 6

(1) Preparation of the iron phthalocyanine absorbent

90 g BPh monomer and 40 mL N-methyl-2- pyrrolidone were added to a 100 mL three neck round bottle flask equipped with a mechanical stirrer and a refluxing condenser. The mixture was heated at 160 °C for several minutes in order to be well dissolved, The solution was then cooled below 100 °C. 3.6 g (4 wt% of BPh monomer) ferrocenecarboxaldehyde, as a kind of catalyst to crosslink the phthalonitrile molecule, was added to the bottle with vigorous stirring. The mixture was refluxed at 200 °C for 2 h.

Finally, a dark green iron phthalonitrile oligomer solution was obtained. It was then poured to water to precipitate the iron phthalonitrile oligomer with vigorous mechanical stirring and dried in air at 80 °C for hours. The oligomer was heated in air at 250 °C isotherm for 4 h, 280 °C isotherm for 4 hours, and post-cured at 300 °C for 4 h. The completely cured iron phthalocyanine polymer was equally divided into three parts and heated under N₂ atmosphere to various elevated temperatures at a heating rate of 1 °C min⁻¹ to 500 °C (isotherm for 4 h); to 700 °C (isotherm for 4 h); to 900 °C (isotherm for 4 h). The final products were labeled as S500, S700 and S900, respectively.

The FePc with the amount of 2 wt%, 3 wt% and 6 wt% ferrocenecarboxaldehyde pyrolyzed under 700 °C were also prepared by the same method as described above. The final materials were named as S2, S3 and S6, respectively.

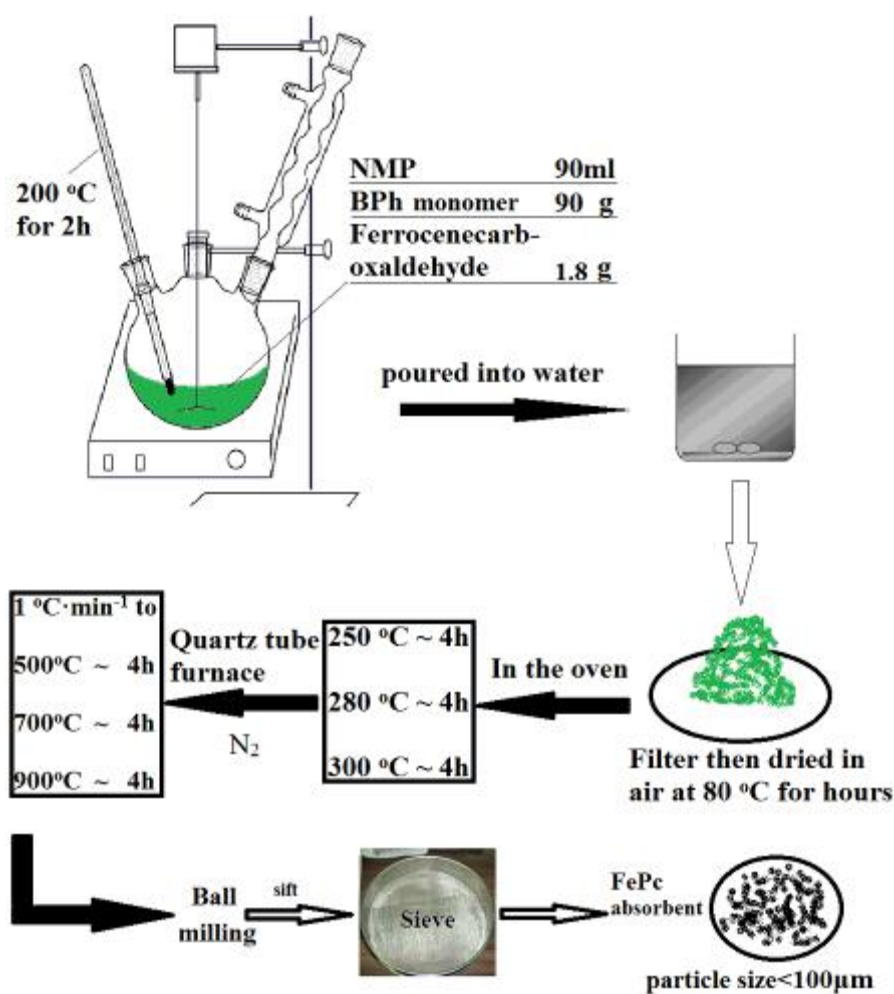


Fig. 2.6 Preparation of iron phthalocyanine absorbent.

(2) Preparation of the FePc/BPh composite

The FePc/BPh composites were prepared through the same melt mixing process as shown in Fig. 2.2. The 4, 4'-bis (3, 4-dicyanophenoxy) biphenyl (BPh) monomer was first melted in a beaker at 250 °C (the melting point of BPh monomer was 235 °C). Ball milled FePc powder (S700, the particle size is smaller than 100 µm) was then added to the melt and after 10 min of stirring 2 wt% of DDS (curing agent) was added, yielding a green pre-polymer mixture containing FePc. Then the resulting melting liquid was transferred into the moulds and cured in the oven by the following sequential mode of temperature program: 250 °C, 4 h; 280 °C, 4 h; 320 °C, 4 h; 350 °C, 4 h; 375 °C 6 h. Finally, the composites with different weight ratios (FePc wt%=0%, 5%, 10%, 15%,) were obtained.

2.3 characterization

2.3.1 Differential Scanning Calorimetry (DSC) analysis

The DSC analysis was performed on a TA-Q100 differential scanning calorimeter (TA, America) in a nitrogen atmosphere. The calibration of the temperature and heat flow scales at the same heating rate was performed with indium. The curing behavior of the iron phthalocyanine prepolymerw obtained using Fe(CO)₅ powder and nano-iron powder as the catalyst was characterized by DSC-Q100 in a nitrogen atmosphere with a flow rate of 50 ml/min and heating rate of 10 °C/min and nitrogen.

2.3.2 Thermogravimetry analysis (TGA)

The thermal decompositions of all the cured BPh and composites were determined by a TA Instruments TGA-Q50 thermogravimetric analyzer with a heating rate of 20 °C/min from room temperature to 800 °C under nitrogen atmosphere.

2.3.3 Rheological measurements

Dynamical rheological measurements were carried out on a rheometer (TA Instruments

Rheometer AR-G2) equipped with a parallel-plate geometry (25 mm diameter). The curing process of the xGnP/BPh pre-polymer system was performed at low strain values (1%) and with a frequency of 1 Hz at 250 °C in air.

2.3.4 X-ray diffraction (XRD) analysis

The X-ray diffraction (XRD) scans were measured by Rigaku RINT2400 at room temperature. The CuK α (wave length=1.542nm) irradiation source was operated at 40 kV and 100 mA. Patterns were recorded by monitoring diffractions from 10 to 80 °, and the scanning speed was 3 %/min. The samples for WAXD tests were taken from the central part of the injection molded bars.

2.3.5 Mechanical Properties analysis

The flexural tests of the composites were performed with a SANS CMT6104 Series Desktop Electromechanical Universal Testing Machine at room temperature, with a crosshead speed of 2 mm/min. The dimensions of the specimens were: 80.0×15.0×4.0 mm³. The flexural strength test was in accordance with the Chinese national standard GB/T1040-2006. The final results were the average values of six replicate measurements.

2.3.6 Resistance measurements

The volume electrical resistivity of the final xGnP/BPh nanocomposites was determined by the two probe method at room temperature using high resistance meters of type ZC36, 10-14 A and 1017 Ω . Samples with dimensions of 1 × 1 × 0.3 cm³ were cut from the middle portion of flexural bars, and their resistivity was measured along the thickness direction (0.3 cm). The two surfaces which were connected to the electrodes were first treated with colloidal silver paint in order to remove the top surface layers which were rich in polymer, and to ensure good contact between the sample surface and the electrodes. The resistivity of the nanocomposites was calculated by equation (2-1):

$$\rho = \frac{RA}{T} \quad (2-1)$$

Where ρ is the volume resistivity ($\Omega \cdot \text{cm}$), R is the volume resistance (Ω), A is the area of the sample contacting the electrode (cm^2), and T is the thickness of the sample (cm).

2.3.7 Intrinsic viscosity measurements

The intrinsic viscosity of the phenolphthalein-based PEN copolymers was measured by Ubbelohde viscometer in a thermostat water bath of 30 °C. A NMP solution with PEN concentration of $c = 0.5 \text{ g}/100\text{ml}$ was first prepared, and the time it (t) and the solvent (t_0) flowing through the Ubbelohde viscometer were then recorded, respectively. The intrinsic viscosity of PEN calculated by equation (2-2):

$$[\eta] = [2(\eta_{\text{sp}} - \ln\eta_r)]^{1/2} / c \quad (2-2)$$

where $\eta_r = t/t_0$, $\eta_{\text{sp}} = 1 - \eta_r$.

2.3.8 Dielectric properties analysis

Microwave complex permittivity ($\epsilon_r = \epsilon' - i\epsilon''$) and permeability ($\mu_r = \mu' - i\mu''$) of CNTs, FePc and FePc/BPh composites in the frequency range of 1.0-18.0 GHz were measured by the transmission/reflection method on an Agilent Vector Network Analyzer (VNA) 8720. A toroidal sample (the inner and outer diameters were 3 and 7 mm, respectively, and the thickness was 5.7 mm) used for electromagnetic measurements were prepared by homogeneously mixing the sample with wax in a mass ratio (CNTs/wax) of 3:1. The edge effect due to the use of a finite size sample (in our case 3 mm×7 mm) was expected to be large for the long-wavelength or low-frequency regime, i. e. 2-4 GHz. For the higher-frequency regime results were more reliable.

2.3.9 Magnetic properties analysis

The magnetization versus magnetic field at room temperature was measured by a Riken Denshi BHV-525 vibrating sample magnetometer (VSM) with a resolution of $1 \times 10^{-8} \text{ emu/g}$.

2.3.10 Fourier-transform infrared spectroscopy analysis (FTIR)

The samples for FTIR analysis were PEN, BPh monomer and cured BPh with 10 wt% of PEN. The FTIR spectra were recorded from 500 to 4000 cm^{-1} by Shimadzu FTIR-8400S spectrometer.

2.3.11 Scanning electron microscopy analysis (SEM)

For morphology observation, the cured BPh and composites were fractured in liquid nitrogen after 30-minute immergence. Then the fractured surfaces were sputtered with gold and observed in a JEOL JSM-5900LV SEM instrument, using an acceleration voltage of 20 kV.

2.3.12 Transmission electron microscopy analysis (TEM)

The morphology of the CNTs and the structure of xGnP were observed with a transmission electron microscope of type Hitach H600, using an acceleration voltage of 10 kV.

2.4 References

- 3 [1] He íold A, Petitjean D, Furdin G, Klatt M. Mater Sci Forum 1994, 152/153: 281.
- 4 [2] Fukushima H. Ph.D. Thesis, Michigan State University, East Lansing, MI, USA, 2003.
- 5 [3] Kalaitzidou K. Ph.D. Thesis, Michigan State University, East Lansing, MI, USA, 2003.
- 6 [4] Zhang JH, Liu XB. Chinese Journal of Synthetic Chemistry 7, 1999, 42.

Chapter 3 Preparation Process and Properties of Exfoliated Graphite Nanoplatelets filled Bisphthalonitrile Nanocomposites

3.1 Introduction

Polymer nanocomposites have been an area of major scientific and technological interest since they have potential to exhibit multifunctional and high-performance characteristics owing to the presence of small amounts of nanofillers in polymer matrices [1-8]. Under such circumstances, the intrinsic properties of the nanofillers as well as the strong polymer-nanofiller interfacial interactions alter the properties of the polymer matrix [1, 2, 9, 10], which may have the potential of significantly improving its mechanical, thermal and electrical properties. All these properties depend on the type of nanofiller. Many nanofillers could be considered for nanocomposite fabrication and property enhancement. Among the most studied nanofillers are layered silicates such as montmorillonite and bentonite [11-15], graphite, and carbon nanotubes [16-20].

Graphite is a layered material consisting of one-atom-thick sheet of carbon. The carbon atoms are bound covalently in a hexagonal arrangement within the layer. These layers are bound to each other by weak van-der-Waals forces which results in highly anisotropic properties. Along the basal plane, graphite could exhibit high modulus, excellent electrical and thermal conductivities as well as low coefficient of thermal expansion (CTE) [21]. Expandable graphite, also called acid-intercalated graphite flake, can be expanded up to hundreds of times more than its initial volume at the high temperature, resulting in the separation of the graphene sheets at the nanoscopic level along the c-axis of the graphene layers [19, 22, 23]. Recently, a new type of nano-reinforcement, exfoliated graphite nanoplatelets (xGnP), has been under investigation [24]. These nanoparticles are a potential alternative to other nano-reinforcements such as nano-clays and carbon nanotubes since they combine the low cost and layered structure of nano-clays and the superior thermal and electrical properties of carbon nanotubes [24, 25].

Phthalonitrile polymers show potential as high-temperature polymers for use in a wide variety of applications such as composite matrices [26], adhesives [27], and electrical conductors [28-31]. To date, several phthalonitrile monomers having structural variations at molecular level have been synthesized and polymerized into thermosets [32, 33]. 4, 4' Bis-(3,4-dicyanophenoxy)biphenyl (BPh) is a typical phthalonitrile monomer that has been effectively used as a matrix resin for composite formulations. Composite panels have been processed by conventional prepreg consolidation, resin infusion and filament winding methods with different reinforcements such as carbon tape [34], carbon fabric, and glass fabric [35, 36]. Due to its relatively low initial melt viscosity (0.1–0.2 Pa.s), BPh-based phthalonitrile composites are amenable to processing by a resin transfer molding process which is more cost-effective. Moreover, the mechanical properties and thermal and oxidative stabilities of BPh-based composites are superior to those of many state-of-the-art high-temperature composites. However, much higher strength, modulus and multifunctional materials are still needed in some special fields such as aerospace and military industry.

In this section, xGnP/BPh nanocomposites are prepared through a simple and efficient process. The state of dispersion of the xGnP in the BPh polymer is characterized by scanning electron microscopy (SEM). The effects of the xGnP on the complex viscosity, storage modulus of the xGnP/BPh pre-polymer system and the mechanical, electrical and thermal properties of the final xGnP/BPh nanocomposites are studied. The as-prepared xGnP/BPh nanocomposites with multifunctional properties are expected to have potential applications in military industry, aerospace, and other fields where solvent resistance and/or exposure to high temperature is necessary.

This part of work has been published on the Journal of Physics and Chemistry of Solids, 2012, volume 73, issue 11, page 1335-1341.

3.2 Results and discussion

3.2.1 Structure of xGnP

Expanded graphite (EG) consists of graphite sheets with thickness of less than 100 nm (Fig. 3.1 (a)). After mechanical agitation, EG is torn to fully exfoliated graphite nanosheets (xGnP), as described in previous reports [37, 38]. The diameter of most xGnP ranges from 5 to 20 μm , as shown in Fig. 3.1 (b). Fig. 3.1 (c) shows the TEM images of xGnP. The thickness of xGnP is in the range of 10 to 30 nm. Thus, their aspect ratio (diameter to thickness) is as high as 200 to 500. Besides, the structure of isolated xGnP is very different from that of the EG.

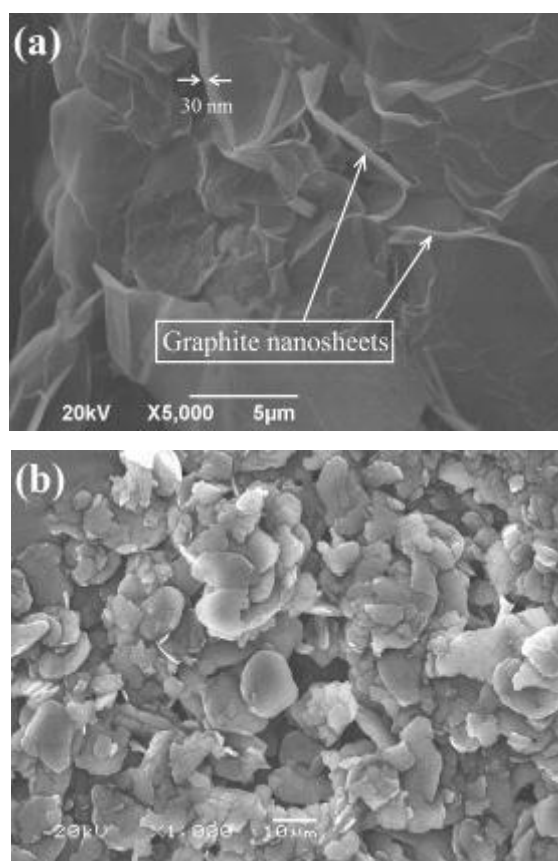




Fig. 3.1 SEM images of expanded graphite and exfoliated graphite nanoplatelets.

(a) Expanded graphite, (b) Exfoliated graphite nanoplatelets

(c) TEM images of exfoliated graphite nanoplatelets

3.2.2 Rheological behavior of the xGnP/BPh pre-polymer system.

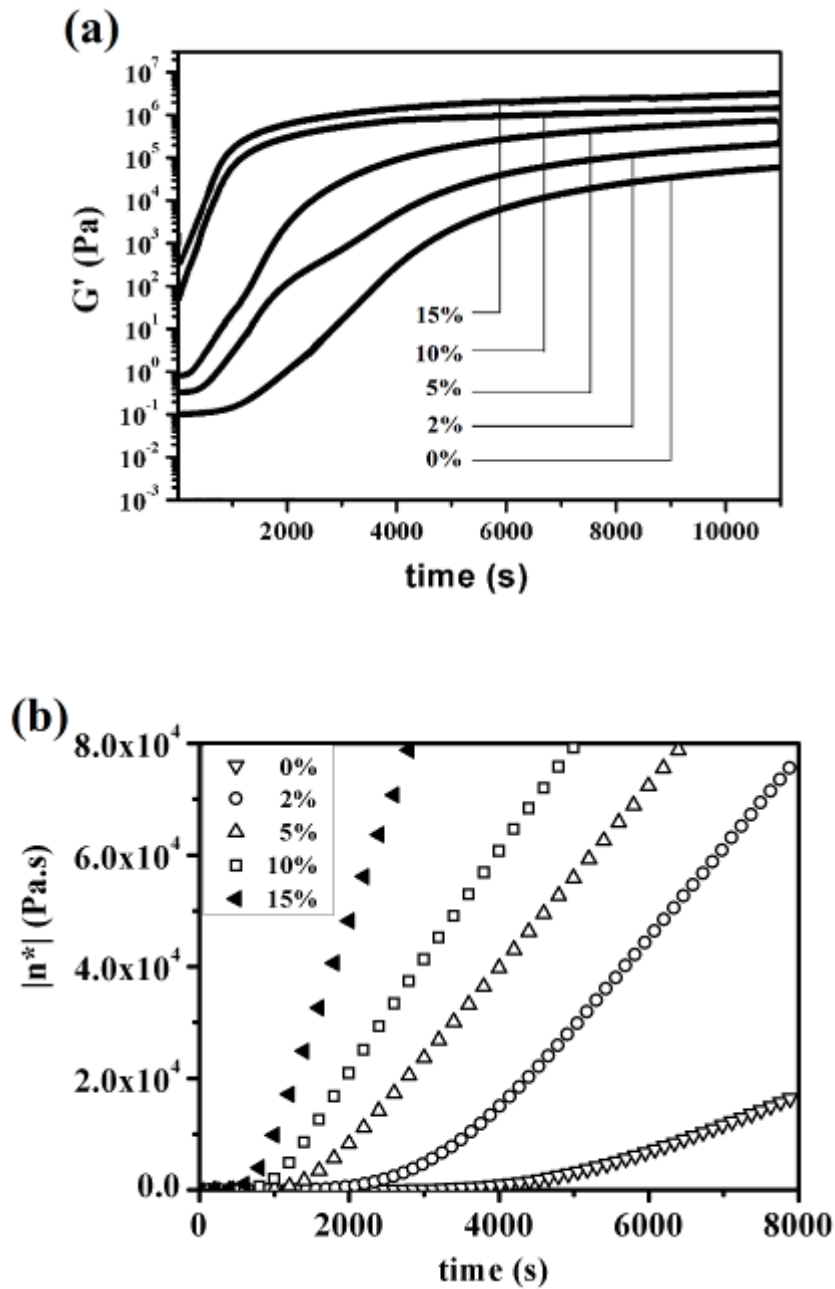


Fig. 3.2 Rheological property of the xGnP/BPh prepolymer system.

(a) Dependence of G' on time at 250 °C for the pure BPh and xGnP/BPh pre-polymer

(b) Time sweep viscosity curves of the pure BPh and xGnP/BPh pre-polymer system

The polymer rheological behavior is a key factor in determining its processability. Fig. 3.2 (a) shows the dependence of the dynamic storage modulus (G') on time at 250 °C for the pure BPh and different weight ratios of the xGnP/BPh pre-polymer system. Three regions can be observed when the weight ratio of xGnP/BPh system is below 5/95. In the first region, the

G' is very small and gradually increases with time. This period is gradually shortened as the content of xGnP increases. When the weight ratio of the xGnP/BPh system is above 5/95, the first region has disappeared. Namely, only the second region is observed. In this region, the curing reaction has occurred and G' has increased quickly because of the network formation. In the third region, G' has reached a plateau, indicating that the network formation has reached an equilibrium state. It is also observed that the rate of increase in G' increases with increasing xGnP content. When the xGnP content in the xGnP/BPh system is low, G' is dominated by the matrix resin. As the xGnP load increases, its contribution to G' becomes important even plays a dominant role. Fig. 3.2 (b) shows the dependence of the melt viscosity on time at 250 °C for the pure BPh and different weight ratios of the xGnP/BPh pre-polymer system. The rate of increase in the complex viscosity increases with increasing xGnP content. To conclude, the xGnP/BPh pre-polymer system possesses higher complex viscosity and storage modulus than the pure BPh pre-polymer, suggesting that the xGnP has great impact on the properties of xGnP/BPh pre-polymer system.

3.2.3 Thermal properties of the xGnP/BPh nanocomposites

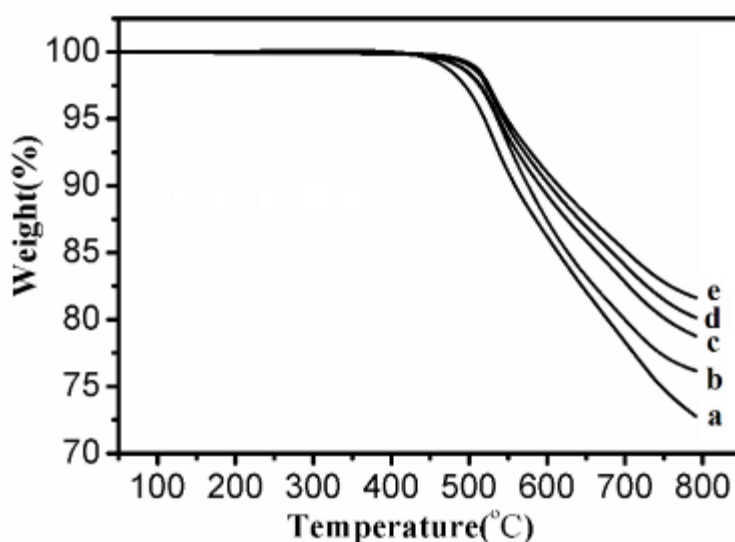


Fig. 3.3 TGA curves of the BPh polymer and xGnP/BPh nanocomposites.

- (a) Pure BPh polymer
- (b) 2 wt% xGnP/BPh nanocomposite
- (c) 5 wt% xGnP/BPh nanocomposite
- (d) 10 wt% xGnP/BPh nanocomposite
- (e) 15 wt% xGnP/BPh nanocomposite

xGnP has good thermal stability. The carbon yield of the pure xGnP at 800 °C is 98.5%, as determined by a thermogravimetric analyzer of type TA Instruments TGA-Q50 with a heating rate of 20°C/min under nitrogen. Fig. 3.3 shows the TGA thermograms of the xGnP/BPh nanocomposites with various xGnP contents. It is seen that the thermal stability of the xGnP/BPh nanocomposite increases with increasing xGnP content. Table 3.1 shows the thermal degradation temperatures of 5 and 10% weight losses ($T_{5\%}$ and $T_{10\%}$) and the carbon yields at 800 °C. The $T_{5\%}$, $T_{10\%}$ and carbon yield of the pure BPh polymer at 800°C are about 519 °C, 559 °C and 72%, respectively. However, all xGnP/BPh composites showed higher $T_{5\%}$ and $T_{10\%}$ than pure BPh. For the xGnP/BPh nanocomposite with 15 wt% of xGnP, they are increased by about 31°C, 56 °C and 10%, respectively. This drastic improvement in thermal stability results from homogeneous dispersion of the xGnP in the BPh matrix which serve as mass transfer barriers against the volatile pyrolyzed products in the BPh matrix, eventually retarding thermal degradation of the nanocomposite.

Tab. 3.1 Thermal properties of BPh and xGnP/BPh nanocomposites

xGnP content (wt%)	0	2	5	10	15
$T_{5\%}$ (°C)	519	532	538	543	548
$T_{10\%}$ (°C)	559	573	591	603	615
Carbon yield at 800 °C (%)	72	77	79	80	82

3.2.4 Mechanical properties of the xGnP/BPh nanocomposites

Fig. 3.4 shows the mechanical properties of the nanocomposites with various xGnP contents. The flexural strength and modulus of the nanocomposites increase dramatically with increasing xGnP content. For example, the addition of 2 wt% xGnP results in about 10% increase in flexural strength and 7% increase in flexural modulus with respect to those of the pure BPh. The maximum values of mechanical properties were observed in the 10 wt% xGnP-filled BPh systems, where about 27% and 69% increments of flexural strength and modulus were resulted respectively in comparison with those of pure BPh. The fracture surfaces of the nanocomposites with various xGnP contents in Fig. 3.5 confirm the enhancement of the mechanical properties. It can be seen clearly that many exfoliated

graphite nanoplatelets are dispersed uniformly in the BPh matrix. The SEM picture with high magnification (Fig. 3.5 (e)) shows that the xGnP are well coated by the BPh resin, which guarantees effective stress transfer at the xGnP/BPh interfaces. The significant improvement in mechanical properties of the BPh matrix by xGnP is due to the excellent mechanical properties of xGnP as well as their good dispersion and large aspect ratio. It is also worthwhile to note that the modulus and strength of the 15 wt % xGnP/BPh nanocomposite are similar to those of the 10 wt % one, due likely to accrued aggregation of xGnP (Fig. 3.5 (f)).

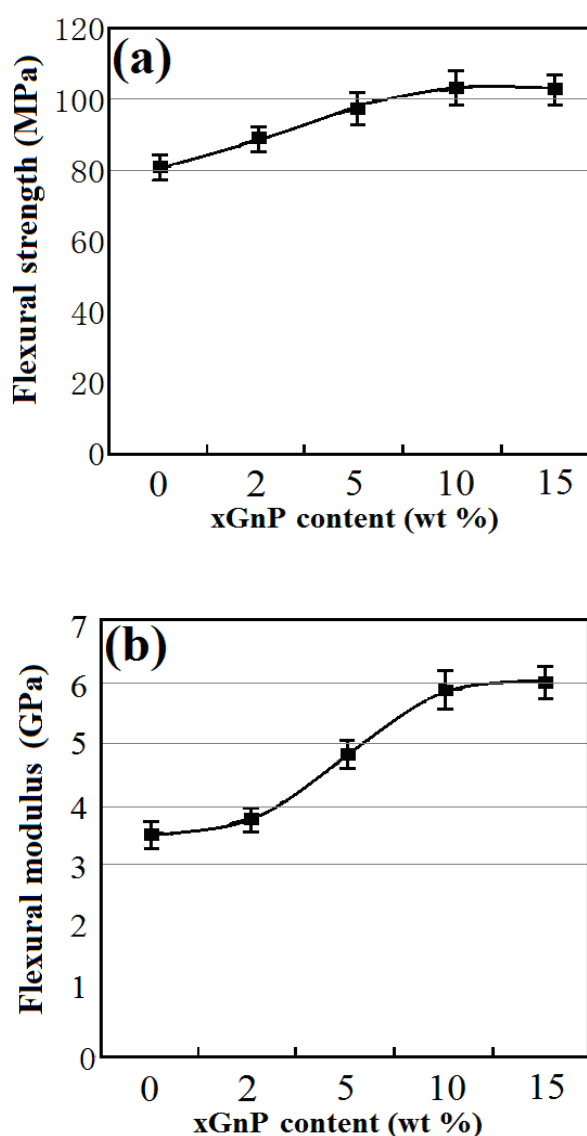


Fig. 3.4 Mechanical properties of the xGnP/BPh nanocomposites.

(a) Flexural strength of xGnP/BPh naocomposites

(b) Flexural modulus of xGnP/BPh nanocomposites

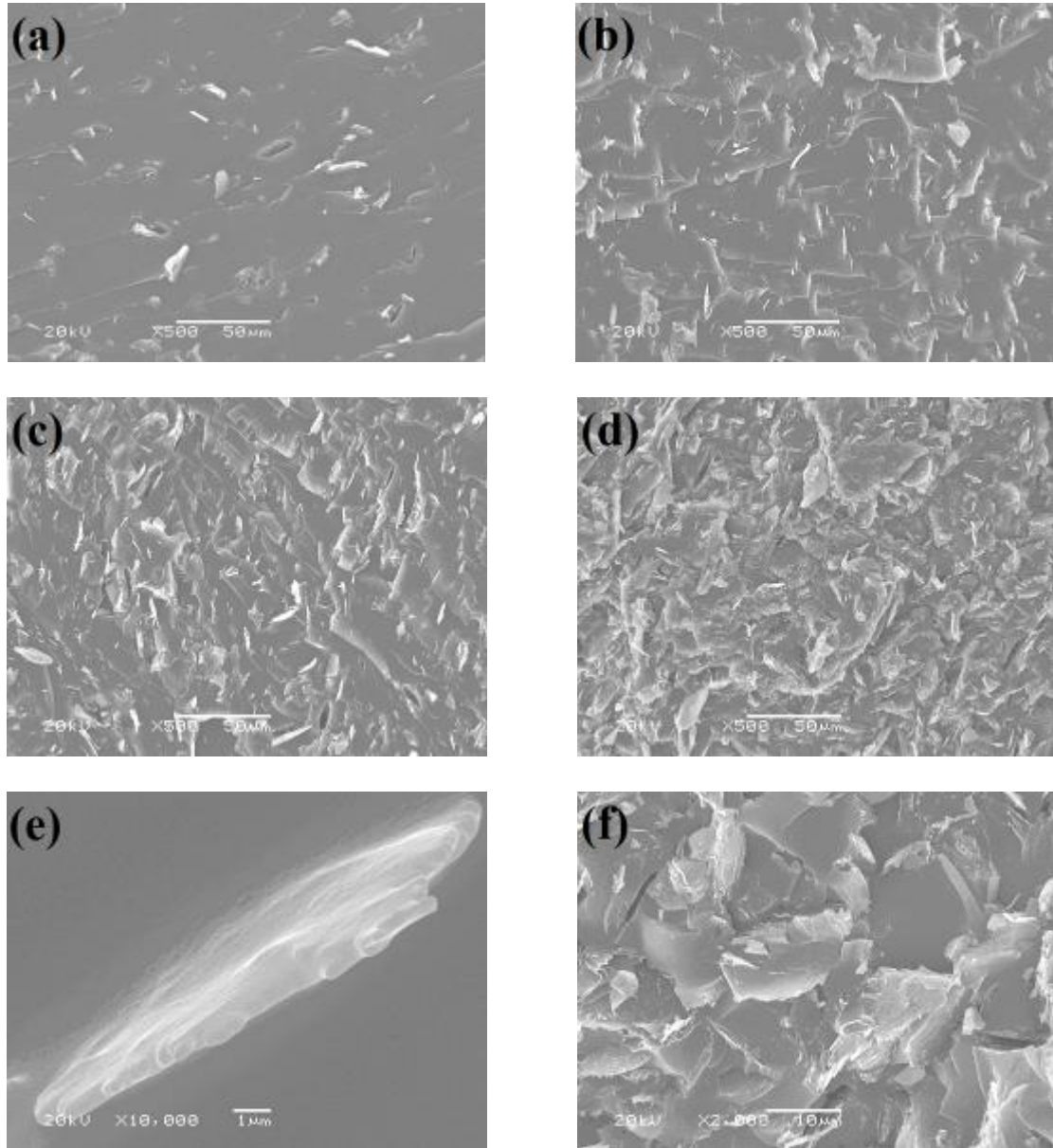


Fig. 3.5 SEM images of the fracture surfaces of xGnP/BPh nanocomposite.

- (a) 2 wt% of xGnP (b) 5 wt% of xGnP
- (c) 10 wt% of xGnP (d) 15 wt% of xGnP
- (e) 5 wt% of xGnP in high magnification
- (f) 15 wt% of xGnP in high magnification

Polymer nanocomposites based on nanofillers, such as xGnP, have been widely reported. Fig. 3.6 gathers the results of mechanical properties reported in references [25] and [37]. Those of the xGnP/BPh nanocomposites are better than those of other xGnP reinforced materials. Owing to its good processability and excellent thermal stability, xGnP/BPh nanocomposites are expected to have potential applications in military industry,

aerospace, and other places where solvent resistance and/or exposure to high temperature is necessary.

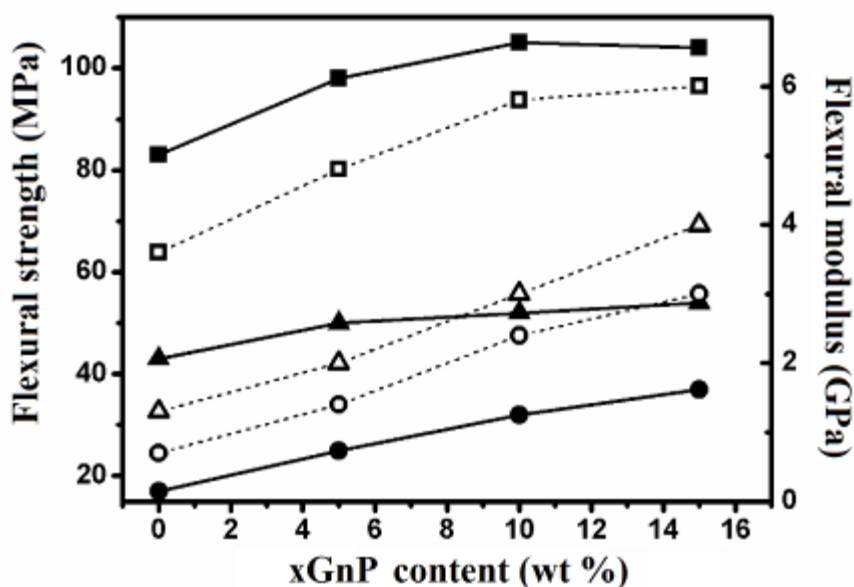


Fig. 3.6 Comparison of the flexural strength (closed symbols) and modulus (open symbols) between the xGnP/BPh (square; this work) and xGnP-15/PP (triangle; ref. [25]) and xGnP-15/HDPE (circle; ref. [37]).

3.2.5 Resistivity of the xGnP/BPh nanocomposites

In contrast to many other types of nanofillers, carbon-based nanofillers such as xGnP have the potential to yield electrically conductive nanocomposites. Electrical conductivity correlates with the “connectivity” of the carbon-based filler particles, which is necessary to provide a pathway for electrical conduction across the samples. At low nanofiller content, a potential prerequisite for achieving electrical conduction is exfoliation and dispersion of the xGnP, with an additional prerequisite being that the dispersion allows for the presence of a network-like structure of the nanofiller across the sample.

The thermoset of BPh resin is an excellent insulating material, with electrical resistivity of about $10^{13} \Omega \cdot \text{cm}$, whereas xGnP have electrical characteristics similar to those of metallic/semimetallic materials. Fig. 3.7 shows the resistivity of the xGnP/BPh nanocomposite as a function of the xGnP content. The incorporation of the xGnP greatly decreases the resistivity of the BPh, with a sharp transition from an electrical insulator to an electrical conductor. The percolation threshold of the xGnP/BPh nanocomposite is between

5% and 10 wt% of xGnP. The percolation threshold for the resistivity depends very much on the geometry of conducting fillers. Fillers with elongated geometry such as sheets can be used to achieve a very low percolation threshold value, due to the fact that sheets with higher aspect ratios have great advantage over spherical or elliptical fillers in forming conducting networks in polymer matrix. This advantage in forming conducting network can be explained by the excluded volume theory [9, 39]. The excluded volume of an object is defined as a volume around it which the center of another similar object is not allowed to penetrate. The overlapping of the two objects is to be avoided. The higher the aspect ratio of the filler particle, the larger its excluded volume and consequently the lower the percolation threshold [40]. The xGnP used in this work possess an average aspect ratio of as high as up to 500. This high aspect ratio might be responsible for the high percolation threshold. The resistivity decreases slowly when the xGnP content is above 10 wt %. This is because once the conductive network is formed a further increase in the xGnP loading does not have much influence on the resistivity of the nano-composite.

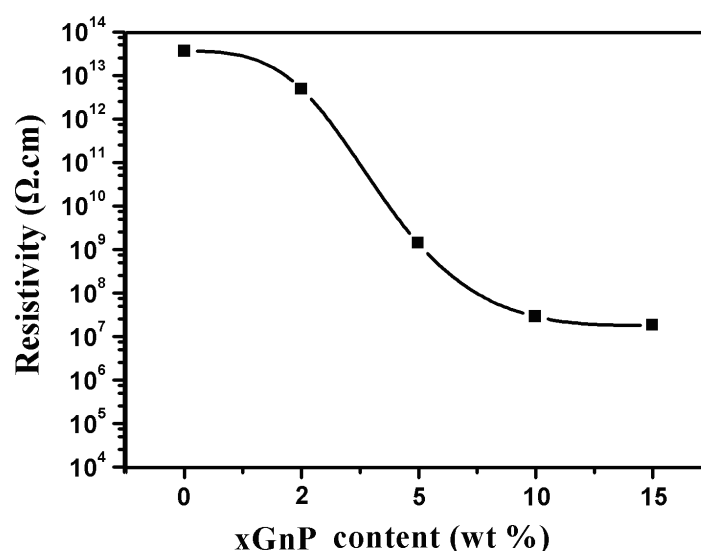


Fig. 3.7 Effect of the xGnP content on the resistivity of the xGnP/BPh nanocomposite.

3.3 Conclusions

xGnP/BPh nanocomposites were successfully prepared via a cost-effective, resin transfer molding method and were characterized for mechanical, electrical, thermal, and

morphological properties.

- (1) The xGnP/BPh pre-polymer possesses higher complex viscosity and storage modulus than the pure BPh, which is closely related to the incorporation of xGnP.
- (2) The flexural strength and flexural modulus of the xGnP/BPh nanocomposites with 10 wt% xGnP exhibit maximum values.
- (3) The incorporation of xGnP greatly decreases their resistivity with a sharp transition from an electrical insulator to an electrical conductor. The percolation threshold of xGnP/BPh nanocomposite is between 5 and 10 wt %.
- (4) The thermal stability of the xGnP/BPh nanocomposites is also much better than that of the pure BPh resin.
- (5) The outstanding properties of xGnP/BPh nanocomposites make them candidates for potential applications in military industry, aerospace, and other extreme situations where solvent resistance and/or exposure to high temperature is necessary.

3.4 References

- [1] Dang, ZM., Yuan, JK., Zha, JW., Zhou, T., Li, ST., Hu, GH. Fundamentals, processes and applications of high-permittivity polymer matrix composites, *Prog. Mater Sci.* 2012; 57: 660-723.
- [2] Yu ZZ., Hu GH., Varlet J., Dasari A., Mai YW. Water-assisted melt compounding of nylon-6/pristine montmorillonite nanocomposites, *J. Polym.Sci., Part B: Polym. Phys.* 2005; 43: 1100-1112.
- [3] Gunes IS, Cao F, Jana SC. Evaluation of nanoparticulate fillers for development of shape memory polyurethane nanocomposites. *Polymer.* 2008; 49: 2223-2234.
- [4] Chinellato AC., Vidotti SE., Hu GH., Pessan LA. Compatibilizing effect of acrylic acid modified polypropylene on the morphology and permeability properties of polypropylene/organoclay nanocomposites, *Compos. Sci. Technol.* 2010; 70: 458-465.
- [5] Mohammed H, Al-Saleh, Sundararaj U. Processing-microstructure-property relationship in conductive polymer nanocomposites. *Polymer.* 2010; 51: 2740-2747.
- [6] Vidotti SE., Chinellato AC., Hu GH., Pessan LA. Preparation of poly(ethylene terephthalate)/organoclay nanocomposites using a polyester ionomer as a compatibilizer, *J. Polym. Sci., Part B: Polym.Phys.* 2007; 45: 3084-3091.
- [7] Chinellato AC., Vidotti SE., Hu GH., Pessan LA. An acrylic acid modified polypropylene as a compatibilizing agent for the intercalation/exfoliation of an organically modified montmorillonite in polypropylene, *J. Polym.Sci., Part B: Polym. Phys.* 2008; 46: 1811-1819

- [8] Pavlidou S, Papaspyrides CD. A review on polymer-layered silicate nanocomposites. *Prog. Polym. Sci.* 2008; 33: 1119-1198.
- [9] Penu C., Hu GH., Fernandez A., Marchal P., Choplin L. Rheological and electrical percolation thresholds of carbon nanotube/polymer nanocomposites. *Polym. Eng. Sci.* 2012, in press. DOI 10.1002/pen.23162
- [10] Kim JY., Han SII, Hong SP. Effect of modified carbon nanotube on the properties of aromatic polyester nanocomposites. *Polym.* 2008; 49: 3335-3345.
- [11] Vaia RA, Giannelis EP. Polymer Nanocomposites: Status and Opportunities. *MRS Bulltin.* 2011; 26: 394-401.
- [12] Cho JW, Paul DR. Nylon 6 nanocomposites by melt compounding. *Polymer.* 2001; 42: 1083-1094.
- [13] Manias E, Touny A, Wu L, Strawhecker K, Lu B, Chung TC. Polypropylene/Montmorillonite Nanocomposites. Review of the Synthetic Routes and Materials Properties. *Chem. Mater.* 2001; 13: 3516-3523.
- [14] Hu GH., Hoppe S., Feng LF., Fonteix C. Nano-scale phenomena and applications in polymer processing. *Chem. Eng. Sci.* 2007; 62: 3528-3537
- [15] Sheng N, Boyce MC, Parks DM, Rutledge GC, Abes JI, Cohen RE. Multiscale micromechanical modeling of polymer/clay nanocomposites and the effective clay particle. *Polymer.* 2004; 45: 487-506.
- [16] Haggenueller R, Gommans HH., Rinzler AG, Fischer JE, Winey KI. Aligned single-wall carbon nanotubes in composites by melt processing methods. *Chem. Phys. Lett.* 2000; 330: 219-225.
- [17] Jiang, FD., Wu, SZ., Wei, YL., Zhang, LQ., Hu, GH. The Study on the Microstructures and High Performances of Melt Blending Polyurethane/Multi-walled Carbon Nanotubes Composites, *Polym. Polym. Compos.* 2008; 16: 509-518
- [18] Ramanathan T, Liu H, Brinson LC. Functionalized SWNT/polymer nanocomposites for dramatic property improvement. *J. Polym. Sci. Part B: Polym. Phys.* 2005; 43: 2269-2279.
- [19] Pan YX., Yu ZZ., Ou YC., Hu GH. A new process of fabricating electrically conducting nylon 6/graphite nanocomposites via intercalation polymerization, *J. Polym. Sci., Part B: Polym. Phys.* 2000, 38: 1626-1633.
- [20] Chen LM., Ozisik R, Schadler LS. The influence of carbon nanotube aspect ratio on the foam morphology of MWNT/PMMA nanocomposite foams. *Polymer.* 2010; 51: 2368-2375.
- [21] Thostenson ET, Li C, Chou TW. Nanocomposites in context. *Compos Sci Technol.* 2005; 65: 491-516.
- [22] Zheng W, Wong SC, Sue HJ. Transport behavior of PMMA/expanded graphite nanocomposites *Polymer.* 2002; 43: 6767-6773.
- [23] Chen GH, Wu DJ, Weng WG, He B, Yan WL. Preparation of polystyrene-graphite conducting nanocomposites via intercalation polymerization. *Polym. Int.* 2001; 50: 980-985.
- [24] Kalaitzidou K, Fukushima H, Drzal LT. Multifunctional polypropylene composites produced by

- incorporation of exfoliated graphite nanoplatelets. *Carbon*. 2007; 45: 1446-1452.
- [25] Kalaitzidou K, Fukushima H, Drzal LT. Mechanical properties and morphological characterization of exfoliated graphite–polypropylene nanocomposites. *Compos. A*. 2007; 38: 1675-1682.
- [26] Keller TM. Synthesis and Polymerization of Multiple Aromatic Ether Phthalonitriles. *Chem. Mater*. 1994; 6: 302-305.
- [27] Keller TM, Roland CM, US Patent. 5242755, (1993).
- [28] Keller TM. High-performance, electrically conductive polymers. *Chemtech*. 1988; 18: 635-639.
- [29] Keller TM. Imide-containing phthalonitrile resin. *Polymer*. 1993; 34, 952–955.
- [30] Warzel ML, Keller TM. Tensile and fracture properties of a phthalonitrile polymer. *Polymer*. 1993; 34: 663–666.
- [31] Guilani JF, Keller TM. Stable Polymer Conductor. *Sens. Mater*. 1989; 1: 2244-2247.
- [32] Narth KA., Keller TM. Phase transition in high molecular weight polyethylene during capillary extrusion: the reversibility of the temperature window. *Polymer* 1991; 32: 2512-2518.
- [33] Armistead JP , Keller TM, Sastri SB. Structure and property changes during pyrolysis of an acetylene-terminated resin. *Carbon*. 1994; 32: 345-348.
- [34] Sastri SB, Armistead JP, Keller TM. Phthalonitrile-carbon fiber composites. *Polym. Compos*. 1996; 17: 816-822.
- [35] Sastri SB, Armistead JP, Keller TM, Sorathia U. Phthalonitrile-glass fabric composites. *Polym. Compos*. 1997; 18: 48-54.
- [36] Sastri SB, Armistead JP, Keller TM, Sorathia U. Flammability characteristics of phthalonitrile composites. *SAMPE Symp. Ser*. 1996; 42: 1032-1038.
- [37] Jiang X, Drzal LT. Multifunctional high density polyethylene nanocomposites produced by incorporation of exfoliated graphite nanoplatelets 1: Morphology and mechanical properties. *Polym. Compos*. 2010; 31: 1091-1098.
- [38] Wu X, Qi S, He J, G Duan. High conductivity and low percolation threshold in polyaniline/graphite nanosheets composites. *J. Mater. Sci*. 2010; 45: 483-489.
- [39] Balberg I, Binenbaum N, Wagner N. Percolation Thresholds in the Three-Dimensional Sticks System. *Phys. Rev. Lett*. 1984; 52: 1465-1468.
- [40] Chen G, Weng W, Wu D, Wu C. PMMA/graphite nanosheets composite and its conducting properties. *Eur. Polym. J*. 2003; 39: 2329-2335.

Chapter 4 Mechanical and thermal properties of graphite nanoplatelets reinforced polyarylene ether nitriles / bisphthalonitrile IPN system

4.1. Introduction

Over the years, phthalonitrile polymers have attracted tremendous attention due to their outstanding properties. The mechanical properties, thermal and oxidative stability of BPh-based composites are superior to that of many state-of-the-art high-temperature composites [1-4]. But much higher strength, modulus and multifunctional materials are still needed in some special fields such as aerospace and military industry. In Chapter 3, the effects of xGnP on the complex viscosity, storage modulus of xGnP/BPh prepolymer and the mechanical, electrical and thermal properties of the final composites were studied. The results showed that flexural strength and flexural modulus of the xGnP/BPh composites with 10 wt% xGnP content exhibited maximum values and thermal stability was greatly improved.

However, the performances of this BPh-based system are still limited by the intrinsic brittleness of the network structure that adversely affects its mechanical properties. To overcome this limitation, the thermoset-thermoplastic interpenetrating polymer networks (IPN) tend to be effective. The IPN, with an intimate combination of two kinds of polymers in network formation [5-7], can exhibit synergistic properties of both component polymers compared with those of each of the single components. As a kind of engineering thermoplastic, polyarylene ether nitrile (PEN) has attracted much interest from both industry and academia due to its excellent property similar to polyether ether ketone (PEEK). Owing to its rigid molecular structure, PEN exhibits high mechanical strength, high toughness, good radiation resistance, and high thermo-oxidative stability [8-10], which make it very attractive for the composites used at toughening mechanism, aggressive chemical environments and so on. Herein, we chose PEN as the guest polymer in BPh

system. However, the introduction of thermoplastic resin always increases the tenacity but decreases the modulus and thermal stability of the thermoset resin. Therefore, it is necessary to introduce a third component to offset losses of the flexural modulus and thermal stability lowered by PEN. xGnP exhibits unique structural features and physical properties. It is known that xGnP has high mechanical strength (Young's modulus of 1060 GPa) and excellent thermal stability. It is a potential alternative to other nano-reinforcements such as nano-clays and carbon nanotubes since it combines the low cost and layered structure of nano-clays and the superior thermal and electrical properties of carbon nanotubes [11, 12].

In this work, PEN-BPh IPN system was prepared and investigated for the effects of the PEN content on the mechanical and thermal properties of the system. The results showed that the toughness and strength of BPh resin could be enhanced with the incorporation of PEN, but the modulus and thermal stability of the IPN composites were decreased. Then the xGnP reinforced PEN-BPh IPN system was prepared and the results demonstrated that xGnP could improve the flexural strength of BPh and also offset losses of the flexural modulus and thermal stability lowered by PEN. The high performance xGnP reinforced PEN-BPh IPN composite is believed to have potential applications in military industry, aerospace, and other places where solvent resistance and/or exposure to high temperature is necessary.

This part of work has been published on the Journal of Applied Polymer Science, 2012, volume 127, issue 5, page 3595-3600.

4.2. Results and discussion

4.2.1 FTIR spectra of the PEN-BPh IPN system

The FTIR spectra were performed to monitor the formation of the PEN-BPh IPN system. In Fig. 4.1 (a) and (b), the absorption at 2231 cm^{-1} is the characteristic symmetrical stretching of $-\text{CN}$ group. Fig. 4 (c) shows the FTIR spectra of PEN-BPh blend after curing. Clearly, the peak at 2230 cm^{-1} shuttles down and new peaks at 1360 cm^{-1} , 1520 cm^{-1} and 1010 cm^{-1} can be observed, indicating the formation of phthalocyanine ring and triazine

ring [14], respectively (the structure of phthalocyanine ring and triazine ring were shown in Fig. 1.3). The results showed that the polymerization of BPh monomer had happened and the crosslink density of PEN was also increased. Both PEN and BPh have $-CN$ groups and the reaction behavior of them are similar, so the $-CN$ groups in PEN chain segment may participate in the cyclization reaction of BPh. Meanwhile, the increase in absorbance from 3450 to 3500 cm^{-1} indicated the presence of hydroxyl groups with the incorporation of PEN. It may be one factor that affects the flexural modulus and thermal stability of resulted composites.

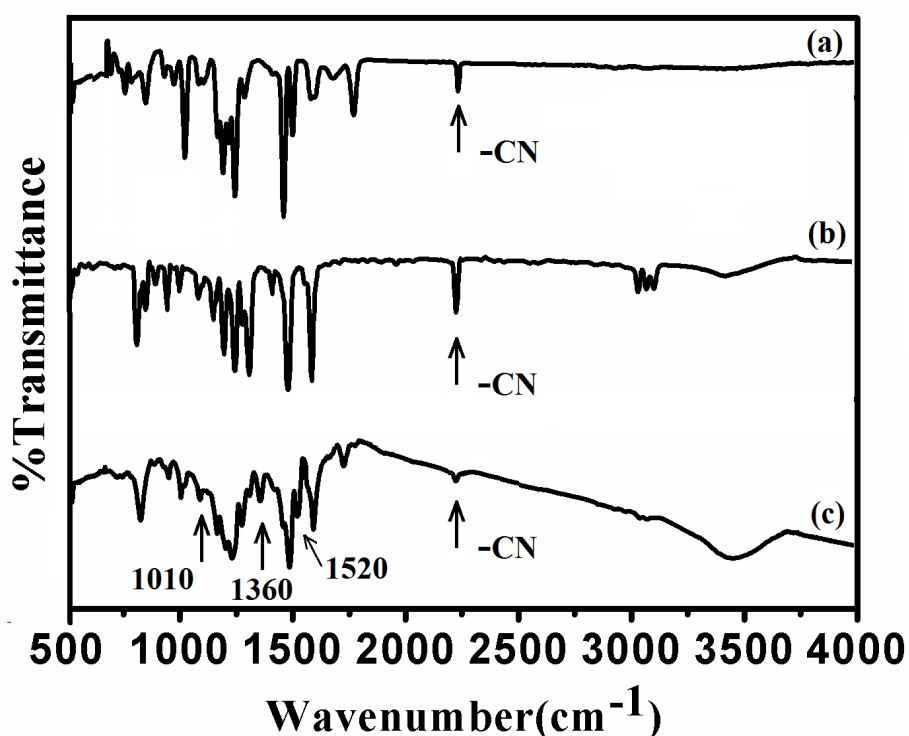


Fig. 4.1 FTIR of (a): pure PEN; (b): pure BPh; (c): BPh with 10 wt% of PEN

4.2.2 Thermal properties of the PEN-BPh IPN system

Fig. 4.2 displays the TGA curves of pure BPh, PEN and PEN-BPh system with various PEN contents. To explore the effect of PEN on the thermal stability of BPh polymer, the thermal degradation temperatures of 5%, 10% weight losses ($T_{5\%}$ and $T_{10\%}$) and the carbon yield at 800 $^{\circ}\text{C}$ were summarized. The pure BPH was rather thermal stable (curve (a)). However, the thermal stability of the PEN-BPh IPN system was reduced with increasing

PEN content. The $T_{5\%}$, $T_{10\%}$ and carbon yield of pure BPh polymer at 800 °C were about 543 °C, 595 °C and 79%, respectively. In cases of PEN-BPh IPN system, the $T_{5\%}$ and $T_{10\%}$ of the composites occurred at lower temperatures than those of pure BPh. For 15 wt% of PEN-BPh IPN system, the $T_{5\%}$ and $T_{10\%}$ and carbon yield at 800 °C were decreased by about 67 °C, 77 °C and 16%, respectively. That is largely because soft polymer chains of PEN reduce the thermal stability of the PEN-BPh system, which is confirmed by TGA curve (e) that pure PEN exhibits poorer thermal stability than that of the pure BPh.

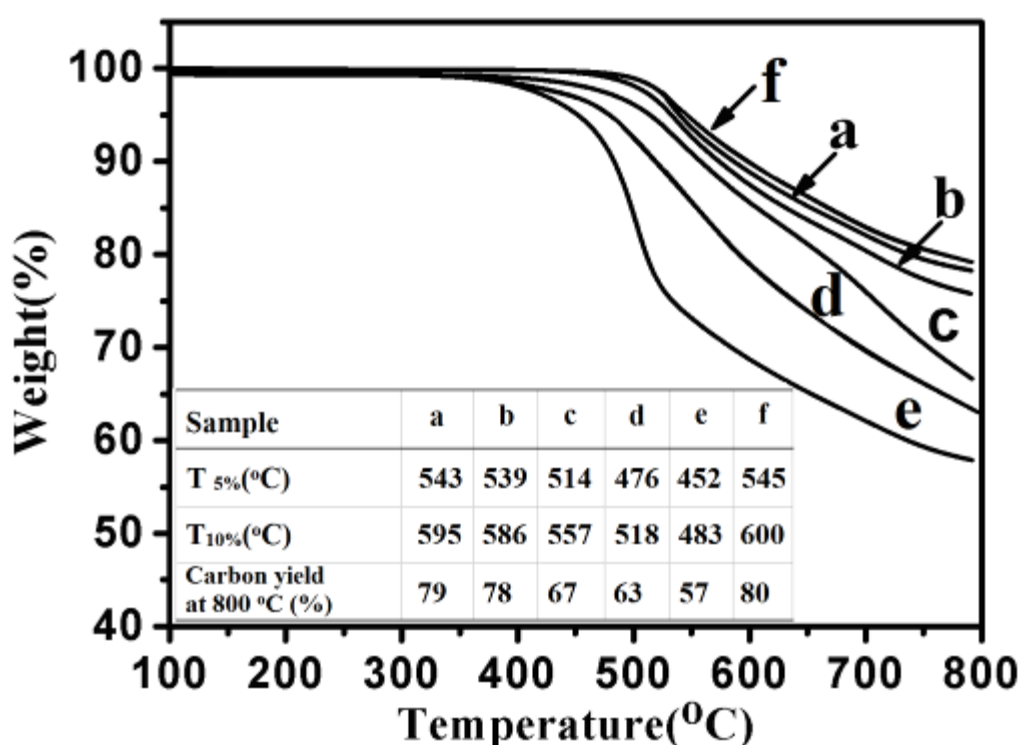


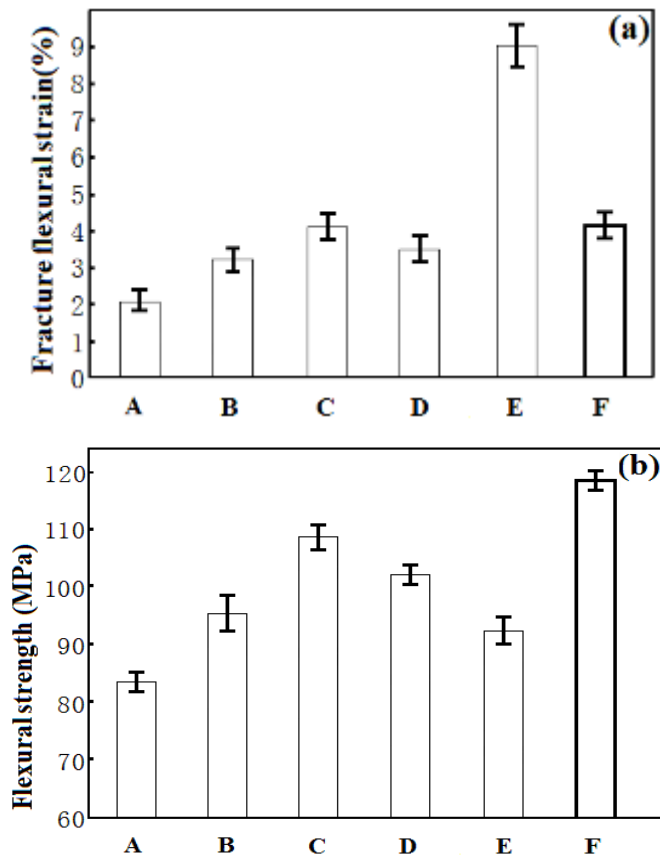
Fig. 4.2 TGA curves of the cured BPh, PEN, PEN-BPh IPN system and xGnP/PEN-BPh composites.

- (a) Pure BPh (b) BPh with 5 wt% of PEN (c) BPh with 10 wt% of PEN
 (d) BPh with 15 wt% of PEN (e) pure PEN (f) BPh with 10 wt% of PEN and 10 wt% of xGnP

4.2.3 Mechanical property of the PEN-BPh IPN system

The mechanical properties of the pure BPh, PEN and PEN-BPh system with various PEN contents are shown in Fig. 4.3. Fig. 4.3 (a) shows that PEN exhibits excellent toughness with fracture flexural strain as high as 9.1%. Because of the intrinsic brittleness of the network structures, the flexural strength and fracture flexural strain of the pure BPh

polymer are only 83 MPa and 2.1%. But its flexural modulus is 3.6 GPa, about 0.9 GPa higher than that of PEN. Compared to the pure BPh polymer, addition of 5 wt% PEN resulted in about 1.0% and 12 MPa increase in the flexural strain and flexural strength but 0.2 GPa decrease in flexural modulus. Flexural strain and flexural strength exhibit maximum values at 10 wt% PEN content, about 2 % and 25 MPa above those of the pure BPh, respectively. These results are due to the good compatibility and high interpenetrating degree between BPh and PEN. In this system, BPh network provided a rigid frame while flexible PEN chains wind around the framework, serving as buffer zone for ambient pressure. Therefore, the strength and tenacity were enhanced largely. Meanwhile, with the introduction of flexible PEN chains, the system tended to soften up to some extent and thus the modulus of BPh is decreased. The flexural modulus of the PEN-BPh IPN system with 10 wt% PEN content was only 3.2 GPa, about 0.4 GPa decrease with regard to the pure BPh. Moreover, the mechanical properties of PEN-BPh IPN system with 15 wt% PEN content were poorer than the composites with 10 wt% PEN content. This may be due to the problems of phase segregation and low interpenetrating degree between BPh and PEN chains.



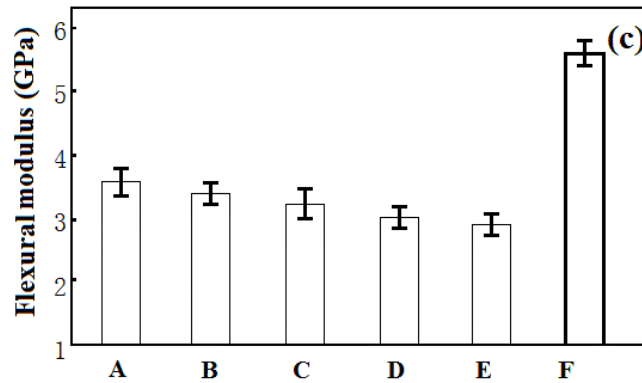


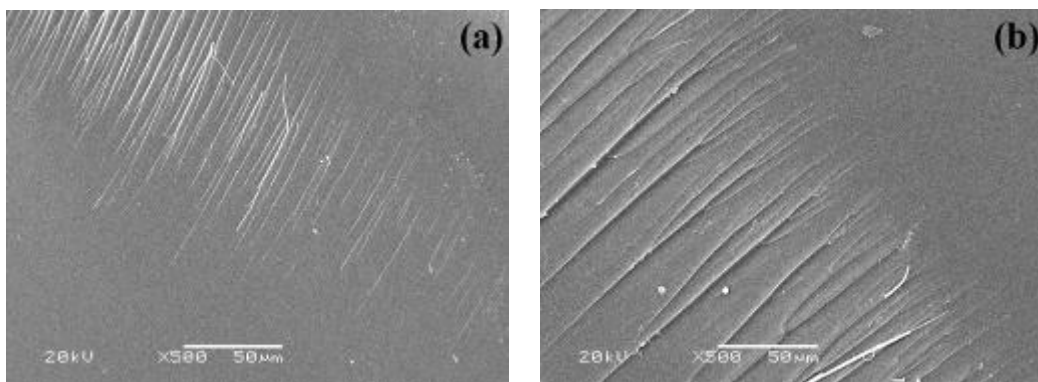
Fig. 4.3 Mechanical properties of the cured BPh, PEN, PEN-BPh IPN system and xGnP/PEN-BPh composites.

(a) Fracture flexural (b) Flexural strength (c) Flexural modulus

A: pure BPh B: BPh with 5 wt% of PEN C: BPh with 10 wt% of PEN,

D: BPh with 15 wt% of PEN E: pure PEN F: BPh with 10 wt% of PEN and 10 wt% of xGnP

The fracture surfaces of the PEN-BPh composites with various PEN contents in Fig. 4.4 also confirmed the mechanical performances investigated above. The fracture surfaces of the pure BPh indicated a smooth, glassy and homogeneous microstructure without any plastic deformation. But the fracture surfaces of PEN-BPh composites reflected different degree of plastic deformation and tearing behavior. These are compelling proof of toughness increase. The homogeneous morphology exhibited by the PEN-BPh IPN system with 10 wt% PEN is due to the good compatibility and interpenetrating between the BPh and PEN chains.



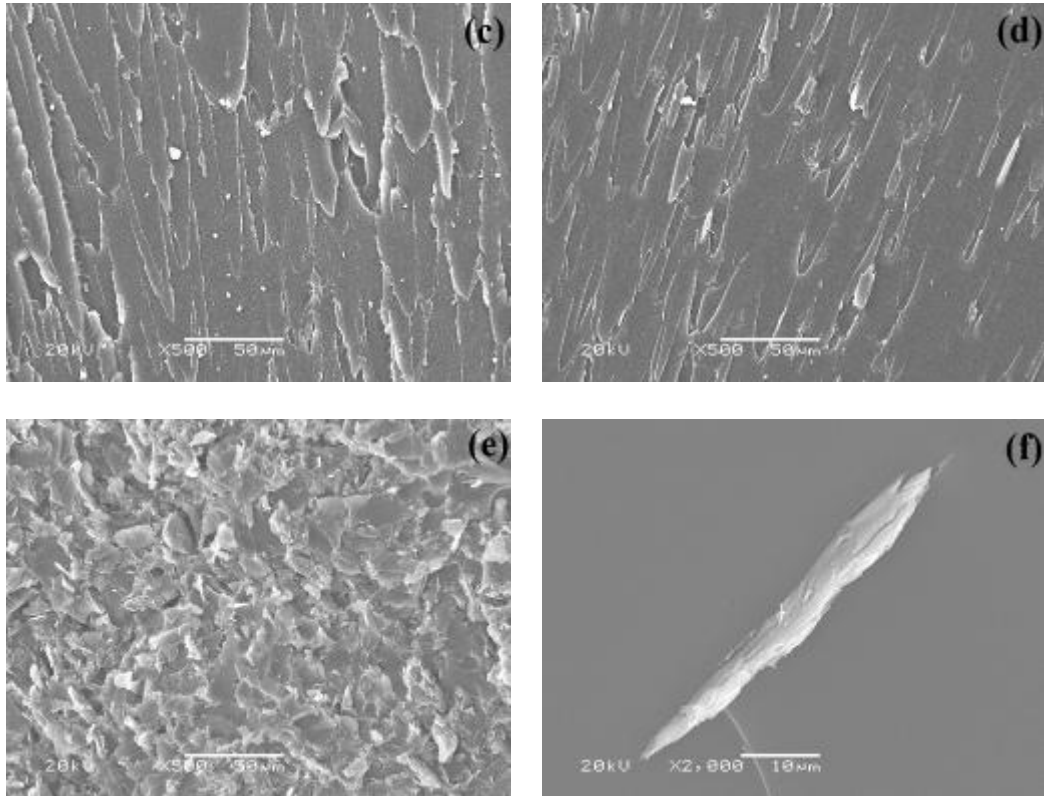


Fig. 4.4 SEM images of fracture surfaces of cured BPh, PEN-BPh IPN system and xGnP/PEN-BPh composites.

(a) Pure BPh (b) BPh with 5 wt% of PEN (c) BPh with 10 wt% of PEN (d) BPh with 15 wt% of PEN
 (e) BPh with 10 wt% of PEN and 10 wt% of GN (f) Image (e) in high magnification

From the above, the PEN-BPh IPN system with 10 wt% PEN exhibit highest strength and toughness, so we choose this ratio for the subsequent studies.

4.2.4 Thermal properties of xGnP/PEN-BPh composite

Based on the study of the PEN-BPH IPN system, xGnP/PEN-BPh composites with weight ratios of BPh/PEN/ xGnP =100/10/10 were prepared. Fig. 4.2 curve (f) shows TGA thermograms of xGnP/PEN-BPh composites. The $T_{5\%}$, $T_{10\%}$ and carbon yield of xGnP/PEN-BPh composites at 800 °C were about 545 °C, 600 °C and 80%, respectively. Compare with the PEN-BPh IPN system (10 wt% PEN content), the thermal property of the xGnP/PEN-BPh composites was improved. With the incorporation of xGnP, the thermal property of the composites reached even a little higher level compared with the pure BPh polymer. This was believed to originate from the fact of xGnP, which were dispersed homogeneously in the PEN-BPh network, serving as the mass transfer barriers

against the volatile pyrolyzed products in the matrix, eventually retarding thermal degradation of the composites.

4.2.5 Mechanical property of xGnP/PEN-BPh composites

The overall performances of PEN-BPh composites were further enhanced by the incorporation of xGnP component. According to Fig. 4.3 (b) and (c), the flexural strain and modulus of the xGnP/PEN-BPh composites were increased to 117 MPa and 5.6 GPa respectively. It is worth emphasizing that the modulus of the xGnP /PEN-BPh composites is 2 GPa higher than that of the pure BPh and 2.4 GPa higher than that of the PEN-BPh system (10 wt% PEN content) by the incorporation of xGnP; the soft materials return to hard. It is well-known and commonly admitted that the mechanical properties of polymer nanocomposites, especially the modulus, depend to a great extent on filler dispersion and interfacial interaction, and are increased only when good dispersion of the nanofiller and effective stress transfer at the polymer/filler interface are guaranteed [16]. In this sense, the improvements in the mechanical properties can also verify the uniform dispersion of xGnP in the PEN-BPh networks. The fracture surfaces of the nanocomposites in Fig. 5 (e) also confirmed the enhancement of the mechanical performances investigated. It can be seen clearly that much vertical graphite nanoplatelets were dispersed uniformly in the PEN-BPh matrix. In addition, SEM photo with high magnification (Fig. 5 f) shows that the xGnP is well coated by PEN-BPh resin and effective stress transfer at the xGnP/resin interface is thus guaranteed. According to the previous researches [17], good dispersion states can increase the average aspect ratio of the nanofillers in the polymer matrix; as a consequence, mechanical properties were improved. Here apparently, xGnP effectively reinforced mechanical properties of the PEN-BPh matrix are due to their good dispersion states, large aspect ratio, as well as excellent mechanical properties of xGnP itself. Moreover, the fracture flexural strain of xGnP/PEN-BPh composites was 4.1%, which is the same as that of the PEN-BPh system (10 wt% PEN content) and about 2.0% higher than that of the pure BPh. The contradiction between the strength and toughness of a material is that higher strength usually results in stress concentration and thus lower toughness. In the

xGnP/PEN-BPh composites, xGnP can restrain the welding cracks effectively during the crack process. As a result, its strength is enhanced and toughness is maintained.

4.3 Conclusions

The xGnP/PEN-BPh composites as a type of thermoset-thermoplastic- nanofiller blend system were successfully prepared via a cost-effective method and characterized for mechanical, thermal and morphological properties.

It was found that the strength and toughness of the xGnP/PEN-BPh composites were much better than those of the pure BPh. Compared with BPh, for 10 wt% of PEN and 10 wt% of xGnP reinforced BPh composite, the flexural strength, modulus and fracture flexural strain were increased by about 34 MPa, 2 GPa and 2.0%, respectively.

The incorporation of PEN enhanced the strength and toughness of BPh polymer while xGnP improved the flexural strength and offset losses of the flexural modulus and thermostability lowered by the PEN. The high performance xGnP/PEN-BPh composites are believed to have potential application in military industry, aerospace, and other places.

4.4 References

- [1] T.M. Keller, Chem. Mater. 1994, 6, 302.
- [2] T.M. Keller, C.M. Roland, US Patent 5242755, 1993.
- [3] T.M. Keller, Chemtech. 1988,18, 635.
- [4] T.M. Keller. Polym. Commun. 1991, 32, 2.
- [5] L.H. Sperling. Interpenetrating Polymer Networks and Related Materials, New York: Plenum Press; 1981.
- [6] V. Huelck, D.A. Thomas, L.H. Sperling, Macromolecules. 1972, 5, 340.
- [7] A.J. Curtius, M.J. Covitch, D.A. Thomas, L.H. Sperling, Polym. Eng. Sci. 1972, 12, 101.
- [8] A. Saxena, R. Sadhana, V. L. Rao, M. Kanakavel, K. N. Ninan, Polym. Bull. 2003, 50, 219.
- [9] A. Saxena, V. L. Rao, K. N. Ninan, Eur. Polym. J. 2003, 39, 57.
- [10] C. Li, Y. Gu, X.B. Liu, Mater Lett. 2006, 60, 137.
- [11] K. Kalaitzidou, H. Fukushima, L. T. Drzal, Carbon. 2007, 45, 1446.
- [12] K. Kalaitzidou, H. Fukushima, L. T. Drzal, Compos. A. 2007, 38, 1675.
- [13] T.M. Keller, J. Polym. Sci: Part A, Polym. Chem. 1988, 26, 3182.
- [14] A.W. Snow, J.R. Griffith, N.P. Marullo. Macromolecules. 1984, 17, 1614.

- [15] X. Wu, S. Qi, J. He, G. Duan. *J. Mater. Sci.* 2010, 45, 483.
- [16] K. Prashantha, J Soulestin, M.F. Lacrampe, M. Claes, G. Dupin, P. Krawczak. *Express. Polym. Lett.* 2008, 10, 735.
- [17] Y. Kojima, A. Usuki, M. Kawasumi, A. Okada, T. Kurauchi, O. Kamigaito, *J. Polym. Sci. A.* 1993, 31, 983.

Chapter 5 Production of empty and iron-filled multiwalled carbon nanotubes from iron–phthalocyanine polymer and their electromagnetic properties

5.1. Introduction

Carbon nanotubes (CNTs), first reported by Sumio Iijima in 1991[1], have attracted tremendous attention due to their unique structural, electronic, magnetic and mechanical properties [2]. CNTs are one of the most interesting one-dimensional (1D) nano-scale materials because of their unique electronic properties and many potential applications. With the help of metal catalysts, CNTs can be prepared by the pyrolysis of hydrocarbons such as ethylene or acetylene. To date, CNTs can be obtained by many methods such as arc-discharge [3, 4], laser ablation [5] and chemical vapor deposition (CVD) [6]. Among them, CVD method is highly preferred for the preparation of aligned CNTs in the presence of carbon sources (e.g. graphite, metal carbonyls, metallophthalocyanines and metallocenes [7, 8]) and catalysts (e.g. pure metals, metal salts and organic metals [9]). Further industrial preparation of CNTs by CVD method, however, is hindered due to cumbersome separation and purification process of catalysts from the CNTs. And the CVD method needs a supply of hydrogen to maintain catalysts activity during the high-temperature process, and the control of tube morphology is also limited.

To solve the problem, solid-state pyrolysis of organometallic precursors for CNT preparation could be effective, simple and controllable [10~12], for that the organometallic materials serve as both the carbon source and the catalyst, and the pyrolysis process could be carried out controllably at “low” temperature in the solid states rather than in the gas phases. Compared with organometallic precursors such as cobalt–oligoalkyne complexes, iron, cobalt and nickel phthalocyanines molecular [13], the use of metal phthalocyanine molecules as carbon sources exhibited excellent performances during the synthesis of CNTs. The corresponding CNTs were cylindrical and bamboo-like structures with a length from 30 to 80 nm when the temperature was increased from 700 to 1000 °C. Their diameters also increased with increasing temperature [14, 15].

Phthalocyanine polymer (PC) containing aryl ether linkages has outstanding thermal properties and high char yields upon thermal treatment to elevated temperatures making them an attractive source of carbon[16]. The planar heterocyclic molecule Pc, with a diameter of about 1.3 nm, is composed of four fused phenyl and pyrrole subunits. The four central nitrogen atoms of the pyrrolic subunits can further enable Pc macromolecule to coordinate with various metallic cations such as FeCl_3 , FeCl_2 , $\text{Fe}(\text{CO})_5$ and nano-iron. And those complexes, with similar curing and cross-linking properties [17, 18], are all called iron phthalocyanine ($\text{FeC}_{32}\text{H}_{16}\text{N}_8$, FePc). Its outstanding thermal properties and high char yields upon thermal treatment to elevated temperatures guarantee a high yield of the CNTs. However, the final CNTs pyrolyzed from these FePc may be different. Phthalocyanine has been previously shown to readily convert into carbon when heated to temperature up to 1000 °C [16]. To our best knowledge, the use of polymer as a carbon source for the formation of various morphology CNTs is an intriguing idea. Synthesis of CNTs using small molecule phthalocyanine as carbon sources has been studied intensively. However the report on the preparation of CNTs from phthalocyanine polymers are few.

In this Chapter, we describe a simple and efficient method for *in situ* synthesis of multi-walled CNTs based on BPh resin. To establish the relationship among the carbon source, catalyst and CNT structure, two kinds of FePc obtained using $\text{Fe}(\text{CO})_5$ powder and nano-iron powder as the catalyst, respectively, were pyrolyzed to acquire CNTs. It is believed that adjusting the cure reaction of the polymers, carbon tubes could be obtained with corresponding electromagnetic properties. Moreover, the field of application of functional BPh resin based materials can be largely expanded.

This part of work has been published on the Chemical Physics Letters, 2010, volume 496, issue 1-3, page 139-142 and Journal of Materials Science: Materials in Electronics, 2012, volume 23, issue 4, page 921-927.

5.2. Results and discussion

5.2.1 DSC analysis of the iron phthalocyanine (FePc) oligomer

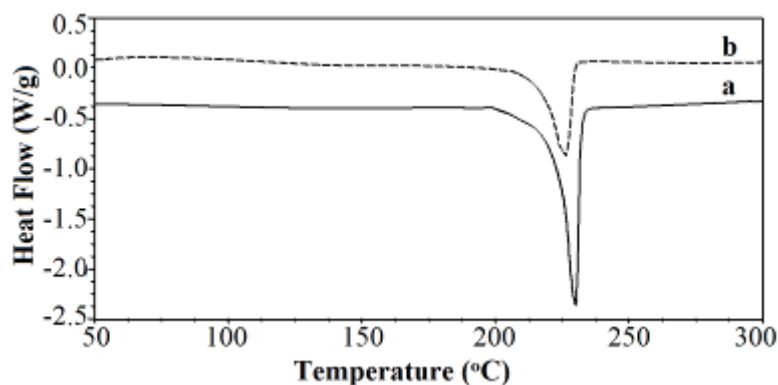


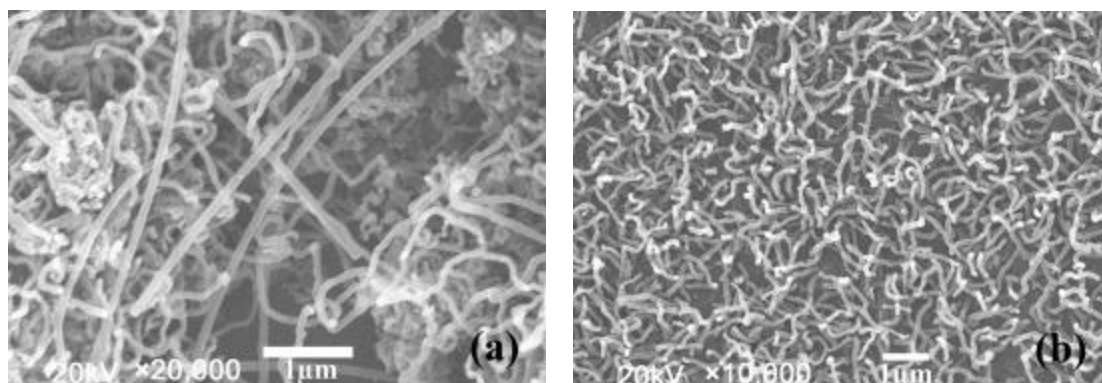
Fig. 5.1 DSC curves of iron phthalocyanine oligomer.

(a) oligomer using $\text{Fe}(\text{CO})_5$ powder as the catalyst

(b) oligomer using nano-iron powder as the catalyst

Fig.5.1 plots the differential scanning calorimeter (DSC) curves of samples (a) and (b). Both samples displayed a characteristic melting transition at 233 °C, but the melting range and enthalpy of sample (b) were narrower and smaller. This indicates that sample (b) had a higher polymerization degree than (a). These differences were due to the fact that the reactivity of the nano-iron powder with Pc was higher than that of $\text{Fe}(\text{CO})_5$.

5.2.2 Microstructure of the CNTs



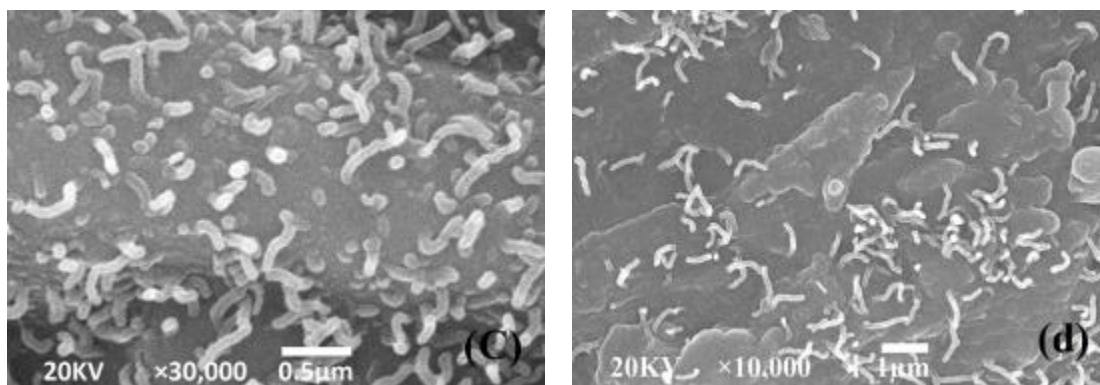


Fig. 5.2 SEM images of CNTs obtained by curing of Pc polymers with the different catalysts.

- (a) CNTs pyrolysed from the oligomer using $\text{Fe}(\text{CO})_5$ powder as the catalyst
- (b) CNTs pyrolysed from the oligomer using nano-iron powder as the catalyst
- (c) Materials pyrolysed from the oligomer using $\text{Fe}(\text{CO})_5$ powder as the catalyst which
Reduces the curing time and increases the heating rate of the pyrolysis temperature
- (d): Materials pyrolysed from the oligomer using nano Fe powder as the catalyst which
reduces the curing time and increases the heating rate of the pyrolysis temperature

The CNTs were obtained by solid-state pyrolysis of cured Pc polymers with the different catalysts at 800 °C for 8 h and their SEM images were shown in Fig. 5.2 From Fig. 5.2 (a), most of the CNTs from sample (a) are long straight ropes up to tens of micrometers, with a diameter of ~ 100 nm. Furthermore, few ropes were coiled or curled. Compared with sample (a), CNTs from the pyrolysis of sample (b) (Fig. 5.2 (b)) have similar length and little winding. However, they are much more uniform, with a reduced diameter of ~ 90 nm. The nano-iron powder was smaller and more uniform than micron-sized $\text{Fe}(\text{CO})_5$, resulting in higher reactivity with Pc and efficient formation of CNTs. Therefore, from these results it can be concluded that particle size and reactivity of catalyst are two key factors influencing the morphology of the CNTs.

Moreover, the curing temperature, duration and pyrolysis temperature also play a very important role in the synthesis of CNTs. It takes a long time and a slow temperature increase profile to obtain completely cured phthalocyanine polymer and then CNTs. In our work, it was found that reducing the curing time or increasing the heating rate of the pyrolysis temperature would not favor the formation of good CNTs from phthalocyanine polymer. The microstructure of the materials pyrolysed from the oligomer using $\text{Fe}(\text{CO})_5$ powder and nano Fe powder as the catalyst which reduce the curing time and increase the

heating rate of the pyrolysis temperature (isotherm for 25 h at 300 °C; 5 °C min⁻¹ from 500 °C to 800 °C) were shown in Fig. 5.2 (c) and (d), respectively. It can be seen that the CNTs grew from the surface of the phthalocyanine, but it can not obtain the whole CNTs materials.

Even if the mechanisms of the nanotubes growth regime cannot actually be emulated in the microscope, the experiments have provided us with valuable information about the initiation and growth of carbon nanotubes. To propose a growth mechanism of the carbon nanotubes, we speculated that iron phthalocyanine polymer first evaporated from the surface of the polymer, where it decomposed into atomic iron and phthalocyanine species under nitrogen at high temperature. Almost simultaneously, the phthalocyanine decomposed into benzene rings while the iron atoms aggregated into nanoparticles as catalytic centers for the growth of the carbon nanotubes. The benzene rings may fragment further, liberating C_n, CH_n. These carbon species then precipitated on or diffused through the metal particles [17-19].

This model may consist of three steps (Figure 5.3): the first step is the nucleation of carbon fragments starts and some of them are melted in metal particles. After the first step, the metal particles are covered with the carbon fragments (step two). Then carbon nanotubes start to grow at eutectic temperature (step three) [20-22].

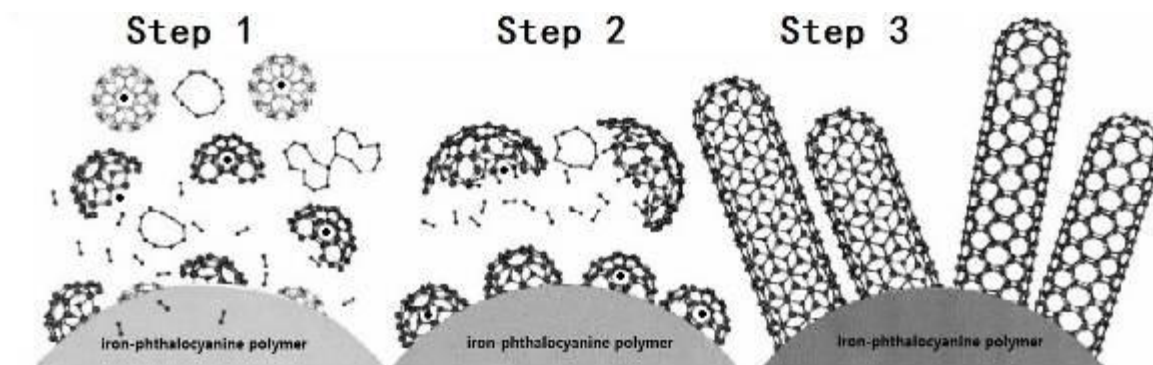


Fig. 5.3 Proposed growth mechanism of the carbon nanotubes from pyrolysis of iron phthalocyanine polymer.

Step 1: the nucleation of carbon fragments starts and some of them are melted in metal particles

Step 2: the metal particles are covered with the carbon fragments

Step 3: the carbon nanotubes start to grow at eutectic temperature.

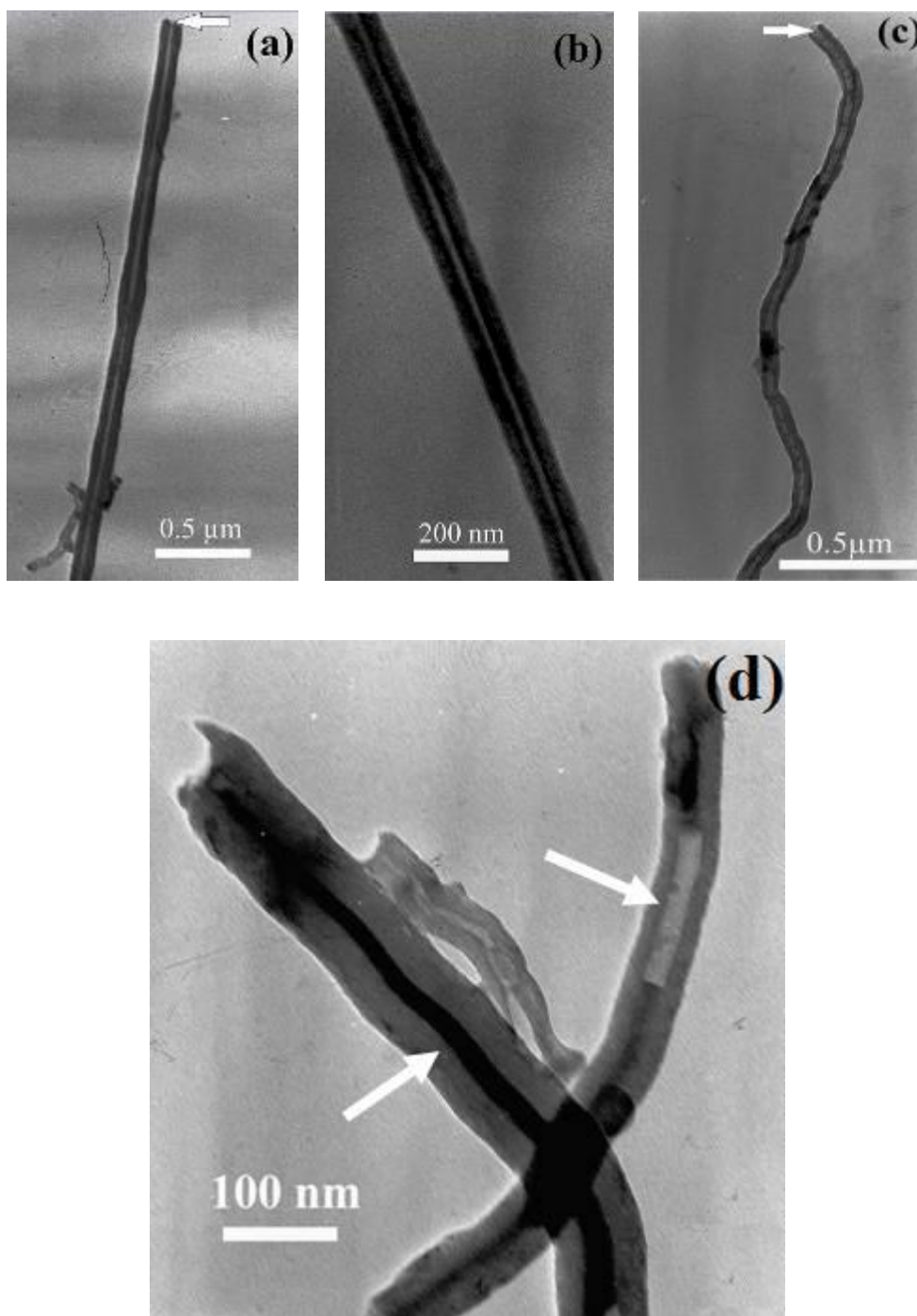


Fig. 5.4 TEM images of CNTs pyrolysed from cured Pc polymers with different catalysts.

- (a), (b), (c) CNTs pyrolysed from the oligomer using $\text{Fe}(\text{CO})_5$ powder as the catalyst
- (d) CNTs pyrolysed from the oligomer using nano Fe powder as the catalyst

TEM was also employed to further characterize obtained CNTs. Fig. 5.4 is the TEM images of CNTs pyrolysed from cured Pc polymers with different catalysts. It is revealed that both pyrolyzed CNTs are multi-walled CNTs (MWCNTs). Among them, figures (a), (b), (c) are the TEM images of the CNTs pyrolysed from cured Pc polymers using $\text{Fe}(\text{CO})_5$

powder as the catalyst and two types of morphologies were obtained. One was long straight tubes (Figure 5.4 (a), (b)) while the other long and crooked bamboo-shaped (Figure 5.4 (c)). All the two types of CNTs possessed open ends, and labeled by the arrows in the images.

Similar to the SEM images, no carbon particles are detected in the TEM images. It is shown in Fig. 5.4 (a) that the size of the CNTs which had a long and straight morphology was about 90 nm in diameter and with a length of several micrometers. With an enhancement in the resolution (Fig. 5.4 (b)), it appears that the nanotube had a wall thickness of ~30nm. The formation of the CNTs pyrolysed from cured Pc with $\text{Fe}(\text{CO})_5$ as the catalyst may be explained as follows. When cured in the presence of $\text{Fe}(\text{CO})_5$, degradation of $\text{Fe}(\text{CO})_5$ occurred at 400 °C to initially produce Fe atoms and clusters, leading to the formation of fcc iron nanoparticles embedded in the polymeric networks. As the iron nanoparticles containing Pc polymer was heated over 500 °C in the inert nitrogen atmosphere, carbonization to a carbonaceous solid occurred in high yield. In short, due to the presence of the iron nanoparticles, CNTs were formed in the carbon during the carbonization process.

Figure 5.4 (c) shows bamboo-shaped nanotubes with an open end. The bamboo-shaped CNTs are comprised of an outer diameter of about 80 nm and an inner diameter of about 25 nm. The bamboo-shaped CNTs was made up of several compartments of almost uniform size and most of the compartments were empty. We proposed the growth mechanism of bamboo-shaped CNTs in terms of surface and bulk diffusion of carbon based on a mechanism proposed in the literature [23]. The carbon atoms, which are produced via pyrolysis of phthalocyanine polymer impinging on metal nanoparticles, form a cap to the metal nanoparticle. If carbon is continuously supplied, they diffuse through the metal nanoparticle due to the gradient in the carbon density within the nanoparticle. Once the formation of the graphitic sheet starts, the diffusion of carbons accelerates into the reaction zone of the catalytic particle, thus the carbons are continuously added to the edge of cap. The hollow and bamboo-shaped carbon nanotubes were formed on different sizes of metal nanoparticles.

The pyrolysis process from cured Pc with the catalysts of $\text{Fe}(\text{CO})_5$ and nano Fe powder were carried out under the same experimental conditions, but the structures of the CNTs

obtained were very different. Fig. 5.4 (d) shows the CNTs pyrolysed from sample (b). About 90% of CNTs were filled with iron wire, thus affording unique metal core/carbon sheath nanocables. The filled part of the CNTs was 1 to 10 μm in length, significantly longer than other metal-filled CNTs prepared by the arc-discharge method [24]. The filled spindle-like tip was closed while the unfilled part of the cable was empty. It is clear that iron particles tended to aggregate and thus formed bigger particles when the temperature was increased too quickly. More micrometer-scale metal particles were generated and the tubes were less well-defined than those formed upon a temperature increase rate of no more than $5\text{ }^{\circ}\text{C min}^{-1}$. This finding is not surprising, since changing the rate of temperature increase affected the conditions of precursor decomposition and carbonization, which were the two most important factors for CNTs formation in this system.

5.2.3 XRD analysis of the CNTs

X-ray diffraction (XRD) scans of the CNTs from the pyrolysis of cured Pc with the catalysts of $\text{Fe}(\text{CO})_5$ and nano Fe powder were obtained using $\text{Cu K}\alpha$ radiation from a rotating X-ray source (Fig. 5.5). The diffraction peaks were identified and indexed based on CNTs, iron metal and cementite (Fe_3C) [13, 14, 25]. It was found that the two samples were very similar. The peaks at 43.58 (110) and 36.34 (311) degrees were assigned to the α -Fe phase and magnetite, respectively. Those at 25.79 (002) and 43.07 (100) degrees were attributed to CNTs [26]. And the interplanar spacing for the CNTs (002) peak was 3.38 \AA [27]. From the XRD, little unordered or amorphous carbon was found, in agreement with SEM and TEM results. This indicates that the yields of the CNTs obtained by the pyrolysis of the two cured Pc polymers were high. Although the exact pyrolysis mechanism remains unclear, the high yields of CNTs appeared to be favored by a higher char yield, a longer pyrolysis time and a higher temperatures.

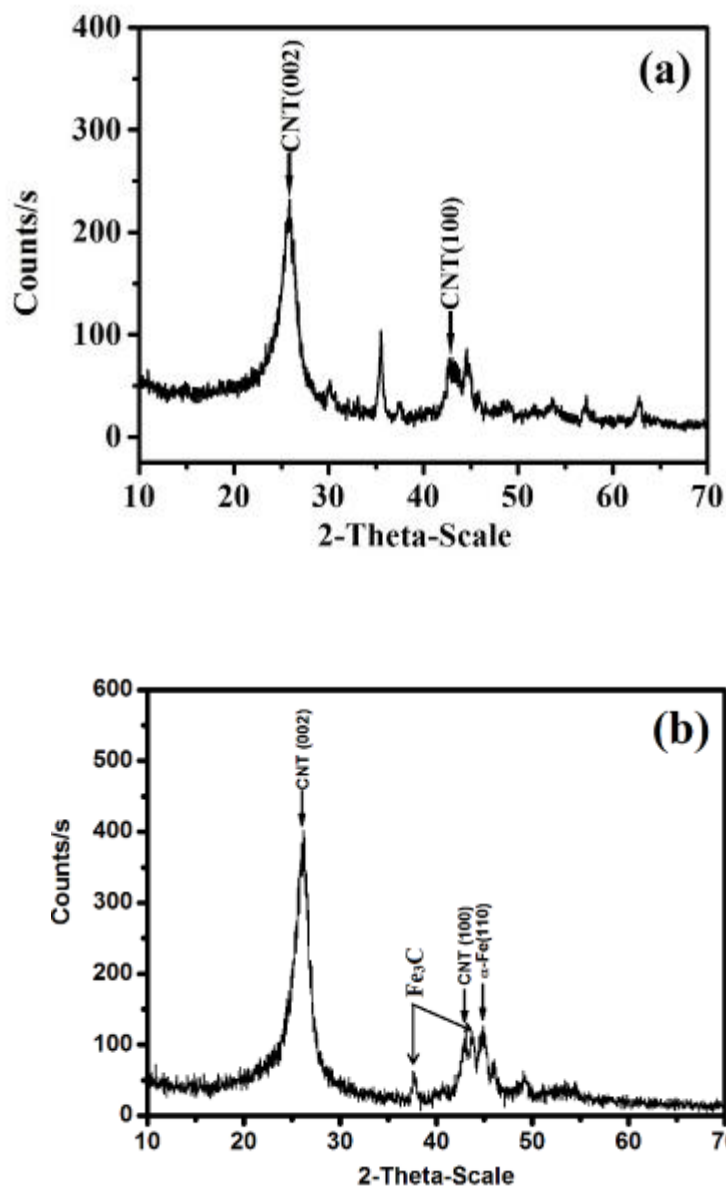


Fig. 5.5 XRD data for CNTs.

(a) CNTs pyrolysed from the oligomer using $\text{Fe}(\text{CO})_5$ powder as the catalyst

(b) CNTs pyrolysed from the oligomer using nano-iron powder as the catalyst

However, the obvious difference of the XRD data between the CNTs pyrolysed from the cured Pc with the catalysts of $\text{Fe}(\text{CO})_5$ and nano Fe powder resides in the intensity of diffraction peaks of Fe_3C . The Fe_3C diffraction peaks of the CNTs pyrolysed from the cured Pc with the catalyst of $\text{Fe}(\text{CO})_5$ is higher than that with the catalyst of Fe. This point coincides with the morphological analysis of the two types of carbon nanotubes. Whether bamboo-like or long straight CNTs had a hollow structure, the iron particles mainly existed in the form of Fe_3C . But in CNTs pyrolyzed from the

cured Pc with the catalyst of Fe, about 90% of CNTs were filled with iron wire. The iron particles mainly existed in the form of iron atom.

5.2.4 Dielectric properties of the CNTs

A Vector Network Analyzer (VNA) is a kind of radio frequency (RF) network analyzer which is typically used for testing circuit systems, and RF and microwave performance of networks and devices. The RF and microwave performance of the materials can be completely characterized by testing the scattering parameters (S-parameters) of the networks and devices. The key element of the VNA is that it can measure both amplitude and phase. In view of the wide application of VNA in the field of RF and microwave test, scientists process the material to a particular shape by a mold, then place it in a matched waveguide box. Test transmission - reflection parameters by the VNA are transformed into microwave electromagnetic parameters according the electromagnetic wave theory.

The basic principle of the electromagnetic properties test by VNA is as follows. The basis of the complex electromagnetic parameters test by the free space test method is that materials are equivalent to a plate (as shown in Figure 5-6) of thickness of d and infinite length to eliminate the scattering effect of the edge.

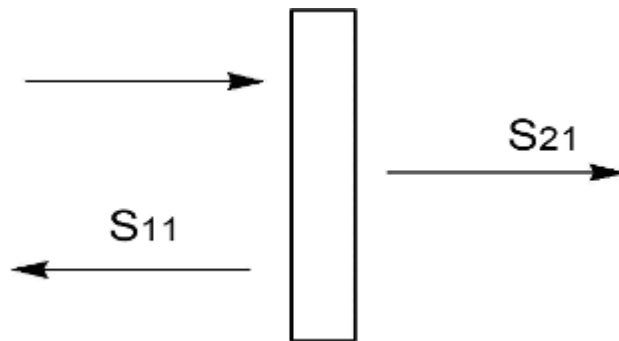


Fig. 5-6 An equivalent diagram of the free space test method

According to the transmission line theory of electromagnetism, the complex dielectric constant and complex magnetic permeability of the material, can be expressed as follows:

$$\varepsilon^* = \varepsilon' + \varepsilon'' = \varepsilon'(1 - j \tan \delta_e) \quad (5-1)$$

$$\mu^* = \mu' + j\mu'' = \mu'(1 - j \tan \delta_u) \quad (5-2)$$

The polarization uniform plane wave with a frequency of ω incident perpendicular to the plate, the reflection coefficient S_{11} and the transmission coefficient S_{21} can be measured by the VNA. According to the sample/air boundary conditions S-parameters S_{11} and S_{21} can be expressed with the Γ parameters and T parameters:

$$S_{11} = \frac{\Gamma(1 - T^2)}{1 - \Gamma^2 T^2} \quad (5-3)$$

$$S_{21} = \frac{T(1 - \Gamma^2)}{1 - \Gamma^2 T^2} \quad (5-4)$$

In the formula above, Γ representative the reflection coefficient at the interface of air and the sample, T representative the transmission parameter:

$$\Gamma = \frac{(Z_{in} - 1)}{(Z_{in} + 1)} \quad (5-6)$$

$$T = e^{-\gamma d} \quad (5-6)$$

In the formula above, Z_{in} is normalized characteristic impedance, γ is propagation constant. They are related o the complex electromagnetic parameters by:

$$\gamma = \gamma_0 \sqrt{\epsilon^* \mu^*} \quad (5-7)$$

$$Z_{in} = \sqrt{\frac{\mu^*}{\epsilon^*}} \quad (5-8)$$

Among them, $\gamma_0 = (j2\pi / \lambda_0)$ represents the free space propagation constant, λ_0 represents the free space wavelength.

According to Formula 5-3 and 5-4, Γ and T can converted to the following forms:

$$\Gamma = K \pm \sqrt{K^2 - 1} \quad (5-9)$$

with $K = \frac{S_{11} - S_{21} + 1}{2S_{11}}$

$$\Gamma = \left(\frac{S_{11} + S_{21} - \Gamma}{1 - (S_{11} + S_{21})\Gamma} \right) \quad (5-10)$$

The selection of the plus-minus must satisfy $|\Gamma| < 1$. According to the formula 5-6, the complex propagation constant can be expressed as:

$$\gamma = [\log_e(1/T)]/d \quad (5-11)$$

According to Formula 5-5 and 5-8, it can be derived that:

$$\sqrt{\frac{\mu^*}{\varepsilon^*}} = \left(\frac{1+\Gamma}{1-\Gamma} \right) \quad (5-12)$$

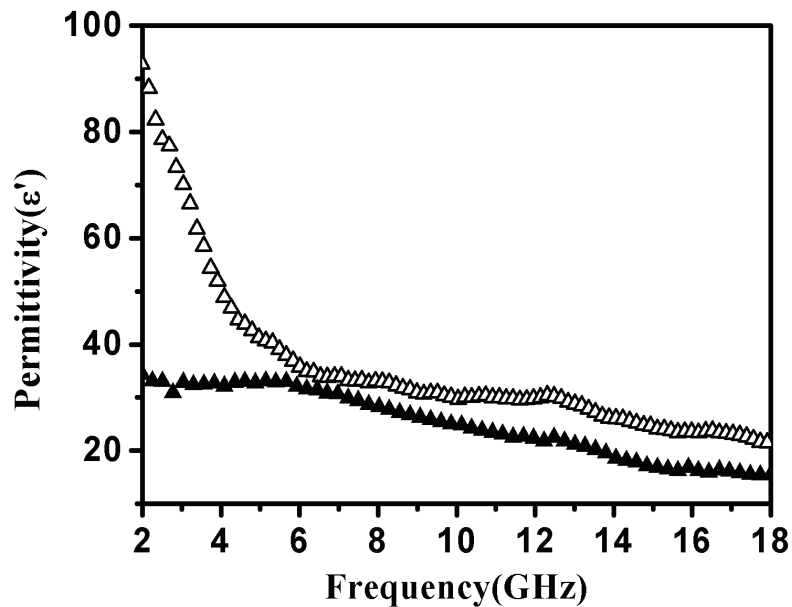
Finally, from 5-7 and 5-12, it can be deduced that:

$$\varepsilon^* = \frac{\gamma}{\gamma_0} \left(\frac{1-\Gamma}{1+\Gamma} \right) \quad (5-13)$$

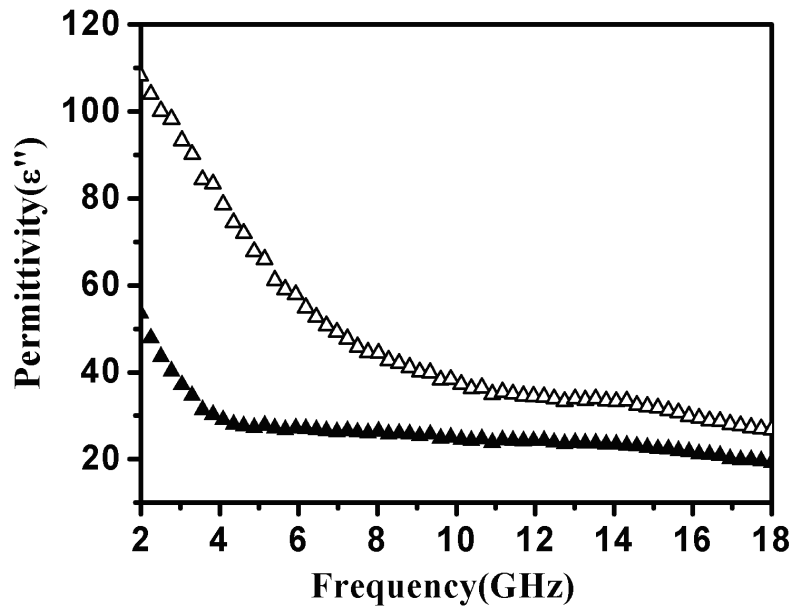
$$\mu^* = \frac{\gamma}{\gamma_0} \left(\frac{1+\Gamma}{1-\Gamma} \right) \quad (5-14)$$

A toroidal sample for electromagnetic measurements (inner diameter: 3 mm, outer diameter: 7 mm, and thickness: 5.7 mm) were prepared by mixing the CNTs with wax in a mass ratio (CNTs/wax) of 3:1. The edge effect due to the use of a finite size sample (in our case 3 mm×7 mm) is expected to be large for the long-wavelength or low-frequency regime, i.e. 2-4 GHz. The results corresponding to the higher-frequency regime are more reliable. Fig. 5.7 shows the frequency dependence of the real part (ε') and imaginary part (ε'') of relative complex permittivity for the CNT. ε' and ε'' stand for the energy storage and loss storage respectively. Fig. 6 (a) and (b) show that over frequency range, the values of ε' and ε'' of CNTs from sample (a) declined from 90.5 to 22.1 and from 105.9 to 26.8, respectively. According to the free electron theory [27], $\varepsilon'' \approx 1/2\pi\varepsilon_0\rho f$, where ρ is the resistivity. The lower ε'' values of CNTs at 2-18 GHz might indicate a higher electric resistivity (with respect to the other CNT materials, e.g. ε'' declined from 51.1 to 19.7 for CNTs obtained by pyrolysis of sample (b). The CNTs pyrolysed from sample (a) have better electric conductivity. Fig. 5.7 (c) demonstrates a higher dielectric loss of the CNTs pyrolysed from sample (a) than

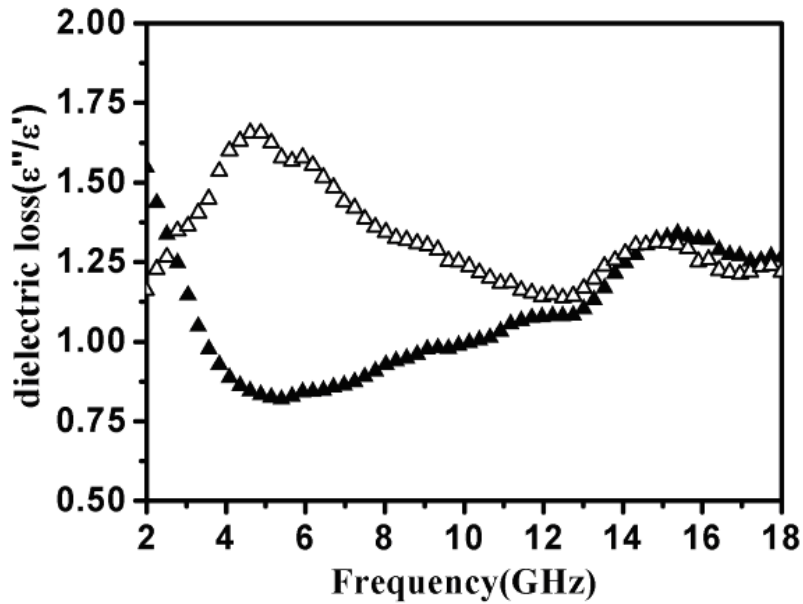
sample (b) from 3 to 15 GHz. According to Refs.[28-32], there are many factors which may have an effect on the dielectric properties: dielectric relaxation, resonance, the motion of conduction electrons, defects in the nanotubes, length, diameter, chirality, etc. Therefore, it will be extremely difficult to describe the permittivity dispersion behaviors of CNTs when taking into account all these factors. For example, the CNT defects do not significantly alter their band structures, but may simply act as polarized centers. Compared with the CNTs pyrolysed from sample (b) and the results reported in references[33, 34], the CNTs pyrolysed from sample (a) have higher electric conductivity and dielectric loss, which are favorable to improve microwave absorption properties.



(a)



(b)



(c)

Fig. 5.7 Dielectric properties of the CNTs

(a) Permittivity (ϵ')

(b) Permittivity (ϵ'')

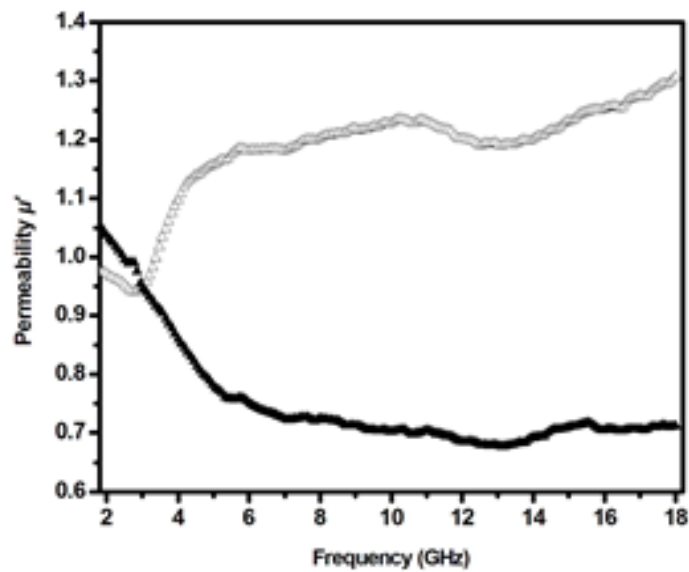
(c) Dielectric loss (ϵ''/ϵ')

Δ : CNTs pyrolysed from sample a (the oligomer using $\text{Fe}(\text{CO})_5$ powder as the catalyst)

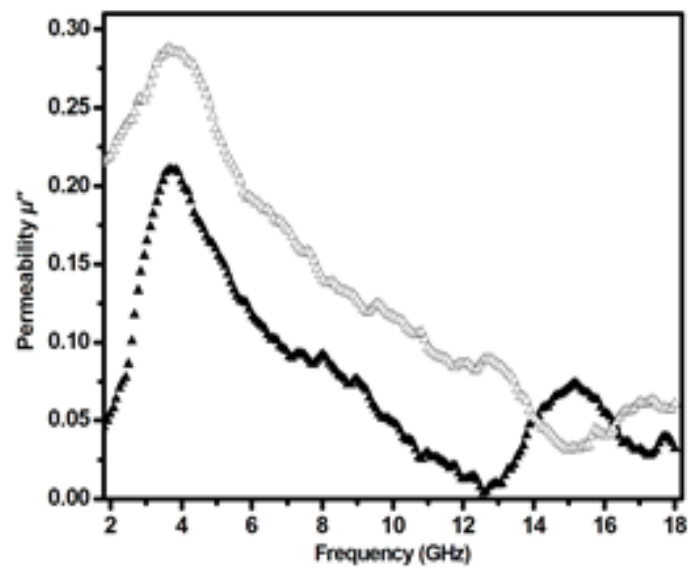
\blacktriangle : CNTs pyrolysed from sample b (the oligomer using nano Fe powder as the catalyst)

Fig. 5.8 shows the relative complex permeability of the two kinds of CNTs. The real part (μ') of CNTs pyrolysed from sample (b) exhibited an abrupt decrease from 1.0 to 0.7 at the 2-7 GHz range and remained almost constant over 7-18 GHz. Meanwhile the

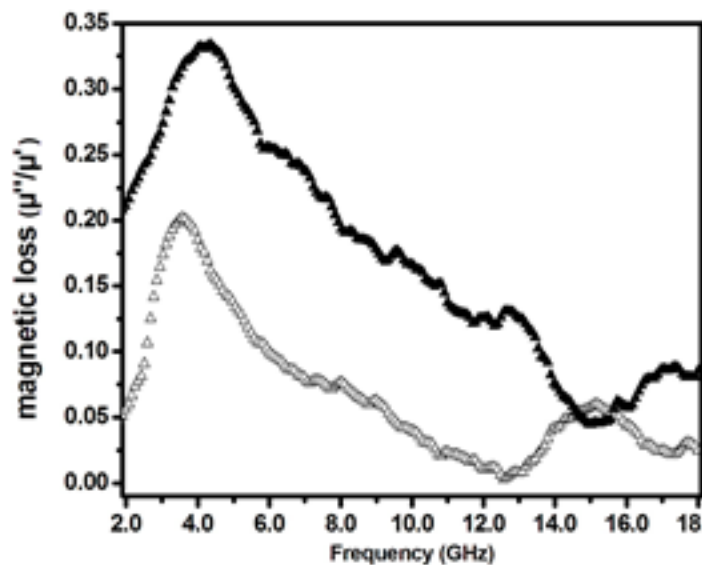
imaginary part (μ'') increased from 0.20 to 0.29 at 2-5 GHz and then decreased in high frequency. The maximum value of the μ'' appearing at 3.6 GHz implies that the natural resonance occurred in the present iron nano-wire. The magnetic loss (μ''/μ') at the frequency range of 2–18 GHz was shown in Fig. 5.8 (c). The maximum value of magnetic loss of iron nanowire inside CNTs was about 0.35, whereas the hollow structure CNTs (CNTs pyrolysed from sample (a)) were no more than 0.20 at the frequency of the 4.0–5.0 GHz. Moreover, in the measured frequency, the iron nanowire inside CNTs always had a higher value magnetic loss than that of the hollow structure CNTs.



(a)



(b)



(c)

Fig. 5.8 Electromagnetic properties of the CNTs

(a) Permeability (μ')

(b) Permeability (μ'')

(c) Magnetic loss (μ''/μ')

△: CNTs pyrolysed from sample a (the oligomer using $\text{Fe}(\text{CO})_5$ powder as the catalyst)

▲: CNTs pyrolysed from sample b (the oligomer using nano Fe powder as the catalyst)

5.2.5 Magnetic properties of the CNTs

The magnetic properties of the CNTs were investigated with a vibrating sample magnetometer at 300 K. The magnetization curves of CNTs are shown in Fig. 5.9, and the data are shown in Tab 5.1. In general, CNTs from the pyrolysis of sample (a) exhibit weak magnetic properties with the saturation magnetization of 1.8 emu/g, remanent magnetization of 0.8 emu/g and the coercive force of 80.0 Oe. However CNTs with iron nano-wire inside exhibit the saturation magnetization of 3.5 emu/g, remanent magnetization of 1.7 emu/g and the coercive force of 594.0 Oe which is much stronger than the CNTs without iron nano-wire filling. This is due to the magnetic iron nano-wire in a homogeneous array. Unlike dielectric properties, the nano-iron filled in CNTs made a great contribution to the magnetic improvement and these nano-iron CNTs can be used as magnetic fillers for composites.

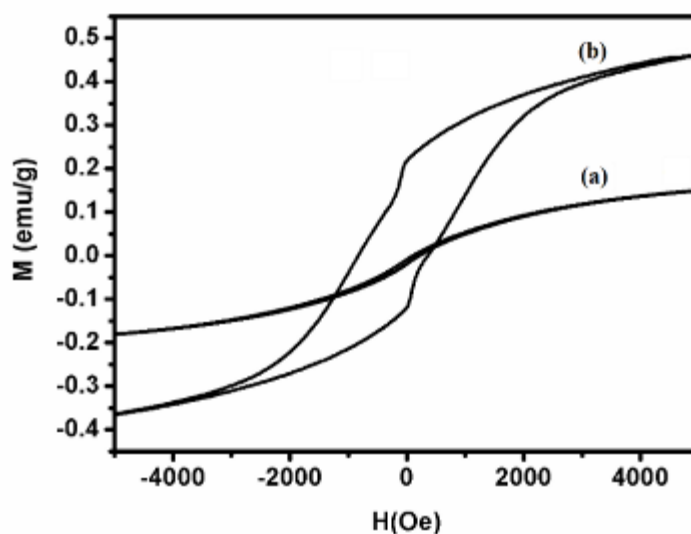


Fig. 7 Room-temperature magnetization curve of CNTs.

(a): CNTs pyrolysed from sample a (the oligomer using $\text{Fe}(\text{CO})_5$ powder as the catalyst)

(b): CNTs pyrolysed from sample b (the oligomer using nano Fe powder as the catalyst)

Tab. 5.1 Room-temperature magnetization data of CNTs

Sample	saturation magnetization M_s (emu/g)	remanent magnetization M_r (emu/g)	coercive force H_c (Oe)
(a)	1.8	0.8	80.0
(b)	3.5	1.7	594.0

5.3. Conclusions

This work shows that pyrolysis of iron-phthalocyanine polymers under nitro atmosphere is a simple and efficient method for bulk synthesis of multiwalled carbon nanotubes. The CNTs are not produced in the vapor phase in a complex apparatus under high pressure and temperature but in the solid phase during carbonization. The choice of the preparation method, the carbon source and the catalysts were important for obtaining the desired type of carbon nanotubes.

The empty CNTs obtained using $\text{Fe}(\text{CO})_5$ powder as the catalyst had better dielectric properties than iron-filled ones. The magnetic properties of the latter exhibited a magnetic saturation value of ~ 3.5 emu/g and a coercive force of ~ 594.0 Oe, which were much

higher than those of the empty CNTs.

To conclude, in situ synthesis of multi-walled carbon nanotubes in a bulk solid composition from the pyrolysis of a mixture formulated by phthalocyanine polymer and $\text{Fe}(\text{CO})_5$ powder or iron nano-powder was a good way to prepare novel electrical or magnetic materials.

More importantly, the field of application of functional BPh resin based materials is extended.

5.4 References

- [1] S. Iijima, *Nature*. 354 (1991) 56-59.
- [2] R. H. Baughman, A. A. Zakhidov, W. A. de Heer. *Science*. 297 (2002) 787-792.
- [3] D. S. Bethune, C. H. Kiang, M. S. de Vries, G. Gorman, R. Savoy, J. Vazquez, R. Beyers, *Nature*. 363 (1993) 605-607.
- [4] C. Journet, W. K. Maser, P. Bernier, A. Loiseau, M. Lamy de la Chapelle, S. Lefrant, P. Denaiard, R. Lee, J. E. Fischer, *Nature*. 388 (1997) 756-758.
- [5] A. Thess, R. Lee, P. Nikolaev, H. Dai, P. Petit, J. Robert, C. Xu, Y. H. Lee, J. E. Fisher, R. E. Smalley. *Science*. 273 (1996) 483-487.
- [6] M. Jose-Yacamán, M. Miki-Yoshida, L. Rendon, T.G. Santieste-ban, *Appl. Phys. Lett.* 62 (1993) 202-204.
- [7] L. C. Qin, *J. Mater. Sci. Lett.* 16 (1997) 457-464.
- [8] H. Hou, J. Zeng, F. Weller, A. Greiner, *Chem. Mater.* 16 (2003) 3170-3175.
- [9] S. C. Lyu, B. C. Liu, S. H. Lee, C. Y. Park, H. K. Kang, C. W. Yang and C. J. Lee, *J. Phys. Chem. B*. 108 (2004) 1613-1616.
- [10] V. S. Iyer, K. P. C. Vollhardt, R. Wilhelm, *Angew. Chem.* 115 (2003) 4515-4519.
- [11] P. I. Dosa, C. Erben, V. S. Iyer, K. P. C. Vollhardt, I. M. Wasser, *J. Am. Chem. Soc.* 121 (1999) 10430-10431.
- [12] M. Laskoski, W. Steffen, J. G. M. Morton, M. D. Smith, U. H. F. Bunz, *J. Am. Chem. Soc.* 124 (2002) 13814-13818.
- [13] W. Y. Tong, A. B. Djurisic, H. Xie, A. M. C. Ng, K. Y. Cheung, W. K. Chan, Y. H. Leung, H. W. Lin, S. Gwo, *J. Phys. Chem. B*, 35 (2006) 17406-17413.
- [14] N. S. Kim, Y. T. Lee, J. Park, J. B. Han, Y. S. Choi, S. Y. Choi, *J. Phys. Chem. B* 107 (2003), 9249-9255.
- [15] A. Milev, N. Tran, G. S. Kamali Kannangara, M. Wilson, I. Avramov, *J. Phys. Chem. C* 112 (2008), 5339-5347.
- [16] T. M. Keller, *Polym. Commun.* 31 (1990), 229.

- [17] M. Matsuda, T. Asari, T. Naito, T. Inabe, N. Hanasaki, and H. Tajima, *Bull. Chem. Soc. Jpn.* 76 (2003) 1935-1940.
- [18] D. C. Li, L. Dai, S. Huang, A. W. H. Mau, Z. L. Wang, *Chem. Phys. Lett.* 316 (2000) 349-355.
- [19] S. Ramo, J. R. Whinnery, T. V. Duzer, *Fields and Waves in Communication Electronics* Wiley, New York, 1984.
- [20] P. M. Ajayan, C. Colliex, J. M. Lambert, P. Bernier, L. Barbe-dette, M. Tenc, O. Stphan, *Phys. Rev. Lett.* 72 (1994) 1722
- [21] H. Kataura, Y. Kumazawa, Y. Maniwa, Y. Ohtsuka, R. Sen, S. Suzuki, Y. Achiba, *Carbon* 38 (2000) 1691-1697.
- [22] Lee, C. J. Park, *J. Appl. Phys. Lett.* 77 (2000) 3397.
- [23] K. Jia, R. Zhao, J. C. Zhong and X. B. Liu, *J. Mater. Sci.* 21 (2010) 708-712.
- [24] S. Ramo, J. R. Whinnery, and T. V. Duzer, *Fields and Waves in Communication Electronics*. Hoboken, NJ: Wiley, 1984-1986.
- [25] Y. Nabae, S. Moriya, K. Matsubayashi, S. M Lyth, M. Malon, L. Wu, N. M. Islam, Y. Koshigoe, S. Kuroki, M. Kakimoto, S. Miyata, J. Ozaki, *Carbon*. 48 (2010) 2613–2624
- [26] C. P. Paul, W. K. Hsu, A. Barres, B. Chamers, *Adv. Mater.* 15 (2003) 600-603.
- [27] A. Burian, J. C. Dore, H. E. Fischer, J. Sloan, *J. Phys. Rev. B* 59(1999) 1665-1668.
- [28] G. S. Zhuang, G. X. Sui, Z. S. Sun, R. J. Yang, *Appl. Polym. Sci.* 102(2006) 3664-3672.
- [29] P. M. Ajayan, C. Colliex, J. M. Lambert, P. Bernier, L. Barbe-dette, M. Tenc, O. Stphan, *Phys. Rev. Lett.* 72 (1994) 1722-1725.
- [30] C. Guerret-Picourt, Y. L. Bouar, A. Loiseau, H. Pascard, *Nature*. 372 (1994) 761-765.
- [31] J.Y. Dai, J. M. Lauerhaas, A.A. Setlur, R. P. H. Chang, *Chem. Phys. Lett.* 258 (1996) 547-553.
- [32] N. Demon, O. Stphan, N. Brun, C. Colliex, A. Loiseau, H. Pascard, *Eur. Phys. J. B* 4 (1998) 185-190.
- [33] M. G. Han, L. Deng, *Appl. Phys. Lett.* 90 (2007) 0111081-0111083.
- [34] L. J. Deng, M. G. Han, *Appl. Phys. Lett.* 91 (2007) 0231191-0231193.

Chapter 6 Electromagnetic and Microwave-Absorbing Properties of Iron-phthalocyanine and its composites based on phthalocyanine polymer

6.1. Introduction

Inorganic materials or metal particles can be used for microwave absorption materials. However, their practical applications are largely hampered by the high specific gravity and complex processing. Thus, lightweight, flexible but structurally sound microwave-absorbing materials with efficient and effective absorption in a wide band range remain to be explored [1-3]. Organic polymers, having extended π -conjugated systems, when doped with specific charge carriers, show conductivity in the semiconductor regime. The conductivity of polymers can be tailored for a given application. It is observed that high conductivity and dielectric constant of the materials contribute to high electromagnetic interference (EMI) shielding efficiency (SE). Therefore, conducting polymers find their application in EMI shielding technology [4].

Phthalocyanine (Pc) is a class of thermoset resins obtained by addition polymerization of phthalonitrile cyano groups at high temperature. It is a planar heterocyclic molecule of about 1.3 nm diameter with four fused phenyl and pyrrole subunits through aza bridges. The Pc macromolecule is also able to coordinate various metal cations (Fe, Ni, Co, etc.) in its center with the four central nitrogens belonging to the pyrrolic subunits. With iron, it is called iron-phthalocyanine (FePc) [5]. FePc, known for high symmetry, planarity, and electron delocalization, is a porphyrin derivative consisting of a central Fe atom bound to a π -conjugated ligand. It has attracted a great deal of attention due to a wide variety of potential applications. Phthalonitrile, as high-temperature polymers, demonstrates potential uses in a wide variety of applications such as composite matrices [6], adhesives [7], and electrical conductors [8-11]. In the last few years, phthalocyanines are being intensively studied as targets for optical switching and limiting devices, organic field effect transistors, sensors, light-emitting devices, low band gap molecular solar cells, optical information recording media, photosensitizers for photodynamic therapy, and nonlinear optical

materials [12, 13], among others. Phthalocyanines will burst also in a very near future into the nanotechnology field.

To date, phthalonitrile monomers with several structures have been synthesized and polymerized into thermosets and mainly used as conventional resin-based composite materials [14, 15]. 4,4'-Bis-(3,4-dicyanophenoxy) biphenyl (BPh) is one of phthalocyanines which has been effectively used as a matrix resin for composite formulations. Composite panels have been processed by conventional prepreg consolidation, resin infusion and filament winding methods using carbon tape [16], carbon fabric, and glass fabric [17, 18] as reinforcements. Because the initial resin melt viscosity is low (0.1–0.2 Pa.s), the phthalonitrile composites are amenable to process by a more cost-effective, resin transfer molding method. The mechanical properties and thermal-oxidative stabilities of BPh-based composites are superior to that of many state-of-the-art high-temperature composites. However the use of BPh as absorbing materials has not been reported yet.

In this chapter, BPh monomer and ferrocenecarboxaldehyde were employed to synthesize FePc via a series of high temperature sintering: 500, 700 and 900 °C. The FePc showed classical electromagnetic shielding properties after 500 °C sintering process but became a strong electromagnetic absorption material above 700 °C. Although conductivity can be controlled by temperature and the amount of the catalyst, the electromagnetic reflection properties seem to be independent of conductivity. From the viewpoint of the electromagnetic match theory, it can be concluded that the best electromagnetic match composites were obtained by a sintering process after 700 °C. Therefore we mainly focus on the microwave absorption properties of the FePc after 700 °C sintering process. Theoretical simulation for the microwave absorption using Cole-Cole semicircle theory agrees well with the experimental results: the microwave absorption of these composites can be mainly attributed to the dielectric loss rather than magnetic loss. Then we choose BPh resin as the vector of FePc (after 700 °C sintering process) absorbent to prepare FePc/BPh composites. After curing reaction, the FePc particles gave the composite with novel dielectric and microwave-absorbing properties and the mechanical properties of the resin were greatly improved. The high values of microwave reflection and mechanical

property suggest that the composite could be used as promising microwave absorbing materials.

This part of work has been published on the Journal of Materials Science, 2012, volume 47, issue 10, page 4473-4480.

6.2. Results and Discussion

6.2.1 Conductivity of the FePc after a series of high temperature sintering

Ordering and planarity are of paramount importance to optimize the electrical conductivity of a polymer system. Therefore individual polymer chains can be packed in an array to transport the charge carriers with minimum resistance through the π orbital of the polymer domains. In essence, the π orbitals permit the transmission of an electrical disturbance or carriers (electron and holes) along the backbone of a molecule, allowing the carriers to move vastly in that direction relative to inter-chain hopping [19]. During the pyrolysis of a polymer, there is a progressive increase in conjugation, and thus π orbital delocalization, owing to the development of planar, polycondensed rings [20]. The overall conductivity will depend on the movement of the charge carriers within the individual polycondensed rings and from one ring system to another. Inter-chain hopping and the lack of long distance ordering must play an important role in the higher resistance to carrier flow of the pregraphite molecules relative to planar, two-dimensional graphite molecules [21, 22]. Figure 6.1 shows the SEM patterns of the FePc after 500 °C (S500), 700 °C (S700), 900 °C (S900) sintering for 4 h. It can be seen that at relative low temperature, the material showed a typical layer structure morphology. As the temperature increased, the ordered layer structure morphology gradually changed to two-dimensional graphite. There was also a progressive increase in the geometric symmetry of the samples.

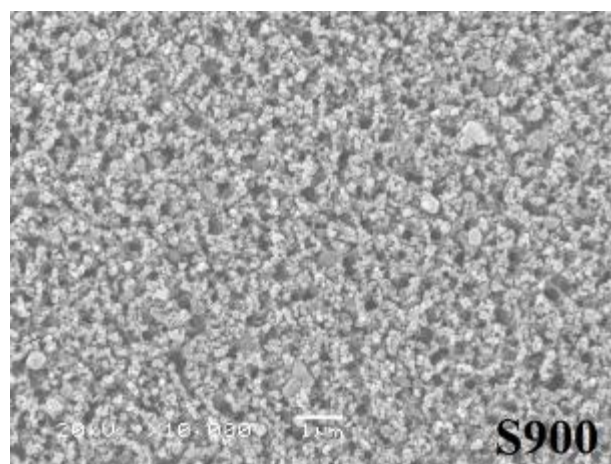
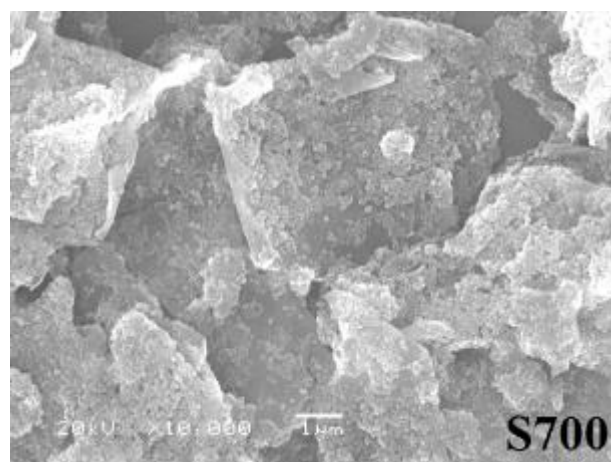
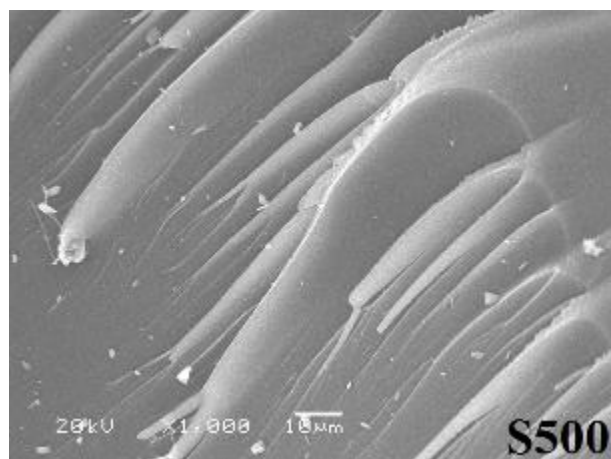


Fig. 6.1 Typical SEM images of the FePc pyrolyzed at various temperatures (S500, S700 and S900).

The electrical conductivity of S500, S700 and S900 were controlled by the pyrolysis conditions. When the iron phthalocyanine polymer was heated to temperature above 500 °C, it started to exhibit conductivity. According to Fig. 6.2, at 500 °C polymer S500 had a conductivity of approximately 10^{-8} S cm⁻¹. When heated at 700 °C for 4 hours, S700

exhibited a conductivity of $10^{-4} \text{ S cm}^{-1}$. At higher temperature $900 \text{ }^\circ\text{C}$, the enhancement in conductivity was significant. After being heated at $900 \text{ }^\circ\text{C}$ in nitrogen for 4 hours, polymer S900 exhibited a conductivity of $10^{-2} \text{ S cm}^{-1}$. In general, most of the stealth materials use dielectric materials as the matrices and the latter must meet two functions: one is to provide a channel for the transmission of electromagnetic waves and the other is to meet the impedance matching function. To meet these two functions, the conductivity of the dielectric material must be in the range of $10^{-4} \sim 10^{-18} \text{ S cm}^{-1}$. According to the analysis above, S500 and S700 meet the conditions. However the thermal/oxidative stability of the phthalocyanine polymer is superior. From Fig. 6.1 it can be seen that S500 still maintains the typical layer structure of phthalocyanine polymer but does not have the functionality as an absorbing material. Moreover, the carbonation level of S900 is too high. Its resistivity is significantly lower than the above-mentioned range, so it is not suitable as an absorbing material either. Therefore, we mainly focus on the microwave absorption properties of the FePc a using the $700 \text{ }^\circ\text{C}$ sintering process.

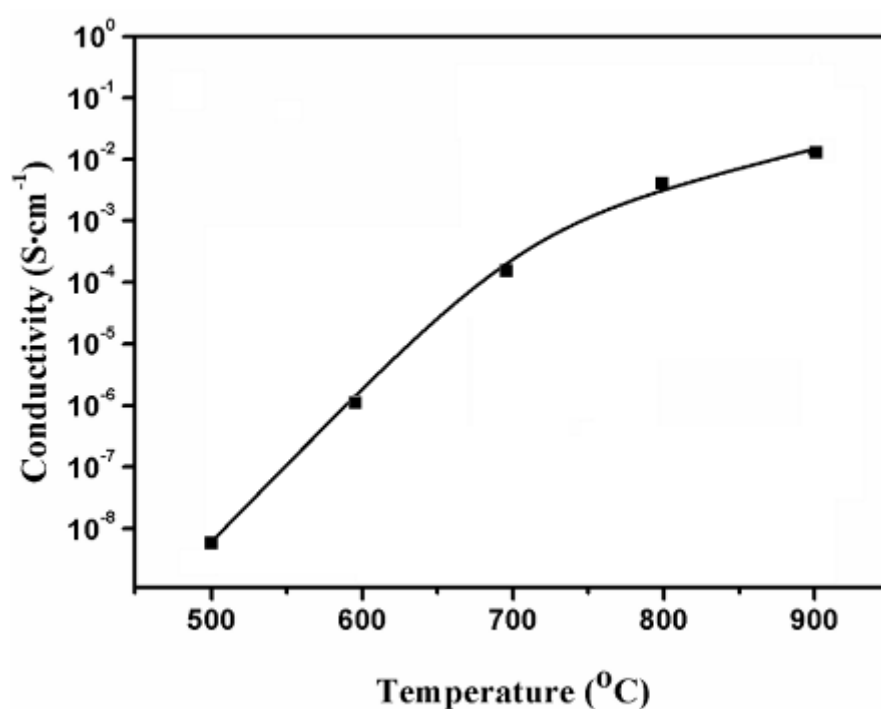


Fig. 6.2 Conductivity of the FePc after a series of high temperature sintering

The conductivity phenomenon in metal phthalocyanine-based polymers was due to the organization of the macro-cycle molecular at supramolecular level with an extended orbital

overlap along the conducting pathway. With the temperature of the pyrolysis increased, the organization of the macro-cycle molecular at supramolecular level along the conducting pathway was more ordered. Fig. 6.3 shows XRD patterns of the three samples pyrolyzed at various temperatures. Diffraction peaks that can be assigned to iron metal and cementite (Fe_3C) were observed above 700 °C. These diffraction peaks became stronger in the sample S900 pyrolyzed at even higher temperature. These observations suggest that iron-based phthalocyanine polymers had decomposed at around 700 °C and formed Fe metal and carbide at high temperature pyrolysis progress. In addition, relatively sharp peaks were observed at 26.0° from samples S700 and S900 at 700 °C and 900 °C, suggesting the formation of turbostratic carbon. From the XRD patterns, sharper peak of S900 than S700 or S500, also indicates that there was a progressive increase in conjugation and development of planar, polycondensed rings, which was in accord with the increase in the conductivity properties of the samples. Although the electrical resistivity and the dielectric loss properties of the composites depended on sintering temperature (500 °C, 700 °C, 900 °C), the best electromagnetic match composite was still obtained using the 700 °C sintering process.

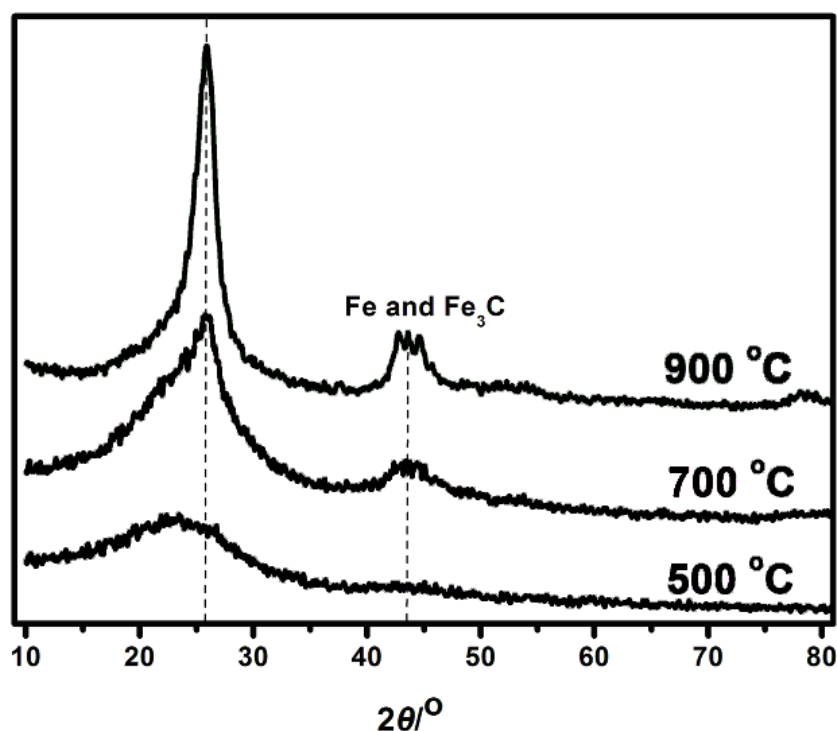


Fig. 6.3 XRD patterns of S500, S700 and S900 samples

6.2.2 Microwave absorption properties of the iron- phthalocyanine (S700)

The S700 sample used for microwave electromagnetic measurements was prepared by homogeneously mixing with wax in a mass ratio of 3:1. From the Fig. 6.4 (a), within the measurement frequency range, the ε' value fluctuated between 24 and 14 while the ε'' value fluctuated between 12 and 2. In the frequency range of 2~9 GHz, the ε' decreased with increasing the frequency. Additionally, the presence of a minimum ε' value (8.60) around 9 GHz was observed. When the frequency was further increased, the ε' spectrum started to rise and retain an approximate constant over the frequency range of 10~18 GHz. Such different ε' behaviors of conducting phthalocyanine in the frequency range of 3~9 GHz and 9~18 GHz have not been given in other papers mentioned above.

To our best knowledge, there are many factors contributing to dielectric properties: dielectric relaxation, resonance, the motion of conduction electron, defects in the materials, length, diameters, chirality, etc [23]. Therefore, it will be extremely difficult to describe the permittivity dispersion behaviors of FePc when taking into account of all these factors. Here, we assume that only two mechanisms made major contributions to the permittivity dispersion of FePc. One is the general permittivity behaviors of dielectric materials which can be described by the Cole-Cole model such as electrons polarization, charges polarization, etc. The other one is due to the motion of conducting electrons [24-26].

Conventionally, the permittivity can generally be represented by the Debye dipolar relation expression:

$$\varepsilon_r = \varepsilon_\infty + \frac{\varepsilon_s - \varepsilon_\infty}{1 + j2\pi f\tau} = \varepsilon'(f) + i\varepsilon''(f) \quad (6-1)$$

Where f , τ , ε_s and ε_∞ were the frequency, relaxation time, stationary dielectric constant, and optical dielectric constant, respectively. From Eq. (6-1), it can be deduced that:

$$\varepsilon'(f) = \varepsilon_\infty + \frac{2\pi f\tau(\varepsilon_s - \varepsilon_\infty)}{1 + (2\pi f)^2 \tau^2} \quad (6-2)$$

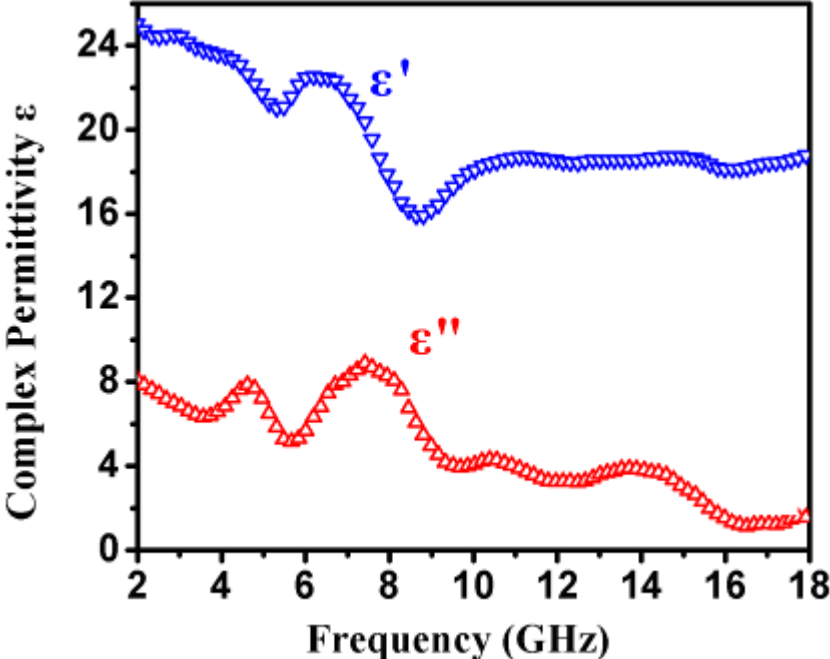
$$\varepsilon''(f) = \frac{2\pi f\tau(\varepsilon_s - \varepsilon_\infty)}{1 + (2\pi f)^2 \tau^2} \quad (6-3)$$

According to Eqs. (6-2) and (6-3), $(\varepsilon' - \varepsilon_\infty)^2 + (\varepsilon'')^2 = (\varepsilon_s - \varepsilon_\infty)^2$, and the plot of ε' versus ε'' would be a single semicircle, which is usually defined as Cole-Cole semicircle. Fig. 6.4 (c) showed the curve characteristics of ε' versus ε'' for the S700 sample. It was worthy to note that the S700 sample presented three segment of semicircles, the presence of three semicircles suggested that there were triple dielectric relaxation processes, and each semicircle corresponds to a Debye dipolar relaxation.

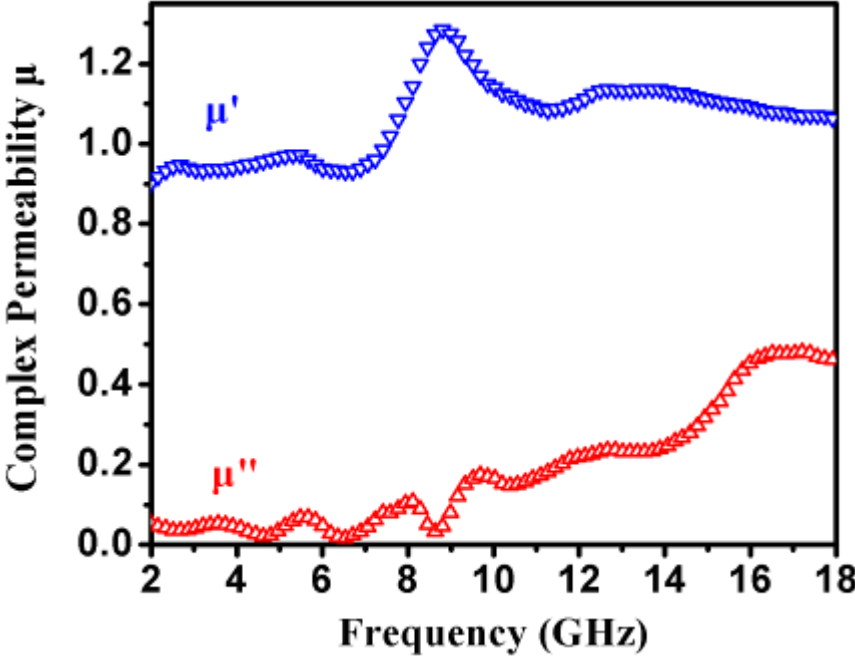
The sole relaxation process of S700 may arise as followings: under the alternating electromagnetic field, the lag of induced charges which countered the external applied field resulted in the relaxation and transferred the electromagnetic energy to heat energy, so the microwave was attenuated [27-29]. Because of numerous delocalized electrons in FePc, this dielectric relaxation process was obvious and a big Cole-Cole semicircle (the first semicircle) emerged as shown in Fig. 6.4. Hence, the dielectric relaxation is the main reason for FePc to absorb microwave. The additional two relaxation processes (the second and third semicircles) of S700 sample were obviously arising from defects and groups. Defects can act as polarization centers would generate polarization relaxation under the altering electromagnetic field and attenuate electromagnetic wave which resulting a profound effect on the loss of microwave. From the microwave permittivity loss ($\varepsilon''/\varepsilon'$) in Fig. 6.4 (d), three peaks of the S700 sample showed at the frequency of 4.5, 7.9 and 14.0 GHz, which were very according with the triple dielectric relaxation processes. The three dielectric relaxation processes also lead to the dual-frequency microwave absorption properties in the reflection loss simulation. Thus, theoretical simulation for the microwave absorption by Cole-Cole semicircle theory agrees well with the experimental results.

Fig. 6.4 (b) also exhibited the permeability real part (μ') and imaginary part (μ'') of the S700, which demonstrated that both μ' and μ'' of the sample were very low due to the weak magnetic characteristic. The real part of permeability showed a peak around the frequency of 10.0 GHz, and the maximum value of μ' was 1.40. The value of imaginary part was no more than 0.2 over the frequency range of 2~10.0 GHz, as the positive imaginary part of μ'' was often used to manifest the magnetic energy loss, such low value of the μ'' assumed the

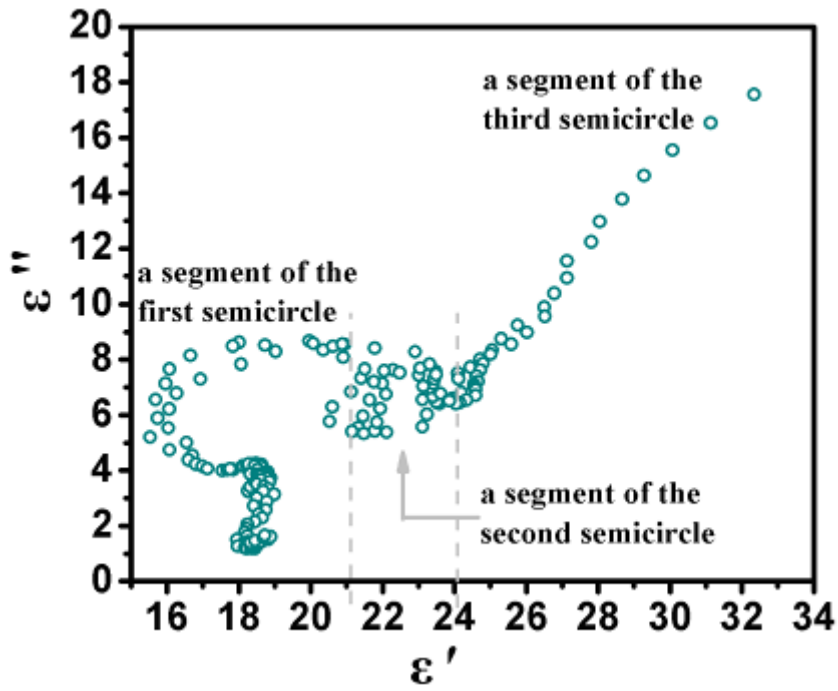
microwave absorption of S700 can be mainly attributed to the dielectric loss rather than magnetic loss.



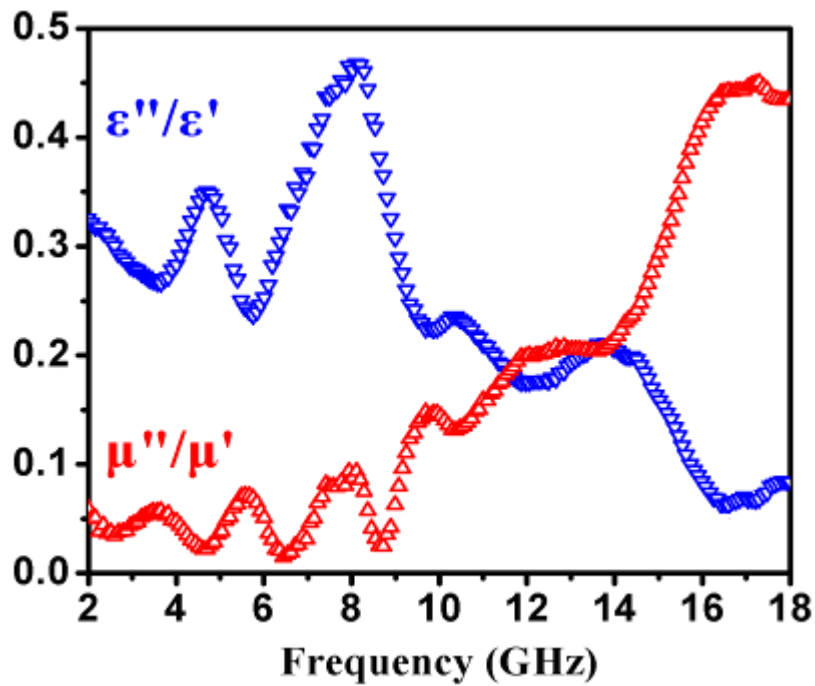
(a)



(b)



(c)



(d)

Figure 6.4 Microwave permittivity and permeability properties of S700.

- (a) complex permittivity (b) complex permeability
- (c) Typical Cole-Cole semicircles (ϵ'' versus ϵ')
- (d) permittivity loss tane (ϵ''/ϵ') and permeability loss tanu (μ''/μ')

Based on the measured data of the complex permittivity and permeability, if it is assumed that single layer of sample/wax composite was attached on a metal plate, then the electromagnetic wave absorption properties usually can be evaluated by the following equation (6-4):

$$RL = 20 \log \left| \frac{Z_{in} - Z_0}{Z_{in} + Z_0} \right| \quad (6-4)$$

Where the RL denoted the reflection loss in decibel unit, Z_0 was the impedance of free space, and Z_{in} was the input characteristic impedance at the absorption/air interface, which can be expressed as equation (6-5):

$$Z_{in} = Z_0 \sqrt{\frac{\mu_r}{\epsilon_r}} \tanh[j(2\pi ft / c) \sqrt{\mu_r * \epsilon_r}] \quad (6-5)$$

Where c was the velocity of light and t was the thickness of an absorber. Here t values were in millimeter unit. μ_r and ϵ_r were the measured relative complex permeability and permittivity, respectively.

The calculated frequency dependence reflection loss of the S700 with different thickness was shown in Fig. 6.5. It can be noted that reflection loss peaks were shifted to a low frequency along with the sample thickness increased from 1.5 mm to 5.0 mm, when the thickness was 1.5 mm, the reflection loss reached its maximum value of -23.0 dB around 11.0 GHz and the frequency band wide at -10.0 dB was more than 2 GHz. Interestingly, when the S700 sample thickness was more than 3.0 mm, two loss peaks was presented as shown in Fig. 6.5 (A), while below the thickness 2.5 mm, only one loss peak were exhibited. From the dielectric relation processes discussion above, the dual-frequency microwave absorption of the S700 sample may be due to the lag of the polarization between the polymer and iron metal interfaces.

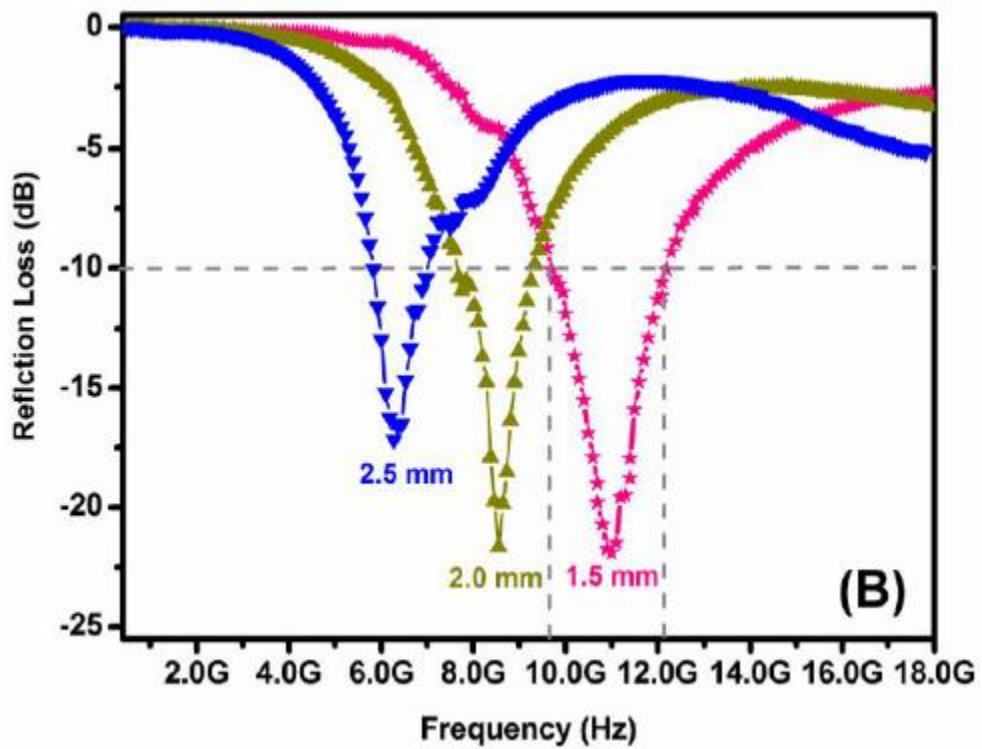
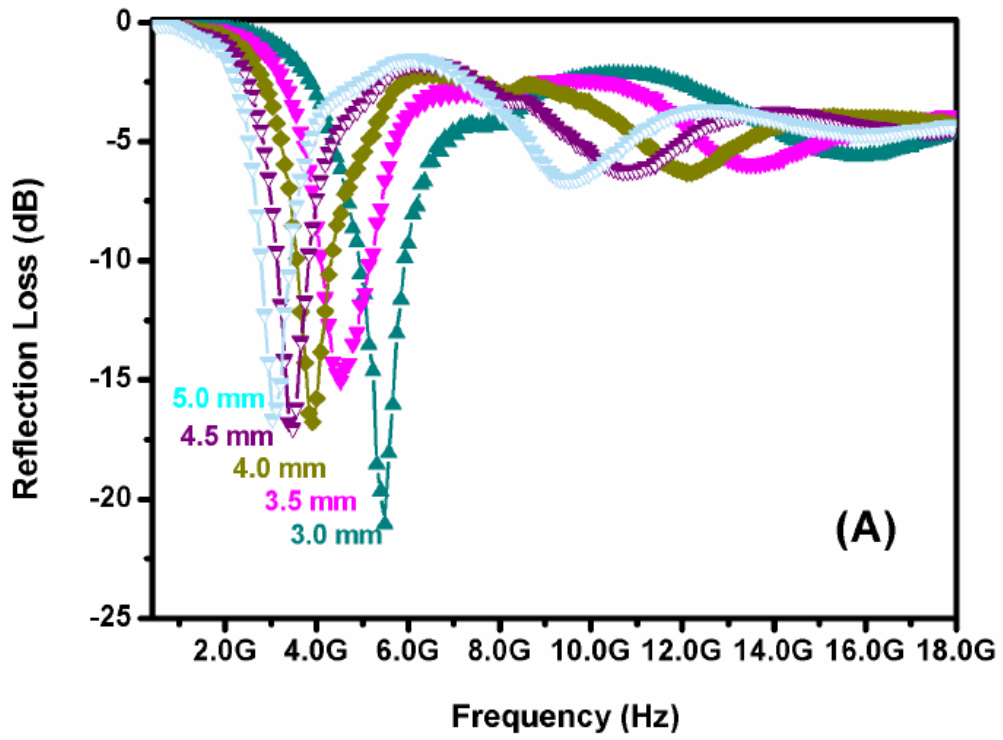


Fig. 6.5 Microwave reflection loss of S700 with different layer thicknesses.

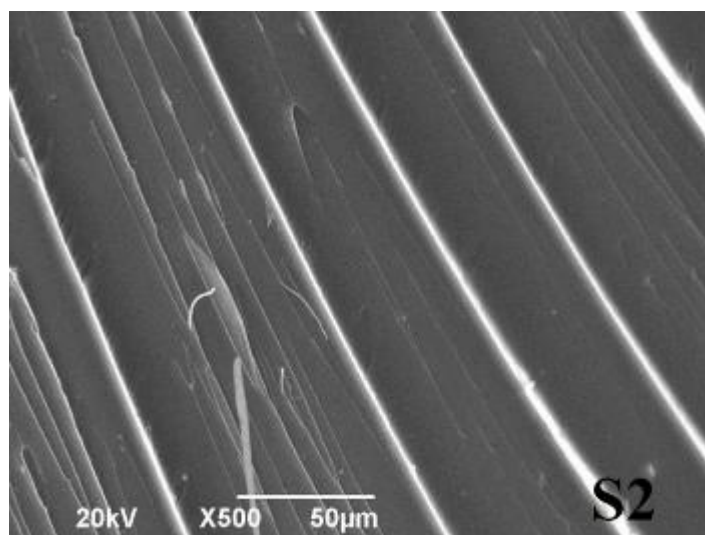
(A) double loss peaks

(B): single loss peak

6.2.3 The effect of catalysis amount on the microwave absorption properties of FePc after 700 °C sintering

The effect of different amount of ferrocenecarboxaldehyde, which acted as the kind of catalyst to crosslink the phthalonitrile molecular, on the final microwave electromagnetic properties of the iron doped conducting phthalocyanine polymer has also been studied in this manuscript. During the experimental section, the ferrocenecarboxaldehyde with the amount of 2 wt%, 0.3 wt% and 0.6 wt% have been added to obtain the three iron phthalocyanine oligomers, the further polymerization and pyrolysis of the iron phthalocyanine oligomers to get the FePc at 700 °C. The three samples with different catalysis loading were labeled as S2, S3 and S6.

From the SEM patterns (Fig. 6.6), at relative low catalysis loading (2 w%), the materials showed the typical layer structure of phthalocyanine polymer, and with the ferrocenecarboxaldehyde content increased the carbonization degree of the materials also increased. From Fig. 6.6 S3, it is to know that with 6 wt% catalysis loading the ordered layer structure of the materials changed to two-dimensional graphite structure.



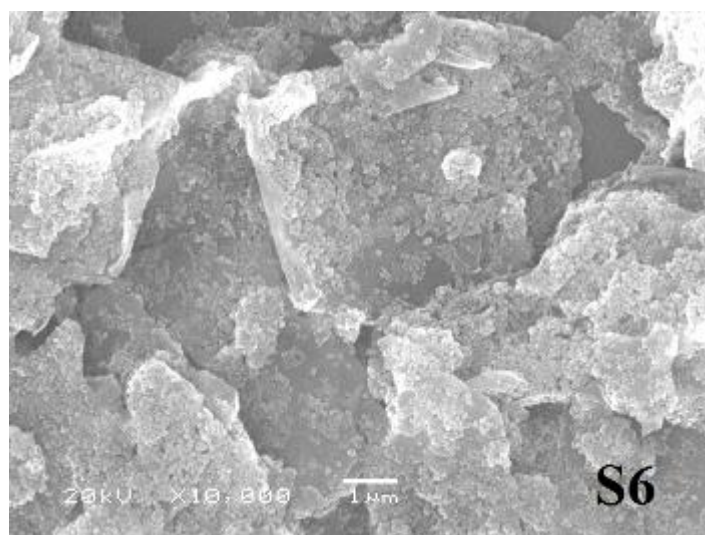
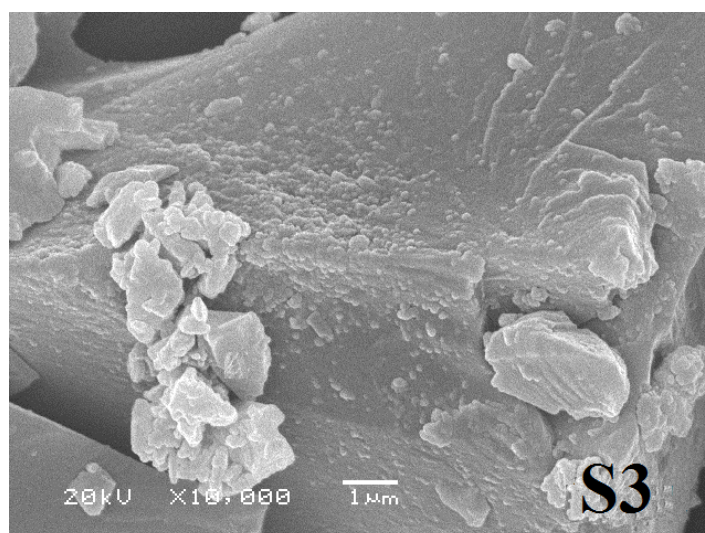


Fig. 6.6 SEM images of the FePc with different amount catalysis loading (pyrolyzed at 700 °C).

The XRD patterns (Fig. 6.7) showed the same peaks belonged to the iron metal and cementite also appeared, these observations suggested that iron-based phthalocyanine polymers had decomposed at around 700 °C and formed Fe metal and carbide at high temperature pyrolysis progress. In addition, relatively sharp peaks were observed at 26.0° from samples S2 to S6, suggesting the formation of turbostratic carbon. From the XRD patterns, more sharper peak of S6 than S3 or S2, also indicted the there was a progressive increase in conjugation and development of planar, polycondensed rings, which was accord with the increased in the dielectric loss properties of the materials.

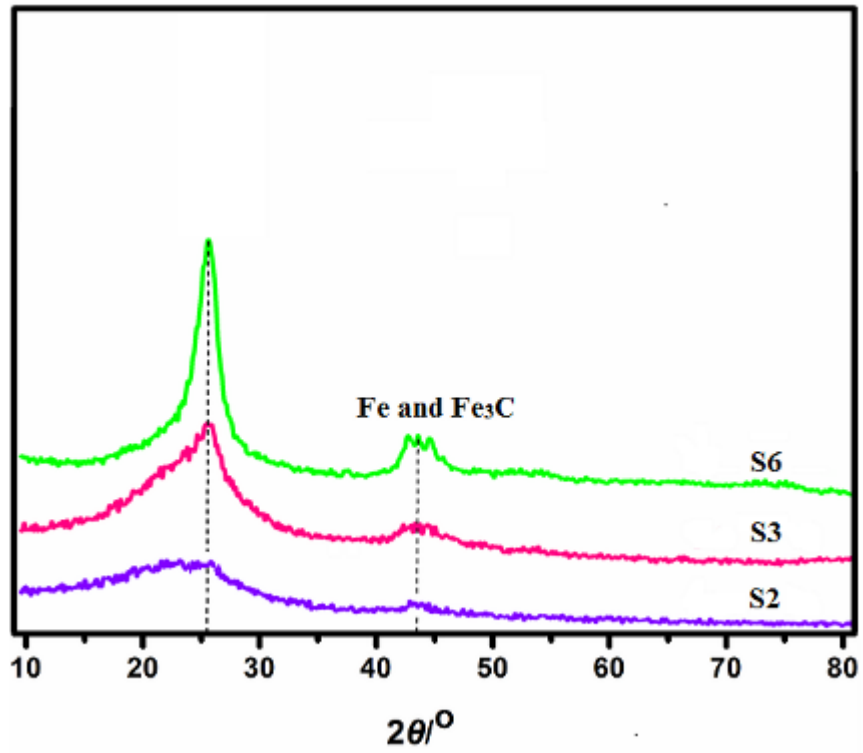
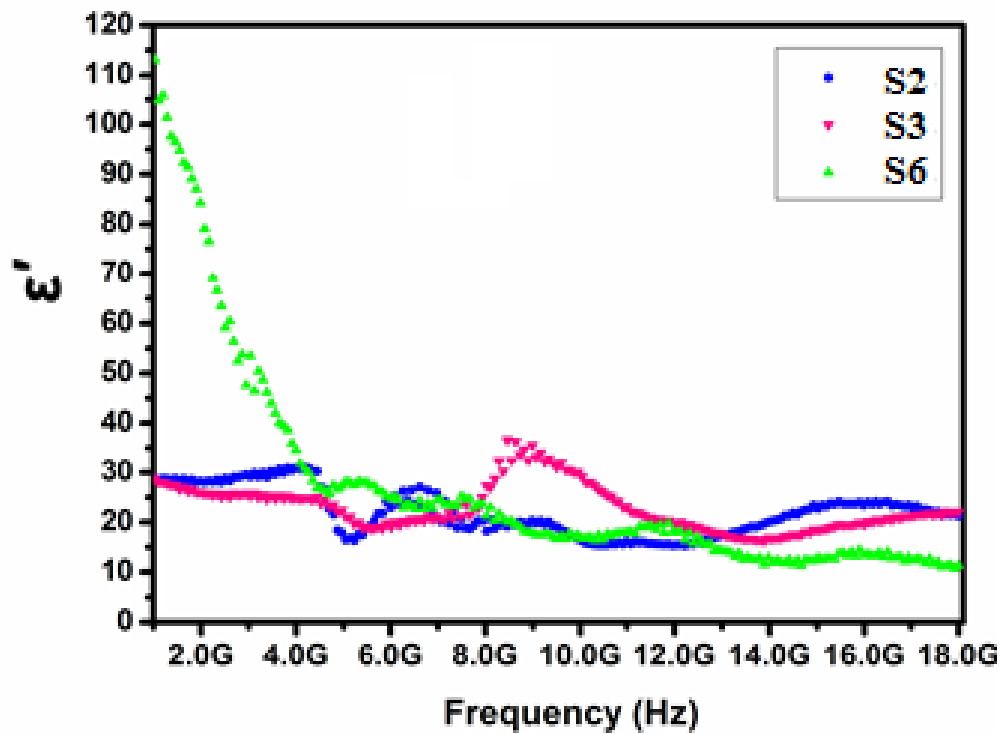
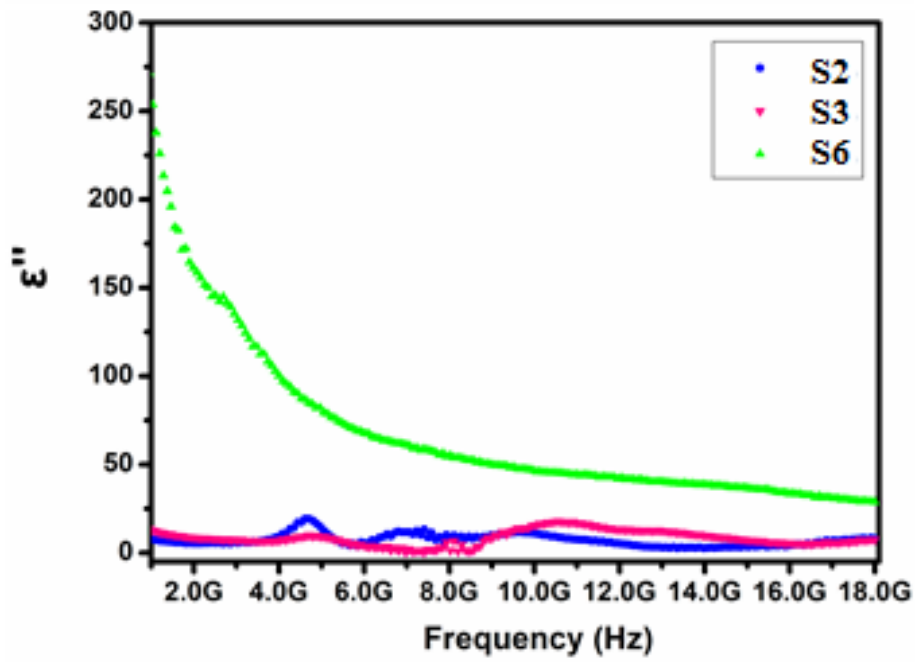


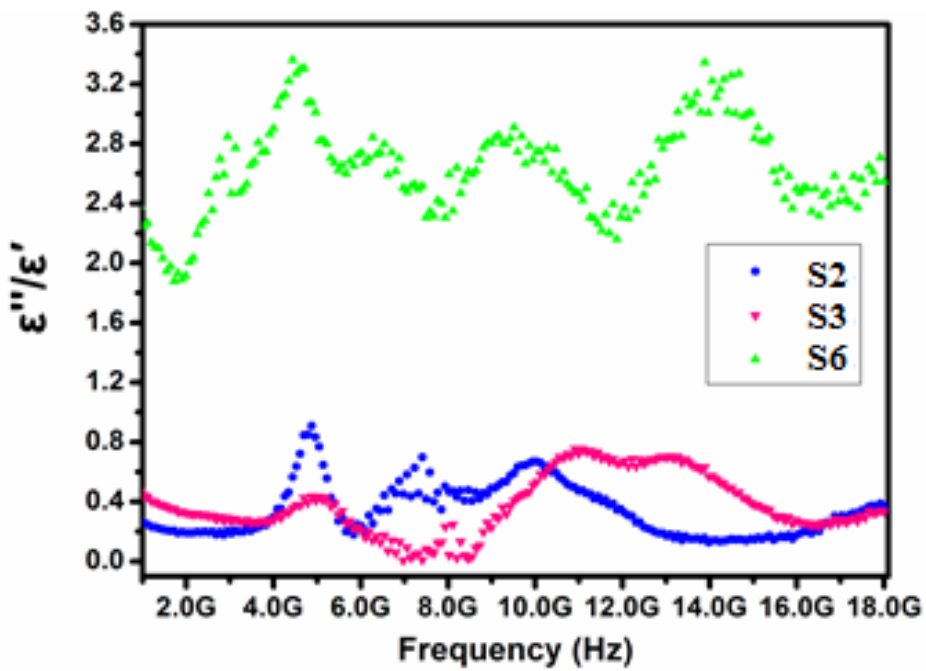
Fig. 6.7 XRD patterns of sample S2, S3 and S6



(a)



(b)

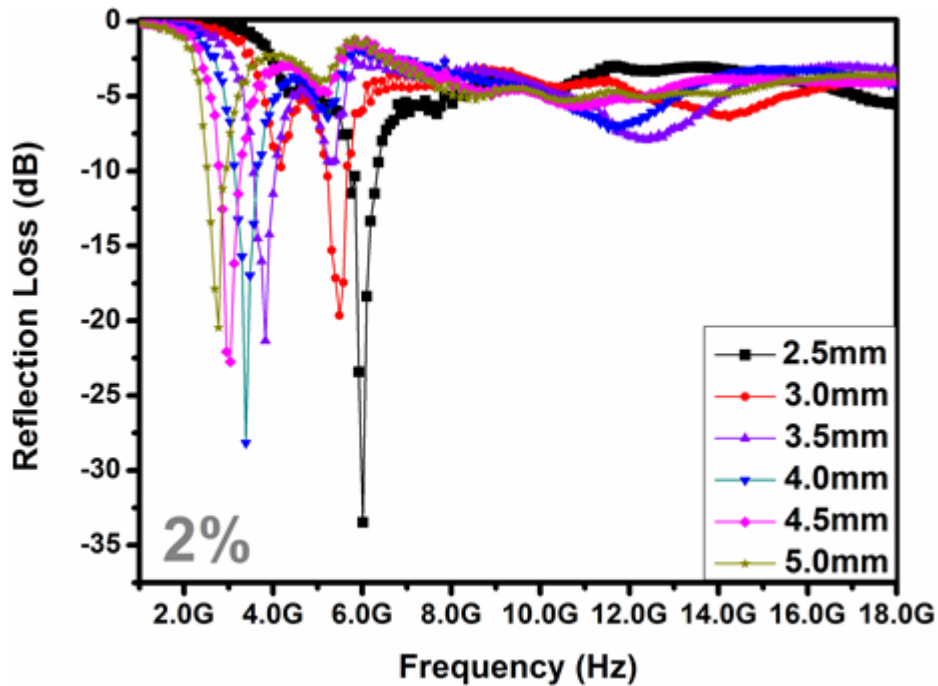


(c)

Fig. 6.8 Dielectric properties of S2, S3 and S6

- (a) Permittivity (ϵ')
- (b) Permittivity (ϵ'')
- (c) Dielectric loss (ϵ''/ϵ')

From the Fig. 6.8, the S6 exhibited a very high value of the permittivity, the value of the dielectric loss ($\tan\epsilon=\epsilon''/\epsilon'$) was 2.0~3.6, and indicated the S6 was a kind of conducting material, different as S2 or S3, the conductivity of S6 is in the semiconductor regime, so the microwave of S6 preferred to reflection properties, not absorption properties. The reason why materials with different catalyst loading showed different sintering properties and how they affected the final microwave properties were not very clear at present, we assumed that with the more loading of the catalysis, the higher crosslink of the phthalonitrile molecular was come to planar, polycondensed rings, as the overall conductivity will depend on the movement of the charge carriers within the individual polycondensed rings and from one ring system to another, the highly crosslink of the phthalonitrile molecular would be high permittivity materials.



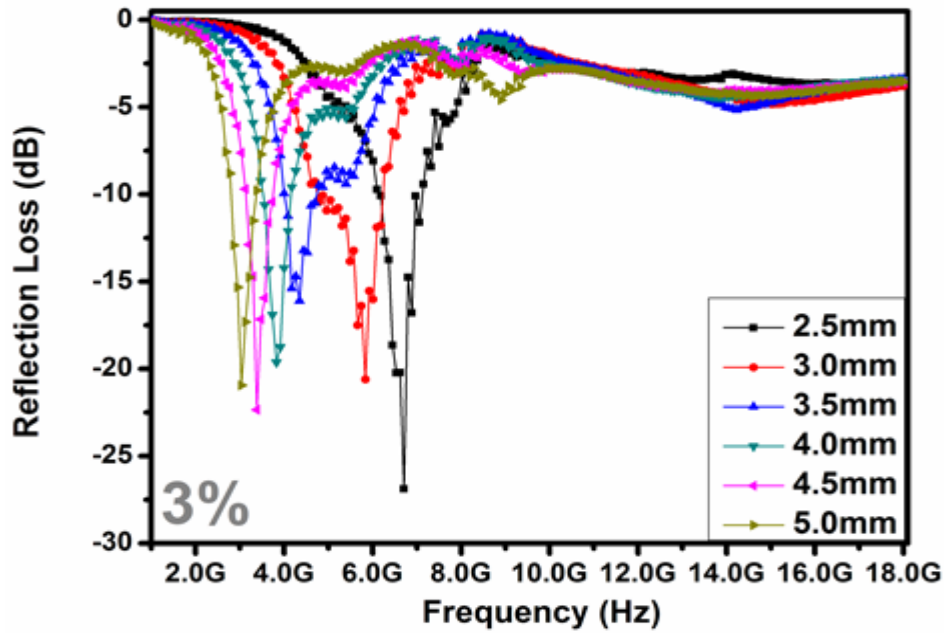


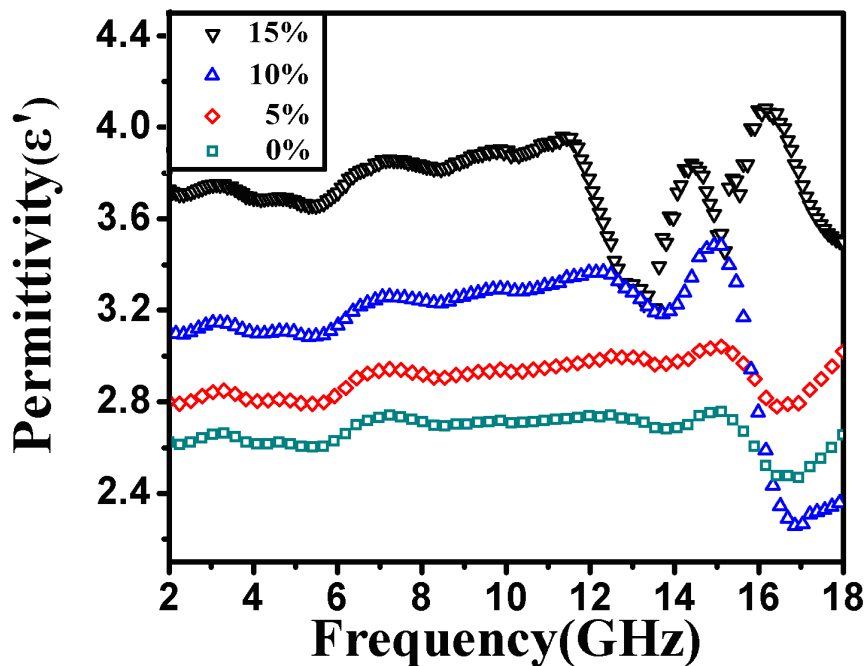
Fig. 6.9 Microwave reflection loss of S2, S3 with different layer thicknesses.

The calculated frequency dependence reflection loss of the S2 and S3 with different thickness was shown in Fig. 6.9 It can be noted that reflection loss peaks shifted to a low frequency along with the sample thickness increased from 2.5 mm to 5.0 mm, when the thickness was 2.5 mm, the reflection loss reached the maximum value of -30.0~-35.0 dB at the frequency of ~6.0 GHz. Interestingly, when thickness of S2 and S3 samples was more than 3.5 mm, another loss peaks was presented at the high frequency range of 12.0~14.0 GHz. From the dielectric relation processes discussion above, the dual-frequency microwave absorption of the samples may due to the lag of the polarization between the polymer and iron metal interfaces.

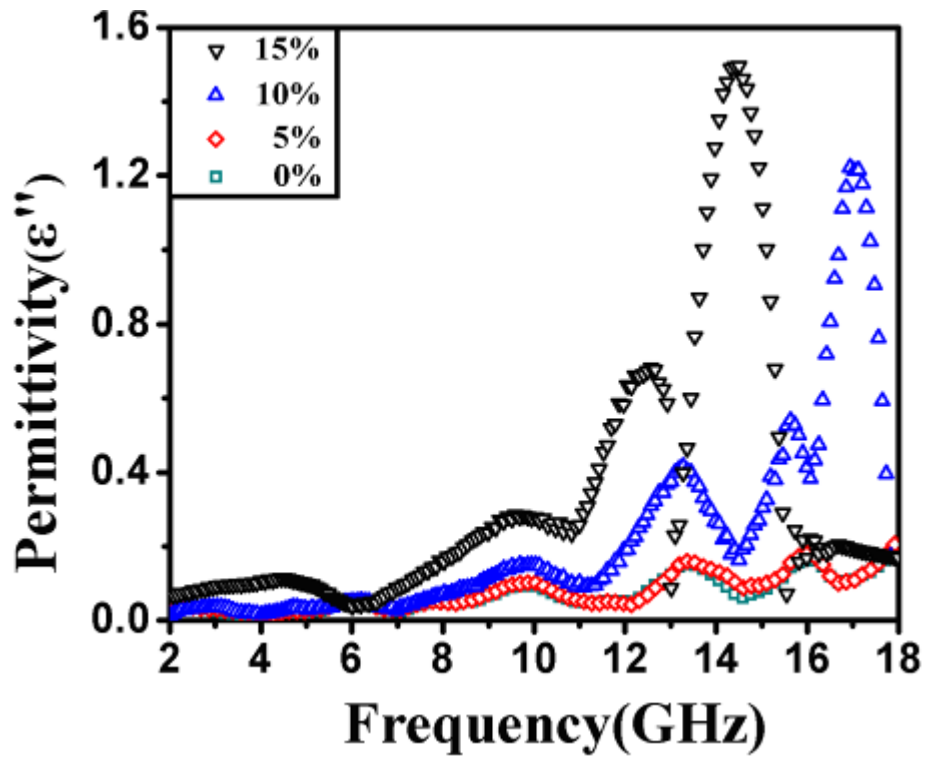
6.2.4 Dielectric and microwave absorption properties of the FePc/BPh composites

The FePc/BPh composite sample used for microwave electromagnetic measurements was firstly ball-milled into powder and then prepared by homogeneously mixing with wax in a mass ratio of 3:1. Fig. 6.10 shows the microwave permittivity and permeability properties of FePc/BPh composites with various FePc contents. The real part (ϵ') and imaginary part (ϵ'') of relative complex permittivity of the FePc/BPh composite was improved with the increment of FePc. The FePc/BPh composites with 15% FePc content exhibited highest value of the permittivity. Within the measurement frequency range, the ϵ'

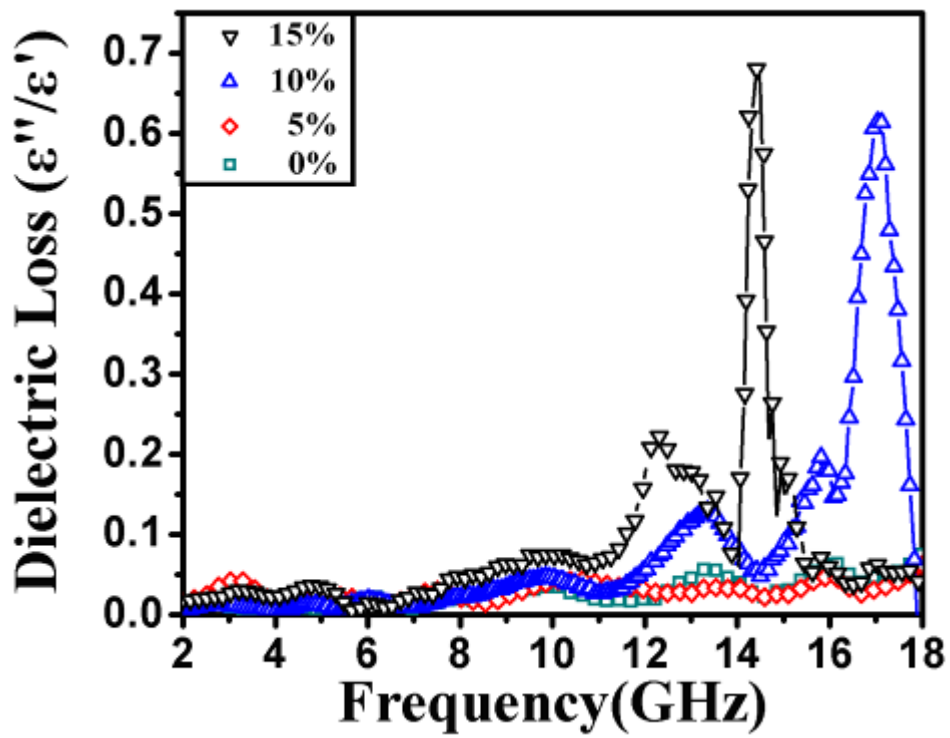
value and ε'' value of the FePc/BPh composites with 15% FePc content fluctuates between 3.2 ~ 4.1 and 0.1 ~ 1.5 respectively. But the ε' and ε'' values of the pure BPh resin were much lower. The higher value of permittivity was due to the contribution of the high performance FePc powder in this complex system. The fluctuation pattern of the permeability of FePc/BPh composites with different FePc contents were not consistent with permittivity properties showed. In the frequency range of 11.0 ~ 15.5 GHz, the FePc/BPh composites with 15% FePc content exhibited highest value of μ' and μ'' , and two peaks were found at 13 GHz and 15 GHz. But in the frequency range of 15.5 ~ 18GHz the composites with 10% FePc content exhibited highest value of μ' and μ'' , and one peak was found at 17 GHz. Figure 4 also shows the microwave dielectric loss and magnetic loss of FePc/BPh composites. The fluctuation pattern of the dielectric and magnetic loss of the FePc/BPh composites with 15% and 10% FePc content were same as the permeability property result. In the frequency range of 7.0 ~ 15.5 GHz, the microwave dielectric and magnetic loss of the composites with 15% content were the highest, only in a narrow frequency range of 15.5~18 GHz, the composites with 10% content were higher than 15% content. To conclude, the FePc/BPh composites with 15% FePc content showed the best electromagnetic properties.



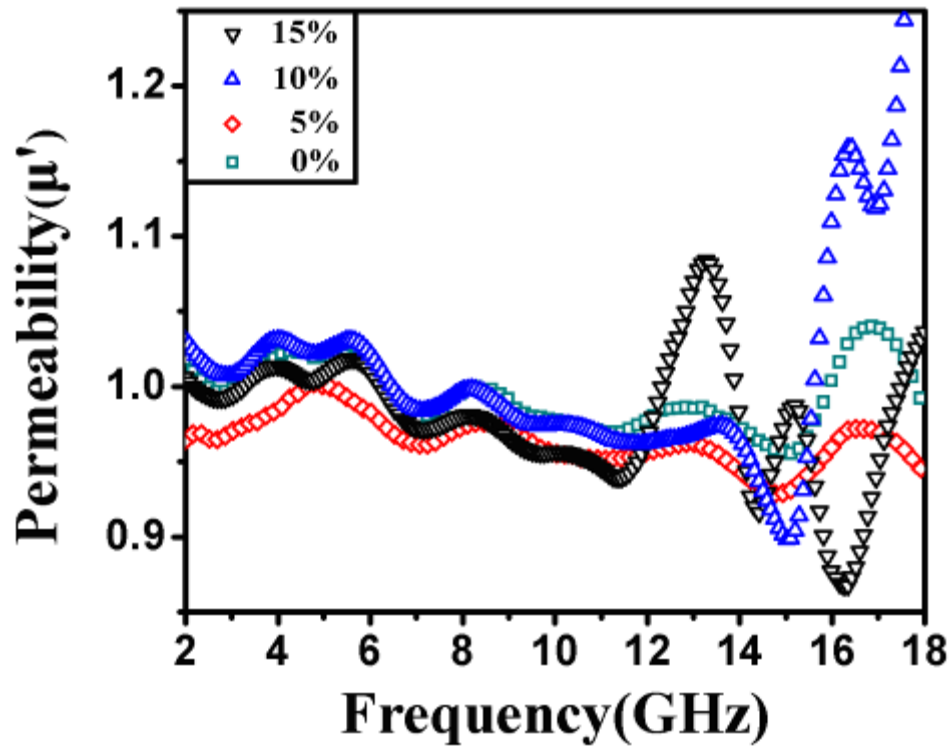
(a)



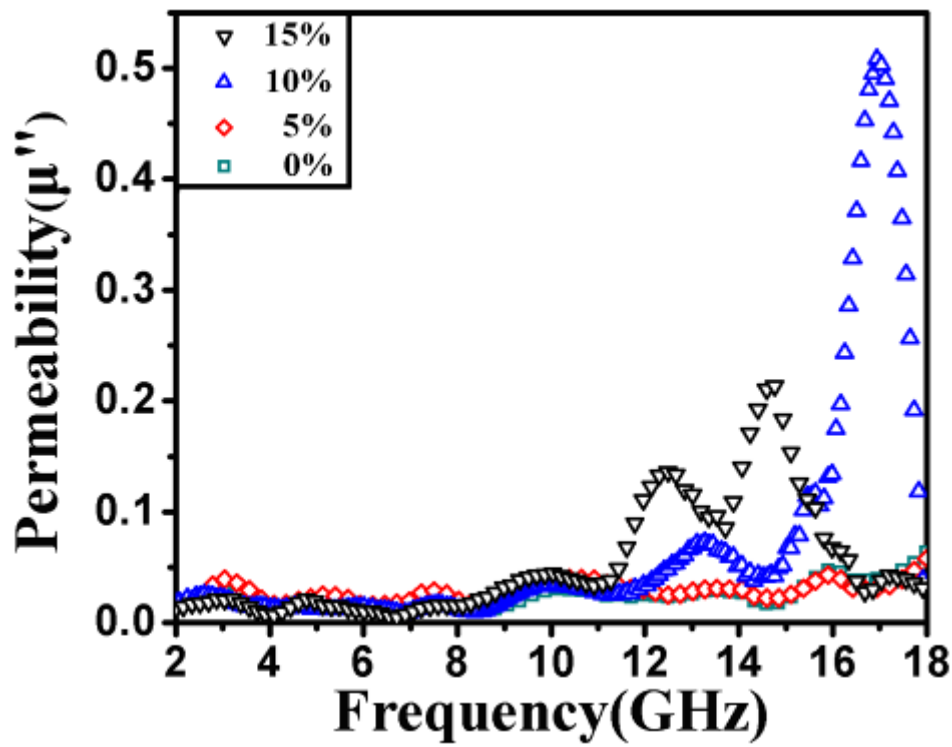
(b)



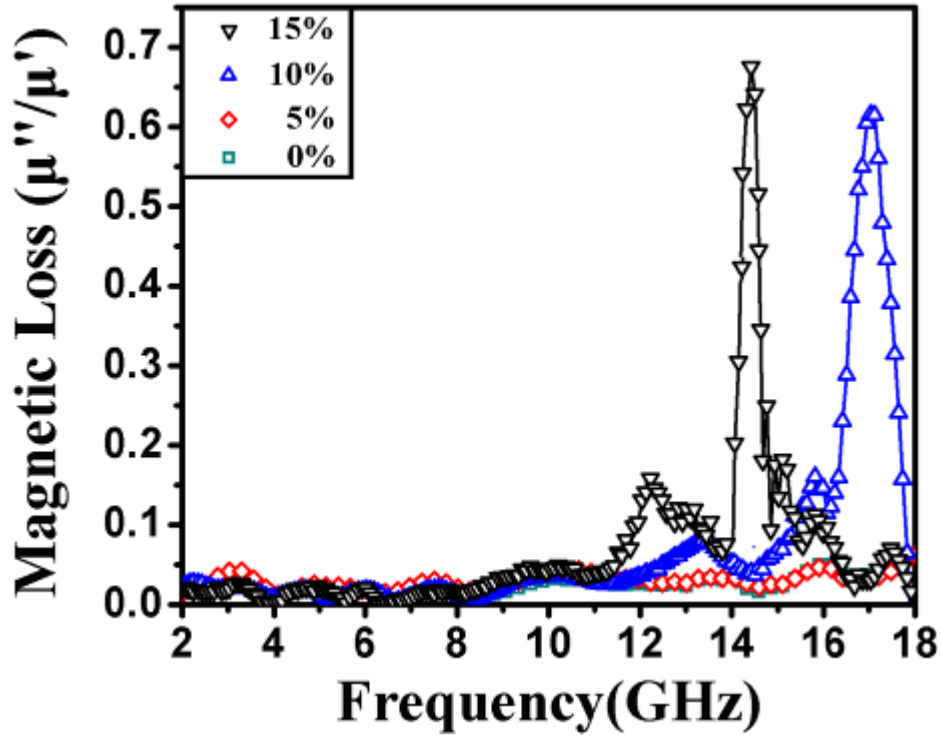
(c)



(d)



(e)



(f)

Fig. 6.10 Dielectric properties of FePc/BPh composites with different FePc content.

- (a) Permittivity (ϵ') (b) Permittivity (ϵ'') (c) Dielectric loss (ϵ''/ϵ')
 (d) Permeability (μ') (e) Permeability (μ'') (f) permeability loss (μ''/μ')

We choose the FePc/BPh composite with 15% FePc content to study its microwave absorption properties. The calculated frequency dependence reflection loss of the the FePc/BPh composite with 15% FePc content with different thickness was shown in Fig. 6.11. It can be noted that reflection loss was increased with the increment of the thickness less than 3.5 mm, when the thickness was 3.5 mm; the reflection loss reached the maximum value of -10.0 dB. At the frequency of 12.2 GHz and the frequency band wide at -10.0 dB was more than 3 GHz. It is also showed in Fig. 6.11 that the composite has three absorption peaks. Multi-peak absorption is very interesting, it may be due to the lag of the polarization between the polymer and the FePc particals or iron metal interfaces.

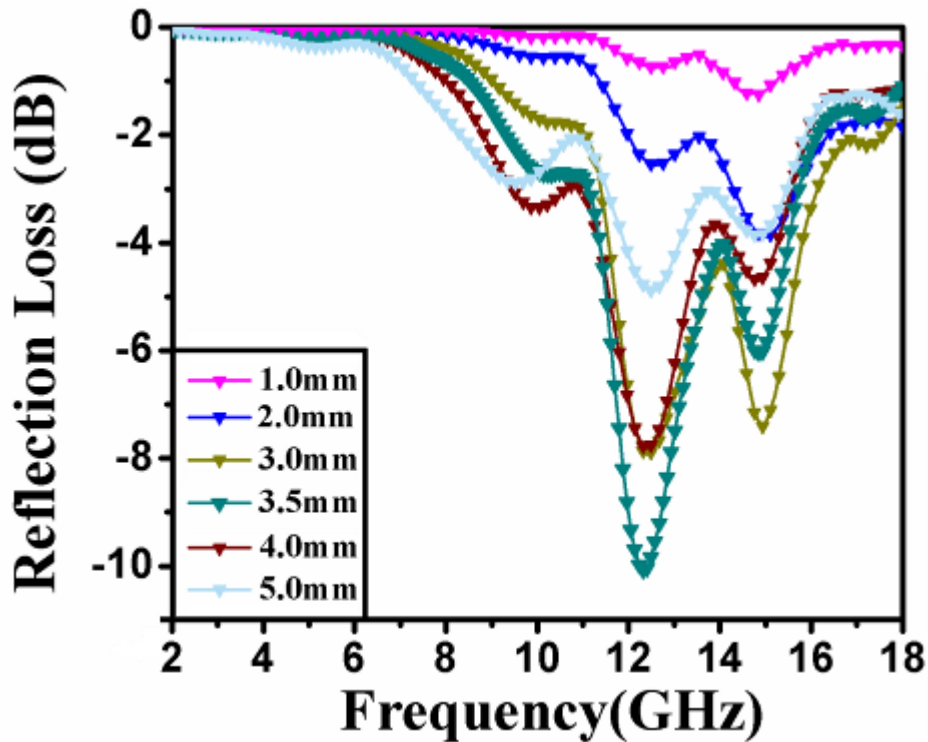


Figure 6.11 Microwave reflection loss of FePc/BPh composites

6.2.5 Mechanical properties of FePc/BPh composites

The mechanical properties of the composites with various FePc contents are shown in Fig. 6.12. It can be seen that the flexural strength and modulus of the composites are dramatically increased with FePc content. The flexural strength and flexural modulus of pure BPh resin is 83 MPa and 3.6 GPa respectively. Relative to neat BPh, addition of 5 wt% FePc particles results in about 10% increase in flexural strength and 6 % increase in flexural modulus. When the content of FePc particle reached 15 wt% the flexural strength and flexural modulus exhibit maximum values of 170 MPa and 5.4 GPa which are about 104% and 50% above those of pure BPh, respectively. It is well-known and commonly admitted that the mechanical properties of polymer composites, especially the modulus, depend to a great extent on filler dispersion and interfacial interaction, and are increased only when good dispersion of the filler and effective stress transfer at the polymer/filler interface are guaranteed [30]. In this sense, the improvements in the mechanical properties can also verify the uniform dispersion and good compatibility of FePc in the BPh matrix.

The FePc is Pc macromolecule coordinate iron cations in its center with the four central nitrogens belonging to the pyrrolic subunits but the peripheral functional groups were similar as Pc macromolecule. This is the basic reason of good compatibility of FePc in the BPh matrix and this is why we choose BPh monomer to prepared FePc first and then added into BPh to prepared for composites.

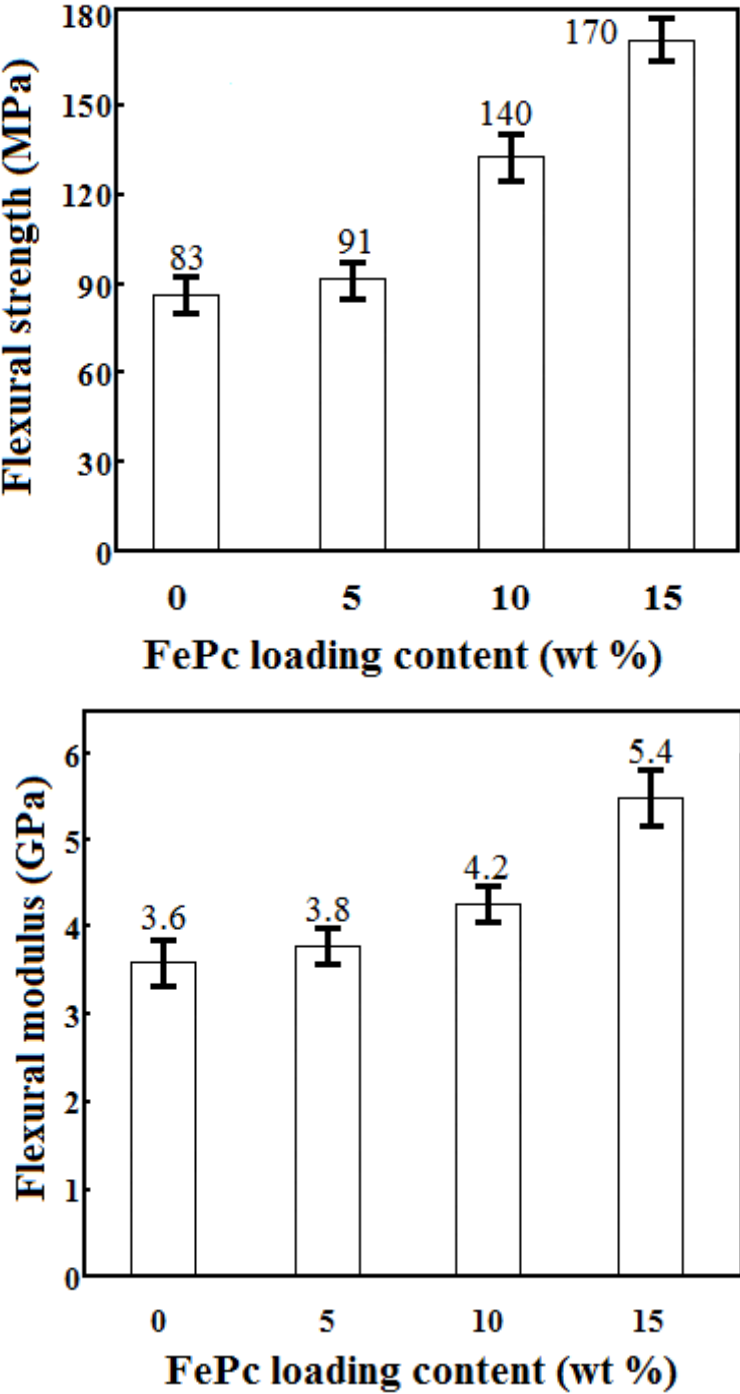
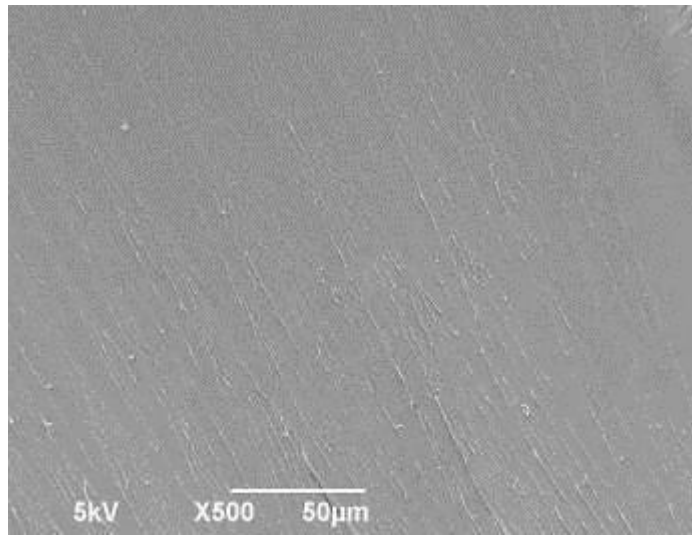
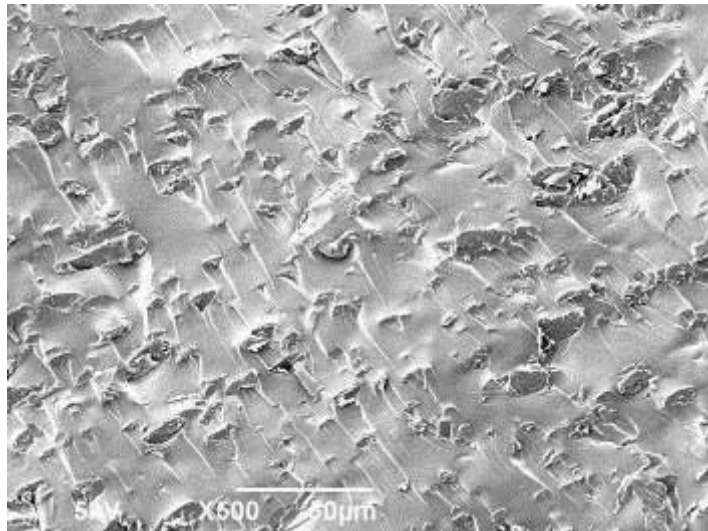


Fig. 6.12 Mechanical properties of FePc/BPh composites.

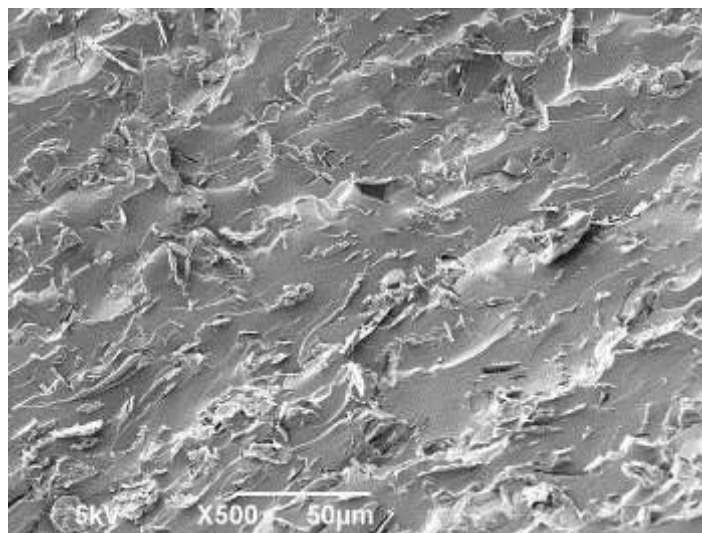
(Effect of FePc content on the flexural strength and flexural modulus of FePc/BPh composites).



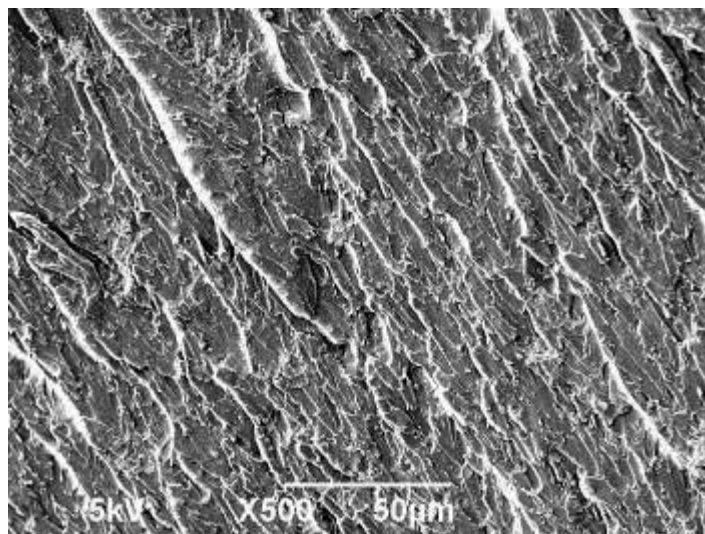
(a)



(b)



(c)



(d)

Fig. 6.13 SEM images of fracture surfaces of pure BPh and FePc/BPh composites

(a) Pure BPh

(b) BPh with 5 wt% of FePc

(c) BPh with 10 wt% of FePc

(d) BPh with 15 wt% of FePc

The fracture surfaces of the composites with various FePc contents in Fig. 6.13 also confirmed the enhancement of the mechanical performances investigated. The fracture surfaces of the pure BPh indicated a smooth, glassy and homogeneous microstructure without any plastic deformation. But in all the FePc/BPh composites it can be seen clearly that the FePc particles were dispersed uniformly in the BPh matrix. In addition, in the FePc/BPh composite with 15% FePc content (Fig. 6.13 (d)) the FePc particles are well coated by BPh resin and effective stress transfer at the FePc/BPh interface are thus guaranteed. According to the previous researches [31], good dispersion states can increase average aspect ratio of the fillers in the polymer matrix; as a consequence, mechanical properties were improved. Here apparently, FePc effectively reinforced mechanical properties of the BPh matrix due to their good dispersion states, good compatibility, combined with excellent mechanical properties of FePc itself.

6.3. Conclusions

In conclusion, FePc exhibits excellent microwave absorption properties in the

frequency range of 2.0~18.0 GHz after 700 °C sintering process. The FePc had a strong microwave absorbing peak at 11.0 GHz and achieved a maximum absorbing value of -23 dB at the thickness of 1.5 mm.

Theoretical simulation for the microwave absorption using Cole-Cole semicircle theory agrees well with the experimental results. The microwave absorption of these materials can be mainly attributed to the dielectric loss rather than magnetic loss. The FePc/BPh composites were also successfully prepared via a cost-effective, resin transfer molding method and characterized for mechanical, electromagnetic and microwave absorption properties.

FePc particles was successfully used as a reinforcing filler for BPh matrix composites. It was found that when the content of FePc particles reached 15 wt% the flexural strength and flexural modulus exhibit maximum values of 170 MPa and 5.4 GPa respectively. The FePc/BPh composites with high performance are believed to have potential uses in microwave absorbing materials.

More importantly, the applications of functional BPh resin based materials in the area of absorbing materials has been greatly enriched.

6.4 References

- [1] A. Ohlan, K. Singh, A. Chandra, S. K. Dhawan, *Appl. Phys. Lett.* 93 (2008) 053114-053116.
- [2] Y. J. Chen, *Appl. Phys. Lett.* 84 (2004) 3367-3369.
- [3] S. S. Kim, S. T. Kim, Y. C. Yoon, K. S. Lee, *J. Appl. Phys.* 97 (2005) 10F905-10F910.
- [4] De la G. Torre, M. Nicolau, T. Torres, In *Supramolecular Photosensitive and Electroactive Materials*. H. S. Nalwa, Ed. Academic Press: New York, 2001; p.1.
- [5] A. S. Milev, N. Tran, G. S. K. Kannangara, M. A. Wilson, I. Avramov, *J. Phys. Chem. C* 112 (2008) 5339-5347.
- [6] T. M. Keller, *Chem. Mater.* 6 (1994) 302-305.
- [7] T. M. Keller, C. M. Roland, US Patent. 5242755 (1993).
- [8] T. M. Keller, *Chemtech.* 18 (1988) 635-640.
- [9] T. M. Keller, *J Polym Sci: Part A: Polym. Chem.* 26 (1988) 3182-3199.

- [10] T. M. Keller, SAMPE Symp. 31 (1986) 528-529.
- [11] J. F. Guilani, T. M. Keller, Sens. Mater. 1 (1989) 2244-2247.
- [12] De la Torre, G, Vázquez, P. Agulló-López, T. Torres, J Mater Chem 8, (1998), 1671.
- [13] De la Torre, G. Vázquez, P. Agulló-López, T. Torres, Chem Rev 104, (2004), 3723.
- [14] T. M. Keller. Polym. Commun. 32 (1991) 2-4.
- [15] T. M. Keller, Polymer. 34 (1993) 949-952.
- [16] S. B. Sastri, J. P. Armistead, T. M. Keller, Polym. Compos. 17 (1996) 814-816.
- [17] S. B. Sastri, J. P. Armistead, T. M. Keller, U. Sorathia, Polym. Compos. 18 (1997) 45-48.
- [18] S. B. Sastri, J. P. Armistead, T. M. Keller, U. Sorathia, SAMPE Symp. Ser. 42 (1996) 1032-1038.
- [19] S. D. Bruck, Polymer, 6, (1965), 319.
- [20] L. Salem, C. Rowland, Angew. Chem. Int. Ed., 11, (1972), 92.
- [21] T. M. Keller, J. Am. Chem. Soc. Div. Polym. Sci. Eng., 52, (1985), 192.
- [22] T. M. Keller, J. Polym. Science: Part A: Polymer Chemistry, 25, (1987), 2569.
- [23] L. Deng, M. Han, Appl. Phys. Lett. 91 (2007) 023119-023121.
- [24] X. L. Dong, X. F. Zhang, H. Huang, F. Zuo, Appl. Phys. Lett. 92 (2008) 013127-013129.
- [25] R. B. Yang, C. Y. Tsay, D. S. Hung, W. F. Liang, Y. D. Yao, C. K. Lin, J. Appl. Phys. 105 (2009) 07A5280-07A5283.
- [26] A. N. Yusoff, M. H. Abdullah, S. H. Ahmad, S. F. Jusoh, J. Appl. Phys. 92 (2002) 976-978.
- [27] T. J. Imholt, C. A. Dyke, B. Hasslacher, J. M. Perez, D. W. Price, J. M. Roberts, J. B. Scott, A. Wadhawan, Z. Ye, J. M. Tour, Chem. Mater. 15 (2003) 3969-3970.
- [28] E. Vázquez, M. Prato, ACS Nano 3 (2009) 3819-3824.
- [29] C. Wang, X. Han, P. Xu, X. Zhang, Y. Du, S. Hu, J. Wang, X. Wang, Appl. Phys. Lett. 98, (2011), 0729060-0729062.
- [30] K. Prashantha, J. Soulestin, M. F. Lacrampe, M. Claes, G. Dupin, P. Krawczak, Express Polym. Lett. 10 (2008) 735-739.
- [31] Y. Kojima, A. Usuki, M. Kawasumi, A. Okada, T. Kurauchi, O. Kamigaito, J. Polym. Sci. A. 31 (1993) 983-986.

Chapter 7 Conclusion

Bisphthalonitrile polymers are an important class of high-performance polymers. Because of their outstanding thermal and thermal-oxidative stability, good mechanical properties, low flammability, water and chemical resistance, and easy processability, bisphthalonitrile polymers are recognized as a better class of excellent candidate matrices for advanced composites than other traditional high temperature/performance resin-based advanced composites, such as epoxy, cyanate resin, polyimide, BMI and so on. However, the performances of bisphthalonitrile polymers are limited by some disadvantages. For example the mechanical properties of bisphthalonitrile polymers are adversely affected by their intrinsic brittleness of the network structure. In some circumstances much higher strength, modulus and multifunctional materials are needed in some special fields such as aerospace and military industry. On this basis, this thesis focuses on the modification and functionalization of bisphthalonitrile resin.

xGnP/BPh nanocomposites are successfully prepared via a cost-effective, resin transfer molding method and are characterized for mechanical, electrical, thermal, and morphological properties. The xGnP/BPh pre-polymer possesses higher complex viscosity and storage modulus than the pure BPh, which is closely related to the incorporation of xGnP. The flexural strength and flexural modulus of the xGnP/BPh nanocomposites with 10 wt% xGnP exhibit maximum values. About 27% and 69% increases in flexural strength and modulus are reached compared the pure BPh. And the incorporation of xGnP greatly decreases their resistivity with a sharp transition from an electrical insulator to an electrical conductor. The percolation threshold of xGnP/BPh nanocomposite is between 5 and 10 wt %. Moreover the thermal stability of the xGnP/BPh nanocomposites is also much better than that of the pure BPh resin. The outstanding properties of xGnP/BPh nanocomposites make them candidates for potential applications in military industry, aerospace, and other extremely situation

To overcome the limitation of the intrinsic brittleness of the network structure of BPh resin, the xGnP/PEN-BPh composites as a type of thermoset-thermoplastic- nanofiller blend system are prepared and characterized for mechanical, thermal and morphological

properties. The strength and toughness of the xGnP/PEN-BPh composites is much better than that of the pure BPh. Compared with BPh, for 10 wt% of PEN and 10 wt% of xGnP reinforced BPh composite, the flexural strength, modulus and fracture flexural strain are increased by about 44 MPa, 2 GPa and 2.0%, respectively. The incorporation of PEN enhanced the strength and toughness of BPh polymer while xGnP improved the flexural strength and also offset losses of the flexural modulus and thermostability lowered by the PEN.

According to the existing report, the processing temperature of bisphthalonitrile resin-based composites are controlled at 500 °C or less, while there is less study on its materials formed above 500 °C. The functionalization of bisphthalonitrile resin has not been abundant enough and its application range needs to be expanded. On this basis, we describe a simple and efficient method for *in situ* synthesis of multi-walled CNTs based on BPh resin. The CNTs are not produced in the vapor phase using a complex high pressure, high temperature apparatus but in the solid phase during carbonization. The choice of the preparation method, the carbon source and the catalyst is important for obtaining the desired type of carbon nanotubes. The empty CNTs which use Fe (CO)₅ powder as the catalyst have better dielectric properties than iron-filled CNTs whereas the magnetic property of the iron-filled CNTs which use iron nano-powder as the catalyst exhibit a magnetic saturation value of ~ 3.5 emu/g and a coercive force of ~594.0 Oe. The latter are much higher than those of the empty CNTs. In situ synthesis of multi-walled carbon nanotubes in a bulk solid composition from the pyrolysis of a mixture formulated by phthalocyanine polymer and Fe (CO)₅ powder or iron nano-powder is a good way to obtain novel electrical or magnetic materials. More importantly, the application field of functional BPh resin based materials has been greatly enriched.

BPh monomer and ferrocenecarboxaldehyde are employed to synthesize FePc via a series of high temperature sintering: 500, 700 and 900 °C. FePc exhibits excellent microwave absorption properties in the frequency range of 2.0~18.0 GHz after 700 °C sintering process. The FePc has a strong microwave absorbing peak at 11.0 GHz and reaches a maximum absorbing value of -23 dB at the thickness of 1.5 mm. Theoretical simulation for the microwave absorption using Cole-Cole semicircle theory agrees well with the

experimental results. The microwave absorption of these materials can be mainly attributed to the dielectric loss rather than magnetic loss. The FePc/BPh composites are also prepared. FePc particles is successfully used as a reinforcing filler for BPh matrix composites. When the content of FePc particles reaches 15 wt%, the flexural strength and flexural modulus exhibit maximum values of 170 MPa and 5.4 GPa respectively. The FePc/BPh composites with high performance are believed to have potential uses in microwave absorbing materials. Moreover, the application field of functional BPh resin based materials in the area of absorbing materials has been greatly enriched.

Acknowledgements

First and foremost I would like to express my best gratitude to my supervisors Profs. Guo-hua HU and Xiao-bo LIU. Their creative ideas of research, patient guidance and consistent encouragement push and inspire me to finish my PhD study. I also would like to express my great appreciation to Dr. Sandrine HOPPE for providing much help and suggestions during my PhD studies.

I am greatly thankful to my mates both in French and Chinese groups, Prof. Jean-Noël JAUBERT, Prof. Paul-Marie Marquaire, Dr. Isabelle Ziegler-Devin, Dr. Niramol, Dr Sara, Dr. Rui Zhao, Ning Yu, Zheng-hui Li, Yu-zhen Xia and Yuan Fang, who kindly helped me a lot during my PhD study. Thank my friends, Mingzhen Xu, Xin Zhao, Xulin Yang, Heng Guo, Jiachun Zhong, Xiaoli Yang, Junji Wei, Kun Jia and Fanbin Meng so much, and they have great contributions to my wonderful life both in China and France.

This study could not been finished without the generous financial support from the National Natural Science Foundation of China (Grant No. 51173021), "863" National Major Program of High Technology (2012AA03A212) and Fundamental Research Funds for the Central Universities (103.1.2.E022050205). Thank China Scholarship Council and University of Electronic Science and Technology of China for supporting my studying in France.

Finally, I would like to express my great appreciation to my parents for their understanding and encouragement which support me to finish my PhD studies.

TITRE

Elaboration de matériaux hautement stables thermiquement par modification et fonctionnalisation de la résine bisphthalonitrile

RESUME

Les polymères de phtalonitrile sont obtenus par des réactions d'addition des groupements cyano à haute température et pour un temps long à partir de dérivés de phtalonitrile. Ils trouvent de nombreuses applications dans les domaines de pointe comme l'aérospatiale et la marine. Cependant, leurs performances sont limitées par les inconvénients suivants : (1) fragilité liée intrinsèquement à leur réseau structural, (2) température de fusion élevée, fenêtre de conditions de mise en forme étroite, température de cuisson élevée, cinétique de cuisson faible, (3) Selon la littérature, le traitement du bisphthalonitrile pour obtenir la résine correspondante s'effectue souvent à des températures inférieures à 500 °C. Il y a peu d'études sur les matériaux formés à des températures supérieures à celle-ci, (4) Il n'y a pas beaucoup d'études sur la fonctionnalisation de la résine bisphthalonitrile et son domaine d'application doit être élargi. Cette thèse porte sur le développement de méthodes permettant la modification et la fonctionnalisation de la résine bisphthalonitrile conduisant à une amélioration des propriétés mécaniques de celle-ci. De plus, des nanotubes de carbone ayant une morphologie différente et des matériaux capables d'absorber les hyperfréquences ont été obtenus par pyrolyse de la résine bisphthalonitrile en présence de différents catalyseurs de fer et sur une plage de température allant de 600 à 900 °C.

MOTS-CLES

Bisphthalonitrile, modification, fonctionnalisation, nanotubes de carbone, matériaux absorbants de micro-ondes

TITLE

Preparation of highly thermostable materials by modification and functionalization of bisphthalonitrile resin

ABSTRACT

Bisphthalonitrile polymers are obtained by addition curing reaction of cyano groups upon heating phthalonitrile derivatives at elevated temperature and for an extended period of time. They have found many applications in advanced technologies such as aerospace and marine. However, their performances are limited by the following disadvantages: (1) high brittleness of the inherent network structure; (2) high melting temperature, narrow processing window, high curing temperature, low curing rate and long curing time; (3) according to the literature, the processing temperature of bisphthalonitrile resin-based composites is controlled at 500 °C or less, whereas there are few studies on materials formed above 500 °C; (4) studies on the functionalization of bisphthalonitrile resins are not abundant and its application range needs to be expanded. Based on the above statement, this thesis is focused on the modification and functionalization of bisphthalonitrile resins. The latter were modified by a variety of methods, resulting in improved mechanical properties. Moreover, carbon nanotubes with different morphologies and microwave absorbing materials were obtained by pyrolysing bisphthalonitrile resins with different metal iron catalysts in the range of 600 to 900 °C.

KEY WORDS

Bisphthalonitrile, modification, functionalization, carbon nanotubes, microwave absorbing materials